Ambient vibration testing of civil engineering structures: development of a Python module and applications to case studies

Dag Pasquale Pasca

Abstract

This thesis treats ambient vibration testing of civil engineering structures with a special attention given to timber structures. It presents an open-source Python module that allows to perform two very much used output-only dynamic identification techniques. One of the reasons behind the open-source release of the module is the hope to attract other persons willing to help extending the module's capabilities also to continuous monitoring applications. Furthermore, the work presents and discusses the application of Operational Modal Analysis methods to three case studies, highlighting the usefulness and potential of such methods. The cases are a prestressed short span concrete girder, an eight storey CLT building and a lightweight timber floor sub-assembly. Through the applications it is shown how Operational Modal Analysis may be of use not only to theoretical research oriented applications, but also very practical tasks. For instance in the framework of maintenance plans it is shown how ambient vibration testing results may be used to infer on the state of health of a bridge. Moreover, experimental modal properties are used to perform sensitivity analysis, update finite element models and draw comparison with analytical solutions. In fact, it is also shown how ambient vibration testing can be a viable and cheaper alternative to force vibration tests.

All in all the goals of this work are to highlight the importance and potential of output-only identification methods and broaden the data-base present with applications to timber structures.

Keywords: Ambient vibration tests, Operational Modal Analysis, Timber structures.

To my family.

Preface

The present work has been submitted to the Norwegian University of Life Sciences (NMBU) as fulfilment of the degree of Philosophiae Doctor (PhD). It has been carried out at the faculty of Science and Technology under the supervision of Prof. Ing. Roberto Tomasi. It is a paper-based thesis containing an introductory part (the so-called "Kappe"), that summarises the research questions and provides the context to the four articles, submitted to international scientific journals, that constitutes the main results of this work.

Acknowledgements

Here I am at the end of this journey. Completing a PhD is not an easy task! It is definitely a stressful one, and if I now find myself here at this point it is also thanks to all the people – family, friends, colleagues and teachers that have accompanied me during this journey. With these few words I therefore wish to thank all of you.

First and foremost I wish to express my gratitude to my supervisor, Prof. Roberto Tomasi, for his guidance, for sharing his experience and knowledge, and for giving me the opportunity to start this PhD. I owe him my increasing interest in timber structures, but also for my interest in research in general.

A grateful acknowledgement is devoted to both my co-supervisor Prof. Olav Høibø and to Prof. Anders Nyrud for their support, their kind words and encouragements not to give up, even in the "darkest hour".

I am also grateful to the mechanical workshop at NMBU, especially to the lover of Italy Øyvind Hansen, always willing to prepare various strange bits and pieces for my endless experiments, and to Roar Økseter of the Timber laboratory.

My encounter with Angelo Aloisio has been particularly important; Angelo, who during these last years has become a valuable friend, thank you for sharing with me your knowledge, and for introducing me to dynamic testing!

Last but not least, I wish to thank my parents, my Italian and Norwegian families, for their endless love, patience and moral support. Two loving and joyful tribes that have accompanied me in this journey.

List of abbreviations

API	*Application Programming Interface*
ASCE	*American Society of Civil Engineers*
AVT	*Ambient Vibration Test/s*
CDF	*Cumulative probability Distribution Functions*
CEN	*European Committee for Normalisation*
CLT	*Cross Laminated Timber*
DE	*Differential Evolution*
DFT	*Discrete Fourier Transform*
DoF	*Degree of Freedom*
EFDD	*Enhanced Frequency Domain Decomposition*
EMA	*Experimental Modal Analysis*
FDD	*Frequency Domain Decomposition*
FE	*Finite Element*
FFT	*Fast Fourier Transform*
FRF	*Frequency Response Function*
FSDD	*Frequency Spatial Domain Decomposition*
FVT	*Forced Vibration Test/s*
IRF	*Impulse Response Function*
LVL	*Laminated Veneer Lumber*
MAC	*Modal Assurance Criterion*
MoE	*Module of Elasticity*
NDE	*Non-destructive Damage Evaluation*
OMA	*Operational Modal Analysis*
PSO	*Particle Swarm Optimisation*
PP	*Peak-Picking*
PSD	*Power Spectral Density*
PDF	*Probability Density Function*
rms	*root mean square*
SD	*Spectral Density*
SNR	*Signal-to-Noise Ratio*
SHM	*Structural Health Monitoring*
SSI-cov	*Covariance driven Stochastic Subspace Identification*
SSI-dat	*Data driven Stochastic Subspace Identification*
SVD	*Singular Value Decomposition*

VDV	*Vibration Dose Value*
ZOH	*Zero Order Hold*

List of publications

Included in the thesis:

I D. Pasca, A. Aloisio, L. De Lauretis (2021) PyOMA A Python module to perform Operational Modal Analysis. *(Submitted to Journal of Open Source Software, March 2021)*.

II A. Aloisio, D. Pasca, R. Alaggio, M. Fragiacomo (2020) Bayesian estimate of the elastic modulus of concrete box girders from dynamic identification: A statistical framework for the A24 motorway in Italy. *Structure and Infrastructure Engineering*, pp. 1–13, 2020. https://doi.org/10.1080/15732479.2020.1819343

III A. Aloisio, D. Pasca, R. Tomasi, M. Fragiacomo (2020) Dynamic identification and model updating of an eight-storey CLT building. *Engineering Structures*, vol. 213, p. 110593, 2020. https://doi.org/10.1016/j.engstruct.2020.110593

IV D. Pasca, A. Aloisio, M. Fragiacomo, R. Tomasi (2020) Dynamic characterization of timber floors sub-assemblies: sensitivity analysis and modelling issues. *(Submitted to Journal of Structural Engineering October 2020, Accepted with minor revisions March 2021, Re-submitted March 2021)*.

Journal papers not included in the thesis:

V M. Izzi, D. Casagrande, D. Bezzi, D. Pasca, M. Follesa, R. Tomasi (2018) Seismic behaviour of Cross-Laminated Timber structures: A state-of-the-art review. *Engineering Structures*, vol. 170, p. 42–52, 2018.

VI D. Pasca, C. Myrvhold, O.A. Høibø, A.Q. Nyrud, R. Tomasi (2020) Assessment of ductility properties of the connections in a prefabricated timber panel. *Proceedings of the Institution of Civil Engineers-Structures and Buildings*, vol. 173, n. 12, p. 939–947, 2020.

Conference papers not included in the thesis:

VII D. Pasca, A. Aloisio, R. Tomasi, M. Fragiacomo (2021) Assessment of the vibrational performance of light timber floors from experimental tests. *WCTE 2021 - World Conference on Timber Engineering*, Santiago del Chile.

VIII E. Furuheim, P.M. Nesse, R. Crocetti, R. Tomasi, D. Pasca, H. Liven, R. Abrahmsen (2021) Connections for post and beam glulam structures using birch plywood plates and screws. *WCTE 2021 - World Conference on Timber Engineering*, Santiago del Chile.

IX A. Aloisio, D. Pasca, R. Tomasi, R. Alaggio, L. De Lauretis, M. Fragiacomo, T. Thiis (2021) Dinamic identification of an eight-storey CLT building. *WCTE 2021 - World Conference on Timber Engineering*, Santiago del Chile.

X T. Reiten, C. Nore, R. Tomasi, D. Pasca, E. Ussher, A. Nyrud (2021) Insulated cross laminated timber wood fibre panels as structural layers within CLT. *WCTE 2021 - World Conference on Timber Engineering*, Santiago del Chile.

XI D. Pasca, C. Myrvhold, R. Tomasi, O.A. Høibø, A.Q. Nyrud (2019) Assessment of the connection properties of a prefabricated wooden sandwich panel under static and cyclic loads. *IABSE Symposium, Guimaraes 2019: Towards a Resilient Built Environment Risk and Asset Management* - Report, pp. 244-250

Contents

Abstract
Preface **vii**
Acknowledgements **ix**
List of abbreviations **xi**
List of publications **xiii**
Contents **xv**
1 Introduction **1**
1.1 Background and Motivation 1
1.2 Scope and contributions 3
1.3 Structure of the thesis 4
2 Background **7**
2.1 Introduction to OMA 7
2.1.1 Fundamental assumptions 8
2.1.2 Random data 9
2.2 Structural dynamics models 17
2.2.1 Finite element models 17
2.2.2 Frequency response models 19
2.2.3 State-space models 22
2.3 Output-only modal identification 30
2.3.1 Frequency domain decomposition 30
2.3.2 Stochastic sub-space identification 33
3 Application of ambient-vibration testing **41**
3.1 PyOMA: a Python module to perform Operational Modal Analysis 42
3.2 The A-24 motorway case study 48
3.3 The Palisaden CLT building case of study 56
3.4 Tests in laboratory 64
4 Conclusions **73**
References **77**
Appendices **83**
Paper I 83
Paper II 85
Paper III 111
Paper IV 131

1 Introduction

1.1 Background and Motivation

It is several years now, that the global interest towards timber buildings is experiencing a constant increase. The global climate change crisis and the well-known carbon storing properties of timber buildings ([1, 2, 3, 4]) are certainly playing a big role in the renewed interest towards wooden products. Moreover, positive effects on the indoor air quality connected to the moisture-buffering behaviour of timber products are also well known and documented ([5, 6, 7]). Some studies ([8, 9, 10]) have also found a positive effect on the psychological and physical well-being of occupants related to the usage of wooden products in indoor spaces. All these reasons are contributing to the increasing interest timber is receiving from stakeholders and architects for the realisation of new buildings.

From a mechanical point of view, the excellent stiffness-to-mass ratio of wood, at least in its strong direction (along the fibres), has been known for a long time. Unfortunately its intrinsic high variability (due to knots, defects etc.) has meant that for engineering applications lower design values had to be used. The advent of new highly engineered wood products such as Cross Laminated Timber (CLT) and Laminated Veneer Lumber (LVL), just to name the most popular, have partially overcome this limitation, and led the way to a "timber renaissance". New technologies are allowing these materials to be produced and shaped into more complex forms and manufactured more efficiently. Moreover, this high degree of prefabrication also means that buildings can be constructed in a far shorter timescale. What is also increasingly apparent is that CLT and other types of timber constructions are finally moving from their more established use in the residential sector to be applied on large commercial buildings. Consequently the need to minimise the building's footprint, in the increasingly overcrowded urban agglomerate, calls for tall timber buildings.

The idea of a wooden high-rise or even mid-rise building would have been laughable thirty years ago. Today, even though we are still in a preliminary phase, dealing with demonstration buildings, some countries seem to have been caught up in a race to build the world's tallest timber building [11, 12, 13, 14]. Historically one of the biggest obstacles to the growth in height of wooden structures has been the commonly spread misconception that large scale timber buildings have a greater risk of burning down. Building codes and fire regulations in many countries have for decades severely limited the maximum height achievable by timber structures. However, even though gradually

codes are moving in the direction of allowing for taller wood structures, there are a lot of open issues that need to be addressed.

The experience accumulated during the last twenty years has shown that for CLT structures there is a kind of "sweet spot" at 8-9 storeys for cost-effectiveness reasons. Due to considerations such as cross-grain crushing of floor panels, which are thought to limit the capacity of the vertical load resisting system in such cases, it is unlikely that massive timber panels can be used as the exclusive load bearing system for buildings above the mentioned limit. Post and beams type of structures seem to be the way to go in such circumstances.

Besides the obvious problems posed by the fact that wood is a living material that shrinks and swells when subjected to humidity content variations, going up in height poses a lot of stability-related challenges. One of the major concerns is in fact related to the accelerations level induced by dynamic loads on top floors of mid- and high-rise buildings. The dynamic behaviour of tall timber buildings is definitely still an open issue. This is true both from a serviceability point of view, e.g. that could cause discomfort to the occupants, and also from an ultimate limit state perspective, which aims at providing life safety measures for extreme loading scenarios. Moreover, the need for open, flexible interior spaces in office buildings worsens the already known issue of walk-induced vibration problems in timber floor decking. In fact, a much more known issue, largely investigated in the past, is the assessment of the vibration performance of timber floors. However, this still remains a very topical subject.

One of the "hot topics" in structural engineering that has gained a lot of attention and produced a considerable amount of literature during the last twenty years, is Operational Modal Analysis (OMA) and its applications. OMA allows the identification of the modal parameters (natural frequencies, mode shapes and damping ratios) of the tested structure from ambient vibration in operational conditions. OMA is a response-only technique, meaning no input forces are measured during the test, as opposed to the classical Experimental Modal Analysis (EMA). Modal testing is not a new field, mechanical and aeronautical engineers, for example, have for decades tested components and smaller structures, using well-established input-output techniques, to gain knowledge over their dynamic behaviour. The difficulties connected to giving a measurable and controlled excitation to massive civil engineering structures, such as buildings and bridges, have somehow limited the diffusion of such techniques in the structural engineers community. The advent of OMA techniques, which completely bypass these difficulties, have completely changed the situation and opened up for modal testing of huge and massive structures. Undoubtedly, its most widespread application is ambient-vibration-based

Structural Health Monitoring (SHM), which basically consists in a constant and automated application of output-only identification algorithms to a continuous stream of data from the monitored structure. However, several useful considerations can also be drawn from once-only tests. The results of OMA may be used, for example, to enhance numerical models of the structure under investigation. The development and refinement of new OMA techniques have encouraged copious research activities, which span from theoretical investigations to practical applications [15, 16, 17, 18, 19, 20, 21, 22]. However, research applications onto timber structures are still scarce, and therefore constitutes the main object of this work.

1.2 Scope and contributions

Presently some good commercial software and Matlab toolbox implementing OMA methods and algorithms can be found. However, being proprietary software or needing additional licenses, these are closed environments that are sold at high prices. On the other hand open source software has gained a lot of attention and popularity during these last years. The open source model has even become a successful business model adopted by several companies, not only for its obvious cost-saving reasons, but also because of several other factors. A major advantage to open-source code is the ability for a variety of different people to edit and fix problems and errors, and this results for instance: in faster development, more flexibility and higher reliability of the code.

The author implemented a set of routines written in Python programming language to perform OMA on data acquired from ambient measurement tests. The programming language Python was chosen because of its high versatility, ease of use and because it is a free-software license, characteristics that have made it very popular in the academic field. Since several efforts were spent preparing and testing the code in order to make it as easy as possible to use, it was decided to share the work done and send the code to be reviewed by the Journal of Open Source Software. A Git hub repository was created to host the source code under a GNU General Public License. The objective is to make the tool available to everyone who is interested in the subject, thus helping in spreading the use of dynamic identification methods in civil engineering, with the hope that other individuals will contribute making improvements to the tool.

As already mentioned, few works can be found in the literature that deal with the identification of the modal parameters of timber structures, or components, from ambient vibration tests. One of the goals of this work is therefore to broaden the current data-base present in the literature for such kind of applications. A better understanding

of the dynamic behaviour of mid-rise and high-rise timber buildings is of paramount importance in order to design future buildings more efficiently. Unfortunately it was not possible to set up a permanent monitoring system of a building during the time frame of this PhD project, however some interesting conclusions could already be drawn from the one-time test performed, the results of which will be introduced in one of the enclosed papers. It is the opinion of the author that monitoring mid-rise and high-rise timber structures represents a big opportunity for the whole branch. This will aid in learning important lessons and enhance the confidence of the engineering community towards the use of this material. Furthermore OMA methods can also be employed as a cheaper alternative to EMA methods for tests in a laboratory controlled environment, since vibration shakers or impact hammers are not needed anymore. These kinds of tests have also been successfully used by the author to validate Finite Element (FE) models of a timber flooring systems and will be presented in another of the enclosed papers.

Moreover, the usefulness of once-only dynamic identification test is also highlighted with an application to short-span bridges made of prestressed concrete box girders. To this day, in fact, dynamic-based Non-destructive Damage Evaluation (NDE) techniques do not have a meaningful role in the arrangement of the maintenance plans by the managing body of bridges. A simple reliability-based procedure for the probabilistic assessment (with a Bayesian updating method) of the elastic modulus from the natural frequency of the first bending mode, is presented in the last of the enclosed papers.

To conclude, this work aims at showing the performance of laboratory tests and full-scale applications, and obtain evidences of their usefulness. Only in this way designers, constructors and owners can be convinced of the potentiality and relevance of dynamic identification and monitoring.

1.3 Structure of the thesis

Beside the first introductory chapter, the work is organised as follows:

- In the second chapter the basic mathematical background to understand OMA methods is given. Firstly the fundamental assumptions in OMA are presented, then the basic concepts behind random data measurements are given. Subsequently the models of structural dynamical systems are summarised. Particular attention is given to state-space models since its formulation, which origins from control theory, adopts advanced mathematical tools and is not treated in standard civil engineering study programs. Finally, two of the most widely used algorithms to perform OMA are presented and discussed.

The third chapter presents the developed Python module and introduces to the research cases that were studied during the time frame of this PhD project:

- The first section describes the functionalities of the uploaded Python module, PyOMA. The program's main functions are presented through an application to a simulated data set. The simulated data set consists in the acceleration time-history responses obtained from a five Degrees of Freedom (DoF) system, with user defined properties. The solution of the equation of motion is obtained and then polluted with a random white noise source. The data is then imported and analysed with the functions of the developed module so as to demonstrate its good functioning.

- In the second section the application of ambient vibration tests (AVT) to a prestressed short span concrete bridge is presented. The paper delivers a reliability-based method for the assessment of the Module of Elasticity (MoE) of concrete in simply supported girders from dynamic identification tests. The correlation between the natural frequencies of the first bending modes and the concrete MoE supports the use of the first natural frequency as a predictor of the MoE value. In the presented application, the MoE of seven girders provides the prior state of knowledge about the considered bridge class. The identified natural frequencies update the prior probability distribution of the MoEs using Bayes inference. The resulting probability of exceeding a specific MoE value expresses the degree of belief of the inspector in the obtained MoE. The posterior probability, compared to a proper threshold, could be used in decision-making processes when prioritising the interventions in the maintenance plans.

- The third section presents the results of the dynamic identification of an eight-storey CLT building. A simplified shear-type analytical model was built and calibrated to match the experimental modal parameter by minimising a proper objective function. To test the hypothesis of a continuum-like behaviour of the panels, with a negligible effect of the connections, and the assumption of a shear-type behaviour, opposed to a cantilever behaviour, an indirect approach was chosen. The storey-masses were the chosen optimisation parameters, and the following reasoning drove the process: let us assume a continuum-like behaviour of the building (hypothesis); the connections are neglected in the model updating process (test); if the updated masses match with the expected ones, the hypothesis is proven (proof). Furthermore, the nonlinear effects of connections over the building's response to higher displacements are discussed, and some simplified and practice-oriented correlations for the first natural frequency estimation are given and compared to other structural systems.

- The fourth section focuses instead on the dynamic identification of a timber flooring system made of glulam beams and plywood decking. Timber floors, compared to other materials, are more prone to exhibit vibration levels that cause discomfort to the occupants. The authors carried out multiple experimental tests of the single components and the entire structural assembly via output-only identification. Then, several finite element (FE) models were developed to assess the impact of the modelling choices on the model updating process. Two optimisation algorithms led to the selection of the best modelling parameters. Specifically, the authors chose the MoE, as the parameters to be optimised. Further, the outcomes of a covariance-based sensitivity analysis of the adopted objective function drove a conclusive discussion about the different modelling strategies.

2 Background

2.1 Introduction to OMA

Modal testing is nowadays a well established field. Through the use of frequency response functions, which basically are the ratio of the output response to the input excitation, it is possible to estimate the modal properties (natural frequencies, modal shapes and modal damping ratios) of the structure under investigation. This way of estimating modal properties is also known as Experimental Modal Analysis (EMA).

The identification of the modal properties is very useful as it can be used for various tasks, e.g.: check, and if necessary update, numerical models of real structures; assess the health state, evaluate the safety of a structure; plan and design rehabilitation intervention; design special vibration control devices as tuned mass dampers. The identification of the modal properties can be performed on the measured response of the structure under different types of controlled excitation. The most used devices to generate such input forces are impact hammers and modal shakers. The first generate a known impact force, that allows to measure the free decay of the structure. The second instead generate a continuous dynamic harmonic force that excite the resonant frequencies of the structure. These type of tests are usually referred to as Forced Vibration Tests (FVT).

In the context of civil engineering, it is not always easy to generate and measure a controllable input on a structure, as these can be huge and massive. Fortunately, in the last two decades, new techniques that allow the identification of the modal properties from ambient excitation, have been devised and refined. These type of tests are designated as Ambient Vibration Tests (AVT), and the techniques used to extract the modal properties are referred to as Operational Modal Analysis (OMA).

In the following sections we will first cover the basic assumptions behind OMA, then basic notions of random data analysis and signal processing will be given. This first step is useful to introduce the widely used Correlation functions and Power Spectral Density functions. In the section section we will briefly cover the basic mathematical procedures to model structural dynamic systems. Finally, in the last section, two very popular OMA algorithms will be presented.

2.1.1 Fundamental assumptions

The assumptions behind OMA methods vary depending on the different techniques that are used. However, there are a few main assumptions that are common to all the methods:

- Uncorrelated white noise input forces, both in time and space.
- Linearity. The system is linear and superposition's principle applies.
- Stationarity. The system's characteristics do not change over time, the system is time invariant.
- Observability. The sensor layout has been properly designed to observe the modes of interest.

The first assumption is needed to ensure that all the modes of the system are excited (uncorrelated inputs), theoretically with the same energy over a broad frequency band (white noise). In reality this is seldom the case, since the excitation has a spatial and spectral distribution of its own. The second assumption is fundamental for all the modal analysis techniques, since only if the system is linear the modal superposition of the most relevant modes can provide a good approximation of the total dynamical response of a certain system. The last assumption is necessary to distinguish, during the system identification phase, between the dynamic properties and the noise. In general, if and only if, the system is stationary the system will behave in a deterministic way with respect to the stochastic behaviour of the noise.

As explained in [23, 24], the fundamental idea of OMA testing techniques is that the structure to be tested is being excited by some type of excitation that has approximately white noise characteristics, that is, it has energy distributed over a wide frequency range that covers the frequency range of the modal characteristics of the structure. However, it does not matter much if the actual loads do not have exact white noise characteristics, since what is really important is that all the modes of interest are adequately excited so that their contributions can be captured by the measurements.

In Fig. 1 (from [23]) the basic idea behind OMA is shown through a graphical depiction of the so-called "combined system". Even if the loading does not have a flat spectrum the output of the loads can be considered as the output from an imaginary loading filter loaded by white noise. It has been proved [25] that including an additional filter describing the colouring of the loads does not change the physical modes of the system. The combined system concept shows that in general what we are estimating in OMA is the modal model for "the whole system" including both the structural system and the loading filter. When interpreting the modal results, this has to be kept in mind,

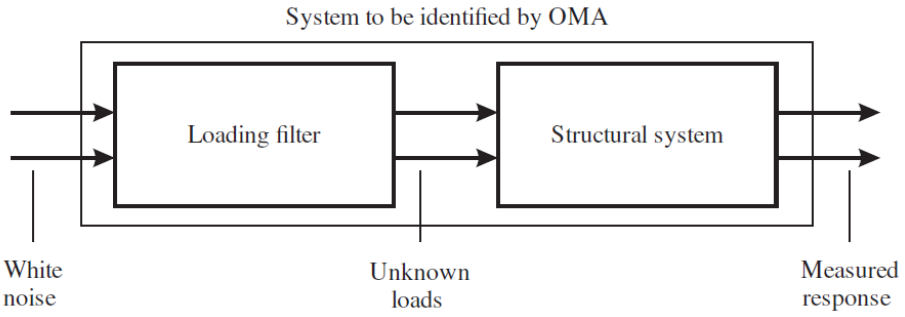

Fig. 1. Combined System.

because, some modes might be present due to the loading conditions and some might come from the structural system.

2.1.2 Random data

Oftentimes external loads imposed on a structure are treated as deterministic, and in such cases these can be expressed through explicit mathematical relationships. Furthermore, also the free vibration response of a system (under a set of initial conditions) is an example of deterministic data, since it is governed by mathematical expressions depending on the mass and stiffness of the system. On the contrary, random data cannot be described by explicit mathematical relationships and they must be described in probabilistic terms.

A random (or stochastic) process $X(t)$, is the collection of all possible N physical realisations of the random phenomenon (i.e contains N number of realisations $x_k(t)$). A sample function is a single time history representing the random phenomenon and, as such, is one of its physical realisations (i.e. each realisation $x_k(t)$, represent an individual time series, that can be thought as the observed result of a single experiment). The collection of realisations from a random process is defined as an ensemble. In Fig. 2 a graphical representation of an ensamble (from [26]) is shown.

Said $x_k(t)$ the k^{th} function in the ensemble, at a certain time instant t the mean value of the random process can be computed from the instantaneous values of each function in the ensemble at that time as follows:

$$\mu_X(t) = \lim_{N\to\infty} \frac{1}{N} \sum_{k=1}^{N} x_k(t) \tag{1}$$

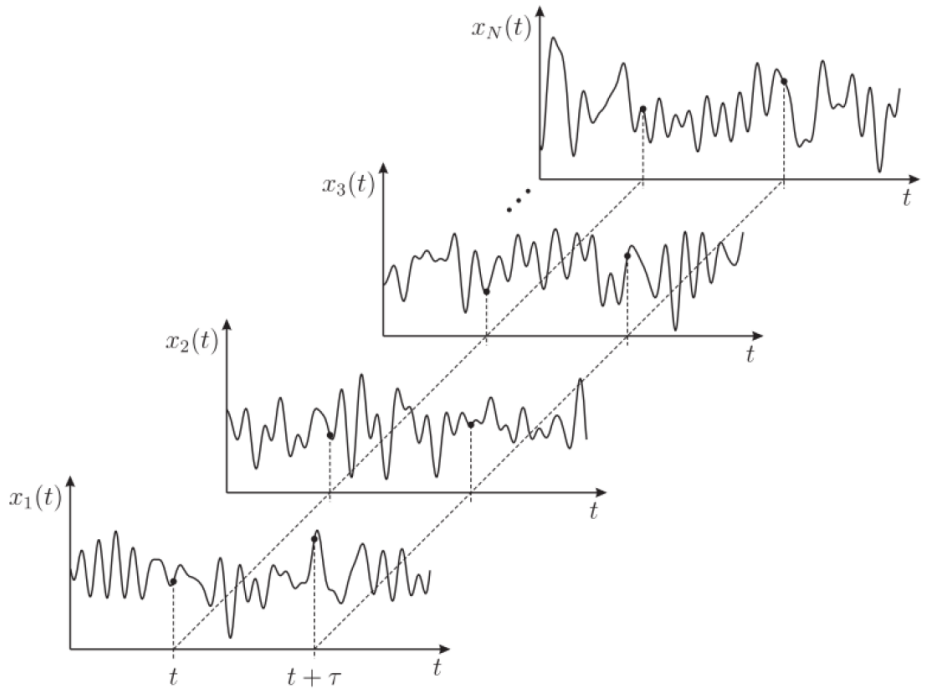

Fig. 2. Ensemble of time history records defining a random process.

In a similar way the auto-correlation function can be computed by taking the ensemble average of the product of instantaneous values at time instants t and $t+\tau$:

$$R_{xx}(t,t+\tau) = \lim_{N\to\infty} \frac{1}{N} \sum_{k=1}^{N} x_k(t) x_k(t+\tau) \tag{2}$$

When Eq.(1) and (2) do not vary with the time instants t, the random process is said to be weakly stationary. For weakly stationary random processes, the mean value is independent of the time t and the auto-correlation depends only on the time lag τ (i.e. $\mu_X(t) = \mu_X$, and $R_{XX}(t,t+\tau) = R_{XX}(\tau)$).

When a random variable assumes values in the range $(-\infty, +\infty)$, its mean value (or expected value) can be computed from the product of each value with its probability of occurrence as follows:

$$E[x_k] = \int_{-\infty}^{+\infty} x p(x)\, dx = \mu_x \tag{3}$$

where $E[\bullet]$ indicates the expected operator, and $p(x)$ is the probability density function. In a similar way it is possible to define the mean square value as:

$$E[x_k^2] = \int_{-\infty}^{+\infty} x^2 p(x)\, dx = \Psi_x^2 \tag{4}$$

and the variance:

$$E\left[(x_k - \mu_x)^2\right] = \int_{-\infty}^{+\infty} (x_k - \mu_x)^2 p(x)\, dx = \Psi_x^2 - \mu_x^2 = \sigma_x^2 \tag{5}$$

The covariance function of two random variables x and y is defined as:

$$C_{xy} = E[(x_k - \mu_x)(y_k - \mu_y)] = \iint_{-\infty}^{+\infty} (x_k - \mu_x)(y_k - \mu_y) p(x,y)\, dx\, dy \tag{6}$$

When dealing with finite records of the structural response, an exact knowledge of parameters, such as mean and variance, and, therefore, of probability density functions is generally not available. Only estimates based on finite datasets can be obtained. Thus, it is desirable to get high quality estimates from the available data. The unbiased estimators for the mean and variance given by:

$$\hat{\mu}_x = \frac{1}{N} \sum_{i=1}^{N} x_i \tag{7}$$

$$\hat{\sigma}_x^2 = \frac{1}{N-1} \sum_{i=1}^{N} (x_i - \hat{\mu}_x)^2 \tag{8}$$

where the hat $(\hat{\bullet})$ indicates that the quantities are estimates of the true values based on a finite number of samples.

Correlation functions

In Eq.(2) the correlation function R_{xx} was introduced. These functions play a primary role in output-only modal identification. For two stationary random processes, $x_k(t)$ and $y_k(t)$, the auto-correlation functions, R_{xx} and R_{yy}, and the cross-correlation function, R_{xy}, are defined respectively as:

$$R_{xx}(\tau) = E\left[x_k(t) x_k(t+\tau)\right], \qquad R_{yy}(\tau) = E\left[y_k(t) y_k(t+\tau)\right] \tag{9}$$

$$R_{xy}(\tau) = E\left[x_k(t) y_k(t+\tau)\right] \tag{10}$$

The assumption of stationary random processes yields mean values, μ_x and μ_y, and covariance functions, $C_{xx}(\tau)$, $C_{yy}(\tau)$ and $C_{xy}(\tau)$, that are also independent of t. If the mean values are both equal to zero, the covariance functions coincide with the correlation functions. When the mean values are not zero, covariance functions and correlation functions are related by the following equations:

$$C_{xx}(\tau) = R_{xx}(\tau) - \mu_x^2, \qquad C_{yy}(\tau) = R_{yy}(\tau) - \mu_y^2 \tag{11}$$

$$C_{xy}(\tau) = R_{xy}(\tau) - \mu_x \mu_y \tag{12}$$

It can be shown [26] that two processes are uncorrelated when $R_{xy}(\tau) = 0$ for all τ only if also either μ_x or μ_y equals zero. Furthermore the maximum values of the auto-correlation and auto-covariance functions occur at $\tau = 0$ and they correspond to the mean square value and variance of the data ($R_{xx}(0) = E\left[x_k^2(t)\right]$, and $C_{xx}(0) = \sigma_x^2$).

When the mean values and covariance (correlation) functions of the considered stationary random processes can be computed by means of time averages on an arbitrary pair of sample records instead of computing ensemble averages, the two stationary random processes are said to be *ergodic*. In other words for ergodic random processes, the time-averaged mean value and auto-correlation function (as well as all other time-averaged properties) are equal to the corresponding ensemble-averaged values. To sum up we have:

$$\mu_x(k) = \mu_x = \lim_{T\to\infty} \frac{1}{T} \int_0^T x_k(t)\, dt \tag{13}$$

$$\begin{aligned} C_{xx}(\tau,k) = C_{xx}(\tau) &= \lim_{T\to\infty} \frac{1}{T} \int_0^T (x_k(t) - \mu_x)(x_k(t+\tau) - \mu_x)\, dt \\ &= R_{xx}(\tau) - \mu_x^2 \end{aligned} \tag{14}$$

$$R_{xx}(\tau,k) = R_{xx}(\tau) \lim_{T\to\infty} \frac{1}{T} \int_0^T x_k(t) x_k(t+\tau)\, dt \tag{15}$$

where the index k denotes that the k^{th} sample function has been chosen for the computation; since the processes are ergodic, the results are independent of this choice ($\mu_x(k) = \mu_x$, $C_{xx}(\tau,k) = C_{xx}(\tau)$, $R_{xx}(\tau,k) = R_{xx}(\tau)$). Similar relations can be defined for μ_y, C_{yy}, C_{xy}, R_{yy} and R_{xy}, see [26].

Ergodic random processes are definitely an important class of random processes. Since the time-averaged mean value and correlation function are equal to the ensemble-averaged mean and correlation function respectively, a single sample function is sufficient

to compute those quantities instead of a collection of sample functions. Fortunately, in practice, random data representing stationary physical phenomena are generally ergodic.

For a stationary record with zero mean ($\mu = 0$) and uniformly sampled data at Δt the unbiased estimate of the auto-correlation function at the time delay $r\Delta t$ is given by:

$$\hat{R}_{xx}(r\Delta t) = \frac{1}{N-r}\sum_{n=1}^{N-r} x_n x_{n+r} \tag{16}$$

where r is also called the lag number and m denotes the maximum lag.

Spectral density functions

Power Spectral Density (PSD) functions are the frequency domain counterparts of the correlation functions. Given the same pair of sample records $x_k(t)$ and $y_k(t)$ of finite duration T from the previously defined stationary random processes $X(t)$ and $Y(t)$, the two-sided auto-spectral and cross-spectral density functions are defined as:

$$S_{xx}(f) = \lim_{T\to\infty} E\left[\frac{1}{T}X_k^*(f,T)X_k(f,T)\right] \tag{17}$$

$$S_{yy}(f) = \lim_{T\to\infty} E\left[\frac{1}{T}Y_k^*(f,T)Y_k(f,T)\right] \tag{18}$$

$$S_{xy}(f) = \lim_{T\to\infty} E\left[\frac{1}{T}X_k^*(f,T)Y_k(f,T)\right] \tag{19}$$

where the operator $(\bullet)^*$ denotes the complex conjugate; the expected value operation is working over the ensemble index k. Two-sided means that $S(f)$ is defined for values of the frequency f in the range $(-\infty, +\infty)$. Eqs.(17, 18 and 19) give the two sided spectrum, the one sided auto-spectral and cross-spectral density functions, $G(f)$, that is with f varying in the range $(0, +\infty)$, can be determined from the two sided spectrum through the relation: $G_{xx}(f) = 2S_{xx}(f)$.

For a zero mean processes, the correlation and PSD functions are Fourier transform pairs, also known as the Wiener-Khinchine relations:

$$S_{xx}(f) = \int_{-\infty}^{+\infty} R_{xx}(\tau)e^{-i2\pi f\tau}\,d\tau \tag{20}$$

The auto-spectral density functions are real-valued functions, while the cross-spectral density functions are complex-valued. In practical applications, PSDs can be obtained by computing the correlation functions first and then Fourier transforming them. This approach is known as the Blackman-Tukey procedure.

Another very used approach is known as the Welch's method. In this procedure the original data segment is split up into n_{DS} data segments of length $T = N\Delta t$, overlapping

by D points. After the data is split up into overlapping segments, the individual n_{DS} data segments have a window applied to them in the time domain. Then, the periodogram is calculated by computing the discrete Fourier transform, and then computing the squared magnitude of the result. The auto-spectral densities are finally calculated through an ensemble averaging operation over the n_{DS} subsets:

$$\hat{G}_{xx}(f) = \frac{2}{n_{DS} N \Delta t} \sum_{i=1}^{n_{DS}} |X_i(f)|^2 \tag{21}$$

The number of data values N in each segment is often called the block size for the computation of each FFT; it determines the frequency resolution of the resulting estimates. The number of averages n_{DS}, instead, determines the random error of the estimates.

Data acquisition and signal processing

High-quality measurements are one of the most important components in OMA, in fact the quality of the acquired data will greatly influence the success of the modal identification. The main components in a modal analysis test are:

– the structure under investigation
– a certain number of motion transducers
– a data acquisition device
– a data processing system (i.e. a Personal Computer)

In an ambient vibration test, the micro tremors of a structure are registered by the motion sensors (usually accelerometers). The motion sensors have the task to convert a physical quantity into an electrical one, typically voltage. Then, the electrical signal in the form of voltage is transferred to the data acquisition hardware for digitisation. Finally, the digitised recorded data is processed and the modal information extracted.

The initial task in dynamic measurement planning is the selection of the sensor locations, directions, and total number of measurements. The choice can be based on experience or can also be based on computer simulations using finite element models of the structure to be tested, or on predictions of the dynamic response of the structure based on simple beam, plate, or shell theories. For all types of measurements, each transducer should be as small and lightweight as possible in order to minimise the influence of the added mass from the sensors. And the sensors should be sensitive enough to pick up the expected operating signals. After measurement numbers, locations, and directions have been selected, the next task is to establish the frequency range for

each measurement, that is, the maximum and minimum frequencies to be recorded and analysed. This parameter usually has the greatest impact on the total data or system bandwidth and on the various instruments of the measurement system.

First of all, when dealing with discrete signals it is worth noting that the sampling interval Δt is the inverse of the sampling frequency f_s and represents the rate by which the analog signal is sampled and digitised:

$$\Delta t = \frac{1}{f_s} \tag{22}$$

In order to extract valid frequency information, digitisation of the analog signal must occur at a certain rate. Shannon's sampling theorem states that the sampling rate must be greater than twice the desired frequency to be measured:

$$f_s > 2 f_{max} \tag{23}$$

For a time record of T seconds, since $T = N\Delta t$ (where N is the number of samples), the lowest frequency component measurable is:

$$\Delta f = \frac{1}{T} = \frac{1}{N\Delta t} \tag{24}$$

The frequency resolution Δf can only be improved at the expense of the resolution in time Δt, and vice versa. As a consequence, for a given sampling frequency, a small frequency spacing Δf is always the result of a long measuring time T (large number of samples N). Assuming that the signal $x(t)$ has been sampled at N equally spaced time instants and that the time spacing Δt has been properly selected, the obtained discrete signal is given by:

$$x_n = x(n\Delta t) \qquad n = 0, 1, 2, \ldots, N-1 \tag{25}$$

Taking into account Eq.(24), the discrete frequency values for the computation of $X(f)$ are given by:

$$f_k = \frac{K}{T} = \frac{k}{N\Delta t} \qquad k = 0, 1, 2, \ldots, N-1 \tag{26}$$

A very important role in signal processing is given to the Discrete Fourier Transform (DFT) algorithm, which allows to analyse the frequency content of a signal and determine if particular frequencies are more predominant. A very efficient version of the algorithm,

known as Fast Fourier Transform, was developed by [27].
The DFT and its inverse are defined by:

$$X_k = \sum_{n=0}^{N-1} x_n e^{\frac{-i2\pi kn}{N}} \qquad k = 0, 1, ..., N-1 \tag{27}$$

$$x_n = \frac{1}{N} \sum_{k=0}^{N-1} X_k e^{\frac{i2\pi kn}{N}} \qquad n = 0, 1, ..., N-1 \tag{28}$$

2.2 Structural dynamics models

This section is meant to provide a brief overview of the basic notion necessary to understand the dynamic identification techniques used in this work. It is assumed that most of those concepts, especially in the first sub-sections, are known to the reader since they are usually well covered during structural dynamics courses in most of civil engineering degrees programmes. Moreover, a few sections of a PhD thesis can not do justice to the breadth and complexity of the subject, and several excellent textbooks are present in the literature that treat the subject [28, 29, 30, 31, 26, 32]. Nevertheless, the basic concepts behind classical modal analysis are briefly presented, along with the concept of impulse response and frequency response function (or transfer function). More attention is devoted to the representation of dynamic systems by state-space models, which is unfamiliar to most structural engineers. These techniques are formulated using concepts and ideas which origin from control theory, and adopt mathematical tools which are more difficult to interpret, an effort will be done in order to highlight the physics behind such methods.

2.2.1 Finite element models

The dynamic response of a discrete multi degree of freedom (MDOF) system, composed by N_m masses, can be described by a set of linear, second order differential equations, expressed in matrix form:

$$[M]\{\ddot{q}(t)\} + [C]\{\dot{q}(t)\} + [K]\{q(t)\} = \{f(t)\} = [B]\{u(t)\} \tag{29}$$

where $([M],[C],[K]) \in \mathbb{R}^{N_m \times N_m}$ are the mass, damping and stiffness matrices, respectively; $(\{\ddot{q}(t)\},\{\dot{q}(t)\},\{q(t)\}) \in \mathbb{R}^{N_m \times 1}$ are respectively the acceleration, velocity, and displacement vectors; $\{f(t)\} \in \mathbb{R}^{N_m \times 1}$ is the force vector, but since usually not all the Degrees of Freedom (DOF) of the system are excited, a load vector $u(t)$, of an inferior dimension ($n_i < N_m$) is often used. This load vector contains the time evolution of the n_i applied inputs and it is multiplied by a matrix $[B] \in \mathbb{R}^{n_i \times N_m}$ composed of ones and zeros that maps the n_i inputs with the N_m DOF of the system. Usually the model described by Eq.(29) is called *spatial model* because it describes the dynamic system by its mass, stiffness, and damping, distributions in the structure. Eq.(29) leads to a system with coupled second order differential equations that need to be solved simultaneously. Coupling, means that the motion of one element affects the motion of the adjacent connected element.

Modal analysis contemplate the transformation of the N_m coupled equations of motion into N_n decoupled single degree of freedom (SDOF) systems, using a convenient

transformation of the coordinates $q(t)$, possible due to the eigenproperties of the system. It can be shown [28] that the eigenvalues, λ_n, and eigenvectors, $\{\psi\}_n$, are intimately tied to the square of the angular natural frequencies, ω_n^2, and the mode shapes, ϕ_n, of the systems, respectively. If we consider the undamped free vibration case the eigensolution is written as:

$$[K][\Psi] = [M][\Psi]diag(\lambda_n) \tag{30}$$

where diag(•) stands for a diagonal matrix, whose entries starting in the upper left corner are $\lambda_1, ..., \lambda_n$. The decoupling of the equation of motion lies in the orthogonality property of the eigenvector matrix (also called modal matrix) with respect to the mass matrix and stiffness matrix, implying that each eigenvector of the modal matrix is independent from others. If we pre-multiply and post-multiply the mass, damping (only true for proportional damping) and stiffness matrices respectively by the transpose of the modal matrix and the modal matrix we are able to diagonalise them. The modal matrix is also used to transform the physical space to the modal space: $\{\eta(t)\} = [\Psi]^{-1}\{q(t)\}$, $f_M(t) = [\Psi]^T[B]\{u(t)\}$. We obtain therefore:

$$[M_M]\{\ddot{\eta}(t)\} + [C_M]\{\dot{\eta}(t)\} + [K_M]\{\eta(t)\} = \{f_M(t)\} \tag{31}$$

where $[M_M], [C_M], [K_M]$ are the (diagonalised) modal mass, modal damping and modal stiffness, respectively; $\{\eta(t)\}$ is the modal coordinates vector, and $\{f_M(t)\}$ is the modal force. The formulation in Eq.(31) is usually known as *modal model*, it allows for an efficient way to solve linear dynamic problems and it provides probably the best physical understanding from an engineering point of view.

It is common practice nowadays to solve models of large civil engineering structures with the aid of Finite Element (FE) software: the structure is divided in elements and from the geometry and material properties of the elements, the global mass matrix $[M]$ and stiffness matrix $[K]$ are assembled. The presence of the damping term is partially based on physical observation and partially on mathematical convenience. In the following only the special case of proportional damping, the so-called Rayleigh damping, is considered. In this case also the damping matrix is diagonalised by the eigenvectors, and can be expressed as a linear combination of the mass and stiffness matrices ($[C] = \alpha[M] + \beta[K]$). As already said, it is very difficult to quantify the true structural damping mechanisms. Therefore one is often satisfied with the mathematically simple proportional damping assumption in a FE analysis [28].

To conclude this brief overview, the Duhamel's integral, which is a way of calculating the response to arbitrary time-varying external loads, is reported. It can be shown [28] that if $f(t)$ is a Dirac delta function (an unit-impulse at instant $t = \tau$), then fundamental

solution for a single degree of freedom (SDOF) system is:

$$h(t-\tau) = \frac{1}{m\omega_D} e^{-\xi\omega_N(t-\tau)} sin\left[\omega_D(t-\tau)\right] \qquad with \qquad t \geq \tau \tag{32}$$

where $\xi = c/(2\sqrt{km})$ is the damping ratio, $\omega_N = \sqrt{k/m}$ is the natural angular frequency of the undamped system (when $c = 0$), $\omega_D = \omega_N\sqrt{1-\xi^2}$ is the damped frequency, m, k, c are respectively the mass, stiffness, damping of the system, and $h(t-\tau)$ is known as the unit-impulse response function. Considering the superposition of effects one obtains the general solution (Duhamel's integral):

$$q(t) = \int_0^t f(\tau)h(t-\tau)\,d\tau = \frac{1}{m\omega_D}\int_0^t f(\tau)e^{-\xi\omega_N(t-\tau)} sin\left[\omega_D(t-\tau)\right]\,d\tau \tag{33}$$

2.2.2 Frequency response models

Unfortunately, the spatial (and modal) model, although giving the best physical understanding from an engineering point of view, is not used in experimental dynamic. Due to the high non linearity of its inverse problem it is not adequate to be directly fitted to experimental data. Consequently, dynamic systems are often modelled with the aid of the so-called Frequency Response Function (FRF).

The application of the Laplace transform to the second order differential equation (29) assuming zero initial conditions, leads to the following algebraic equation:

$$\left(s^2[M] + s[C] + [K]\right)\{Y(s)\} = \{F(s)\} \tag{34}$$

where s is the Laplace variable, and $\{Y(s)\}$ and $\{F(s)\}$ are the Laplace transforms of $\{q(t)\}$ and $\{f(t)\}$, respectively. Defining the dynamic stiffness matrix $Z(s)$:

$$s^2[M] + s[C] + [K] = [Z(s)] \tag{35}$$

we can then rewrite Eq.(35) as:

$$[Z(s)]\{Y(s)\} = \{F(s)\} \tag{36}$$

The inverse of the dynamic stifness matrix $[Z(s)]$ gives the system transfer matrix:

$$[H(s)] = [Z(s)]^{-1} = \frac{adj\left([Z(s)]\right)}{|Z(s)|} = \frac{[A(s)]}{|Z(s)|} \tag{37}$$

with $adj([Z(s)])$ and $|Z(s)|$ the adjoint matrix and the determinant of the dynamic stiffness matrix, respectively. The system transfer function is a complex valued surface,

the numerator of this equation is $[A(s)]$, which is referred to as the *residue matrix*; the denominator of this equation is $det[Z(s)]$, which is a scalar quantity and is called the *characteristic equation*. The solution of the characteristic equation ($det[Z(s)] = 0$) yields $2N_m$ solutions where N_m is the number of equations. If the damping is less than critical damping then the solution to this equation contains roots that are referred to as the *poles* of the system and occur in complex conjugate pairs given by:

$$\lambda_k, \lambda_k^* = -\sigma_k \pm i\omega_{d,k} = -\xi_k \cdot \omega_k + i \cdot \sqrt{1-\xi_k^2} \cdot \omega_k \tag{38}$$

The real part depends on the natural frequency and on the modal damping ratio, whereas the imaginary part coincides with the damped natural frequency, which is close to the natural frequency when damping is small. The Frequency Response Function (FRF) is the transfer function substituting s with $i\omega$ (which effectively takes a slice out of the transfer function surface (see Fig. 3 from [31]), and can be expressed in terms of modal parameters through a partial fraction expansion (see [29]):

$$[H(\omega)]_{s=i\omega} = \sum_{k=1}^{N_m} \frac{[A_k]}{i\omega - \lambda_k} + \frac{[A_k]^*}{i\omega - \lambda_k^*} = \sum_{k=1}^{N_m} \frac{Q_k\{\phi_k\}\{\phi_k\}^T}{i\omega - \lambda_k} + \frac{Q_k^*\{\phi_r\}^*\{\phi_k\}^{*T}}{i\omega - \lambda_k^*} \tag{39}$$

where N_m denotes the number of modes, $\{\phi_k\}$ is the mode shape, $Q_k = 1/(2im_k\omega_d,k)$ is the the modal scaling factor, and λ_k is the, previously defined, pole of the k^{th} mode. The operator $(\bullet)^*$ denotes the complex conjugate of a matrix or vector, the operator $(\bullet)^T$ indicates the transpose of a matrix or vector.

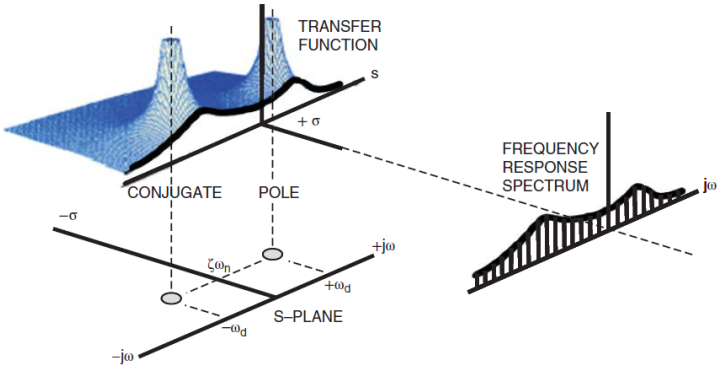

Fig. 3. System Transfer Function, S-plane and Frequency Response Function for a SDOF system.

The structure of the FRF matrix expressed by Eq.(39) highlights some useful results for modal analysis. First of all, it shows that each mode gives a contribution to the

response of the system at any frequency. However, near a resonance this summation can be approximated by the term related to the corresponding mode. SDOF identification methods are based on this assumption. Moreover, Eq.(39) shows that every element of the FRF matrix has the same denominator. Thus, the eigenvalues (poles) of the system are given by the common denominator and they can be estimated either from any individual FRF or from multiple FRFs measured on the same structure. The selected approach leads to the classification of modal analysis techniques as local or global, respectively. The residue matrix $[A_k]$, which is a complex-valued matrix holds the information about mode shapes. It can be shown that $[H(s)]$, when it is evaluated at a pole, is singular and of rank = 1 and can be decomposed as:

$$[H(s)]_{s=\lambda_k} = \{\phi_k\}\frac{Q_k}{s-\lambda_k}\{\phi_k\}^T \tag{40}$$

From this a relationship between the residue matrix and the mode shapes of the system can be written as:

$$[A_k] = Q_k\{\phi_k\}\{\phi_k\}^T \tag{41}$$

The relation between input and output through the FRF matrix:

$$\{Y(\omega)\} = [H(\omega)]\{F(\omega)\} \tag{42}$$

can be manipulated to obtain a fundamental equation of OMA. In fact, taking into account the definition of Power Spectral Density (PSD) function (see [26]) and the properties of transpose, the product $Y(\omega) * Y(\omega)^T$ can be computed and the following relation between PSD matrix of the output and FRF matrix can be obtained:

$$[S_{YY}(\omega)] = [H(\omega)]^*[S_{FF}(\omega)][H\omega)]^T \tag{43}$$

Assuming that the PSD matrix of the input is constant (in OMA the input to the combined system is a stationary, zero mean Gaussian white noise), the output PSD matrix carries the same information and can be expressed in pole-residue form as the FRF matrix:

$$[S_{YY}(\omega)] = \sum_{k=1}^{N_m} \frac{\{\phi_k\}\{\gamma_k\}^T}{i\omega-\lambda_k} + \frac{\{\phi_k\}^*\{\gamma_k\}^H}{i\omega-\lambda_k^*} + \frac{\{\gamma_k\}\{\phi_k\}^T}{-i\omega-\lambda_k} + \frac{\{\gamma_k\}^*\{\phi_k\}^H}{-i\omega-\lambda_k^*} \tag{44}$$

where the operator $(\bullet)^H$ denotes the Hermitian of a matrix (transpose of complex conjugate); $\{\gamma_k\}$ is the operational reference vector associated to the k^{th} mode, that corresponds to the modal participation vector $Q_k\{\phi_k\}^T$ in the pole-residue form of the FRF matrix but, unlike this, it depends on all the modal parameters of the system, the input locations, and the input correlation matrix [33]. In Eq.(44) the poles hold the

information about natural frequencies and damping ratios, while the residues hold the information about the mode shapes. However, since the input is not measured, only un-scaled mode shapes can be obtained. Equation (44) clearly shows that, for each mode, the output PSD provides four poles in complex conjugate pairs (λ_k, λ_k^*, $-\lambda_k$, $-\lambda_k^*$). Taking into account that FRF and IRF on one hand, and spectral density functions and correlation functions on the other hand are Fourier transform pairs, similar analogies are possible between IRFs and correlation functions in the framework of OMA.

Eq.(32) can be rearranged considering the previously defined quantity, into:

$$[h(t)] = \sum_{k=1}^{N_m} \left([A_k] e^{\lambda_k t} + [A_k]^* e^{\lambda_k^* t} \right) \tag{45}$$

Eq.(45) shows evident analogies with the mathematical structure of the FRF reported in Eq.(39). The poles hold the information about natural frequencies and damping ratios, while the information about the mode shapes is in the $[A_k]$ matrices.

2.2.3 State-space models

The idea at the core of this type of models is to represent the dynamic by system states. A state is the smallest set of variables that are able to completely define the system behaviour, or rather the energy of the system. For the second order equation, used to model mechanical systems, 2 states are needed: displacements and velocities of the system. In this way, on one hand we are able to reduce the second order differential equation to a first order differential equation, on the other hand we are doubling the system dimension.

Continuous state-space model

The second order equation (29) can be converted into a system of two first-order equations (the *state equation* and the *observation equation*) using a so-called *state-space model*. These type of models allow to describe a diverse range of dynamical systems and are very popular in control engineering.

Firstly we rewrite Eq.(29) as:

$$\{\ddot{q}(t)\} + [M]^{-1}[C]\{\dot{q}(t)\} + [M]^{-1}[k]\{q(t)\} = [M]^{-1}[B]\{u(t)\} \tag{46}$$

Then we define the *state vector*:

$$\{s(t)\} = \left\{ \begin{array}{c} \{q(t)\} \\ \{\dot{q}(t)\} \end{array} \right\} \tag{47}$$

and we substitute it in the set of equations consisting of Eq.(46) and the identity $[M]\{\dot{q}(t)\} = [M]\{\dot{q}(t)\}$, yielding:

$$\{\dot{s}(t)\} = \begin{bmatrix} [0] & [I] \\ -[M]^{-1}[K] & -[M]^{-1}[C] \end{bmatrix} \{s(t)\} + \begin{bmatrix} [0] \\ [M]^{-1}[B] \end{bmatrix} \{u(t)\} \tag{48}$$

From Eq.(48) the *state matrix* $[A_c] \in \mathbb{R}^{2N_m \times 2N_m}$ and the *input influence matrix* $[B_c] \in \mathbb{R}^{2N_m \times n_i}$ can be defined as follows:

$$[A_c] = \begin{bmatrix} [0] & [I] \\ -[M]^{-1}[K] & -[M]^{-1}[C] \end{bmatrix} \tag{49}$$

$$[B_c] = \begin{bmatrix} [0] \\ [M]^{-1}[B] \end{bmatrix} \tag{50}$$

and the state equation can be written as:

$$\{\dot{s}(t)\} = [A_c]\{s(t)\} + [B_c]\{u(t)\} \tag{51}$$

where the pedix $(\bullet)_c$ denotes continuous time.

The observation equation, instead, establishes the relation between a subset of l measured outputs organised in the vector $\{y(t)\}$ and the displacement, velocity and acceleration associated with all DOF. Under the assumption that measurements of the structural response are taken at l locations and the sensors are accelerometers, velocimeters, and displacement transducers, we have:

$$\{y(t)\} = [C_a]\{\ddot{q}(t)\} + [C_v]\{\dot{q}(t)\} + [C_d]\{q(t)\} \tag{52}$$

$[C_a]$, $[C_v]$ and $[C_d] \in \mathbb{R}^{l \times 2N_m}$ are the output location matrices for acceleration, velocity, and displacement, respectively. It is worth emphasizing that, while a real structure is characterised by an infinite number of DOFs (which becomes a finite but large number in the lumped mass models usually set for numerical analyses), in a practical vibration test this number decreases down to a few dozens or even less. Substitution of the expression for $\{\ddot{q}(t)\}$ obtained from Eq.(46) into Eq.(52) yields the following equation:

$$\begin{aligned} \{y(t)\} = &\left([C_d] - [C_a][M]^{-1}[K]\right)\{q(t)\} \\ &+ \left([C_v] - [C_a][M]^{-1}[C]\right)\{\dot{q}(t)\} \\ &+ \left([C_a][M]^{-1}[B]\right)\{u(t)\} \end{aligned} \tag{53}$$

from Eq.(53), taking into account the definition of state vector Eq.(47) and the following definitions:

$$[C_c] = \begin{bmatrix} [C_d] - [C_a][M]^{-1}[K] & [C_v] - [C_a][M]^{-1}[C] \end{bmatrix} \tag{54}$$

$$[D_c] = [C_a][M]^{-1}[B] \tag{55}$$

where $[C_c]$ is the output influence matrix and $[D_c]$ is the direct transmission matrix. We can then write the observation equation as:

$$\{y(t)\} = [C_c]\{s(t)\} + [D_c]\{u(t)\} \tag{56}$$

The state equation Eq.(51) and the observation equation Eq.(56) define the continuous-time state-space model:

$$\begin{aligned} \{\dot{s}(t)\} &= [A_c]\{s(t)\} + [B_c]\{u(t)\} \\ \{y(t)\} &= [C_c]\{s(t)\} + [D_c]\{u(t)\} \end{aligned} \tag{57}$$

Once the model has been constructed, the modal parameters of the dynamic system can be extracted from the state matrix $[A_c]$. In [33] it is shown that the matrices with the eigenvalues and eigenvectors of $[A_c]$ ($[\Lambda_c]$ and $[\Psi]$, respectively) have the following structure:

$$\begin{aligned} [A_c] &= [\Psi][\Lambda_c][\Psi]^{-1} \\ [\Lambda_c] &= \begin{bmatrix} \Lambda & 0 \\ 0 & \Lambda^* \end{bmatrix}, \quad [\Psi] = \begin{bmatrix} \Phi & \Phi^* \\ \Phi\Lambda & \Phi^*\Lambda^* \end{bmatrix} \\ [\Lambda] &= \begin{bmatrix} \ddots & & \\ & \lambda_k & \\ & & \ddots \end{bmatrix}, \quad [\Phi] = [\dots\ \Phi_k\ \dots] \quad k = 1, \dots, N_m \end{aligned} \tag{58}$$

$[\Lambda_c] \in \mathbb{C}^{2N_m \times 2N_m}$ and $[\Psi] \in \mathbb{C}^{2N_m \times 2N_m}$, while Λ, Φ are the eigenvalues and egenvectors of the original second order equation (29).

A very important property of the state-space model is that it is not unique, there exist an infinite number of representations that produce the same input-output description [30]. An alternative model can be established by the application of a transformation to the state vector: $\{x(t)\} = [T]\{z(t)\}$, where $[T]$ is an arbitrary non-singular square matrix. This property is known as *similarity transformation*, and leads to:

$$\begin{aligned} \{\dot{z}(t)\} &= [T]^{-1}[A_c][T]\{z(t)\} + [T]^{-1}[B_c]\{u(t)\} \\ \{y(t)\} &= [C_c][T]\{z(t)\} + [D_c]\{u(t)\} \end{aligned} \tag{59}$$

the matrices $[T]^{-1}[A_c][T]$, $[T]^{-1}[B_c]$, $[C_c][T]$, $[D_c]$ describe the same relationships as the matrices $[Ac]$, $[Bc]$, $[Cc]$ and $[Dc]$. However, unlike $\{y(t)\}$ the new state vector $\{z(t)\}$

has not the meaning of physical displacements and velocities [33]. This means that a state-space model identified from experimental data is one over an infinite number of possible models that are able to describe the given data. One can obtain the modal state-space form, as shown in [33], by substituting $[T]$ with $[\Psi]$.

Discrete state-space model

In practical applications the signal recorded by the sensors is taken at discrete time instants, while all the equations considered up to now were written in continuous time. The continuous-time state-space model needs, therefore, to be converted into a discrete-time model. For a given sampling period Δt, the continuous-time equations can be discretized and solved at all discrete time instants $t_k = k\Delta t$, $k \in \mathbb{N}$. An assumption about the behaviour of the time-dependent variables between two samples has to be made to this aim. For instance, the Zero Order Hold (ZOH) assumption states that the input is piece-wise constant over the sampling period. Under this assumption the continuous-time state-space model can be converted to the discrete-time state-space model:

$$\begin{aligned} \{s_{k+1}\} &= [A]\{s_k\} + [B]\{u_k\} \\ \{y_k\} &= [C]\{s_k\} + [D_c]\{u_k\} \end{aligned} \tag{60}$$

where $\{s_k\} = \{s(k\Delta t)\}$ is the discrete-time state vector yielding the sampled displacements and velocities; $\{u_k\}$ and $\{y_k\}$ are the *sampled input* and *sampled output*, respectively; $[A]$ is the discrete state matrix, $[B]$ is the *discrete input matrix*, $[C]$ is the *discrete output matrix* and $[D]$ is the *direct transmission matrix*. The relations between continuous-time matrices and the corresponding discrete-time matrices are:

$$[A] = e^{[A_c]\Delta t} \tag{61}$$

$$[B] = ([A] - [I])\,[A_c]^{-1}[B_c] \tag{62}$$

$$[C] = [C_c] \tag{63}$$

$$[D] = [D_c] \tag{64}$$

The interested reader can refer to the literature [30] for more details.

Stochastic state-space model

The model expressed by Eq.(60) is a deterministic model since the system is driven by a deterministic input $\{u_k\}$. Stochastic components have to be included in order to

describe actual measurement data. When stochastic components are included in the model, the following *discrete-time combined deterministic-stochastic state-space model* is obtained:

$$\begin{aligned} \{s_{k+1}\} &= [A]\{s_k\} + [B]\{u_k\} + w_k \\ \{y_k\} &= [C]\{s_k\} + [D_c]\{u_k\} + v_k \end{aligned} \tag{65}$$

where $\{w_k\} \in \mathbb{R}^{2N_m}$ is the process noise due to disturbances and model inaccuracies, while $\{v_k\} \in \mathbb{R}^l$ is the measurement noise due to sensor inaccuracies.

In the context of OMA, structures are excited by immeasurable inputs. Since the information about the input $\{u_k\}$ is not available, the measured system response $\{y_k\}$ is generated only by the two stochastic processes $\{w_k\}$ and $\{vk\}$, and the following *discrete-time stochastic state-space model* is obtained:

$$\begin{aligned} \{s_{k+1}\} &= [A]\{s_k\} + \{w_k\} \\ \{y_k\} &= [C]\{s_k\} + \{v_k\} \end{aligned} \tag{66}$$

In the absence of $\{u_k\}$, its role is implicitly modelled by process noise and measurement noise. In particular, the process noise becomes the input that drives the dynamics of the system, while the measurement noise accounts for the direct disturbance of the response of the system. Thus, when a stochastic state-space model is adopted, the objective is the determination of the order $N_o = 2N_m$ of the unknown system and of a realisation of the matrices $[A]$ and $[C]$ from a large number of measurements of the output $\{y_k\}$ generated by the system itself. The state matrix $[A]$ transforms the current state of the system $\{s_k\}$ in the next state $\{s_{k+1}\}$, while the product of the observation matrix $[C]$ with the state vector provides the observable part of the dynamics of the system. More precisely, the response vector $\{y_k\}$ is given by the observable part of the state plus the measurement noise. The process noise and the measurement noise are both immeasurable. They are assumed to be zero mean, stationary white noise processes with covariance matrices given by:

$$E\left[\begin{Bmatrix} \{w_p\} \\ \{v_p\} \end{Bmatrix} \langle \{w_q\}^T \{v_q\}^T \rangle\right] = \begin{cases} \begin{bmatrix} [Q^{ww}] & [S^{wv}] \\ [S^{ww}]^T & [R^{vv}] \end{bmatrix} & p = q \\ [0] & p \neq q \end{cases} \tag{67}$$

where p and q are two arbitrary time instants. The estimation of the matrices $[Q_{ww}]$, $[R_{vv}]$ and $[S_{wv}]$ is also part of the identification process. The assumption of white noise for $\{w_k\}$ and $\{v_k\}$ is fundamental in the proof of SSI methods (see [32] for more details). Thus, if the unmeasured input includes some dominant frequency components, they

appear as poles of the state matrix $[A]$ together with the eigenvalues of the system. This is equivalent to the identification of the dynamic properties of both the structure under investigation and the excitation system forming the combined system (driven by stationary, zero mean Gaussian white noise as input) that is the generally assumed objective of identification in OMA. In agreement with the stochastic framework of OMA, the system response in the state-space model is represented by a zero mean Gaussian process. The output covariance matrices are given by:

$$[R_i] = E\left[\{y_{k+1}\}\{y_k\}^T\right] \tag{68}$$

and they carry all the information to describe the process. A covariance equivalent model can be then defined as the estimated state-space model characterised by correct covariance and, therefore, able to describe the statistical properties of the system response. The estimator producing this model is referred to as an optimal estimator. The state $\{s_k\}$ is also a zero mean Gaussian process described by its covariance (which is independent of the time instant k):

$$[\Sigma] = E\left[\{s_k\}\{s_k\}^T\right] \tag{69}$$

and it is uncorrelated with the process noise and the measurement noise:

$$\begin{aligned} E\left[\{s_k\}\{w_k\}^T\right] &= [0] \\ E\left[\{s_k\}\{v_k\}^T\right] &= [0] \end{aligned} \tag{70}$$

The "next state - output" covariance matrix (covariance between the response of the system $\{y_k\}$ and the updated state vector $\{s_{k+1}\}$), is defined as:

$$[G] = E\left[\{s_{k+1}\}\{y_k\}^T\right] \tag{71}$$

Taking into account the previous assumptions about the noise terms, the system response and the state, mathematical manipulations of the state-space equations (66) lead to the following fundamental relations:

$$[\Sigma] = [A][\Sigma][A]^T + [Q^{ww}] \tag{72}$$

$$[R_0] = [C][\Sigma][C]^T + [R^{vv}] \tag{73}$$

$$[G] = [A][\Sigma][A]^T + [S^{wv}] \tag{74}$$

$$[R_i] = [C][A]^{i-1}[G] \tag{75}$$

The property expressed by Eq.(75) is very important, in fact since the output covariance sequence $[R_i]$ can be directly estimated from the measured data (eq. 68), its

decomposition according to Eq.(75) permits the estimation of the state-space matrices and the solution of the system identification problem. For stochastic systems, the matrices $([A],[G],[C],[R_0])$ play the role of the deterministic system matrices $([A],[B],[C],[D])$. Thanks to this equivalence, input-output impulse-response-driven identification methods are easily translated into output-only covariance-driven methods.

An alternative formulation for stochastic systems, is the so-called *forward innovation model*, which is obtained by the application of the so-called *steady-state Kalman filter*[33, 24]. The forward innovation model is written as:

$$\begin{aligned} \{\hat{s}_{k+1}\} &= [A]\{\hat{s}_k\} + [K]\{e_k\} \\ \{y_k\} &= [C]\{\hat{s}_k\} + \{e_k\} \end{aligned} \tag{76}$$

where $[K]$ is the Kalman gain. The aim of the Kalman filter is to produce an optimal prediction for the state vector by making use of observations of the outputs up to time $k-1$ and the available system matrices together with the known noise covariances. In this formulation the predictor of the state vector $\{\hat{s}_k\}$, replaces the state vector $\{s_k\}$, and the two processes $\{w_k\}$ and $\{v_k\}$ are converted into a single process, the innovation, $\{e_k\}$. The one-step-ahead predictor of the state vector $\{\hat{s}_k\}$, is defined as the conditional mean of $\{s_k\}$ given all previous measurements:

$$\{\hat{s}_k\} = E\left[\{s_k\}|[Y^{k-1}]\right] \tag{77}$$

The system's response can be optimally predicted if an optimal predictor of the states is available. The quality of the predictor of the states is quantified by the state prediction error:

$$\{\varepsilon_k\} = \{s_k\} - \{\hat{s}_k\} \tag{78}$$

In a similar way it is possible to define the innovation:

$$\{e_k\} = \{y_k\} - \{\hat{y}_k\} \tag{79}$$

where the one-step-ahead predictor $\{\hat{y}_k\}$ is defined as the conditional mean of $\{y_k\}$ given all previous measurements:

$$\{\hat{y}_k\} = E\left[\{y_k\}|[Y^{k-1}]\right] = E\left[\left([C]\{s_k\} + \{v_k\}\right)|[Y^{k-1}]\right] = [C]\{\hat{s}_k\} \tag{80}$$

Given the initial state estimate $\{\hat{s}_0\}$, the initial covariance of the state estimate $[P_0] = E[\{\hat{s}_0\}\{\hat{s}_0\}^T] = [0]$ and the output measurements $[Y^{k-1}]$, the nonsteady-state Kalman state estimate at time t_k can be obtained from the following recursive formulas that provide the Kalman state estimate, the Kalman gain, and the Kalman state covariance, respectively:

$$\{\hat{s}_k\} = [A]\{\hat{s}_{k-1}\} + [K_{k-1}]\left(\{y_{k-1}\} - [C]\{\hat{s}_{k-1}\}\right) \tag{81}$$

$$[K_{k-1}] = \left([G] - [A][P_{k-1}][C]^T\right)\left([R_0] - [C][P_{k-1}][C]^T\right)^{-1} \tag{82}$$

$$\begin{aligned}[P_k] = [A][P_{k-1}[A]^T + \\ \left([G] - [A][P_{k-1}][C]^T\right)\left([R_0] - [C][P_{k-1}][C]^T\right)^{-1}\left([G] - [A][P_{k-1}][C]^T\right)^T\end{aligned} \tag{83}$$

Eq.(83) is known as the *Ricatti equation*. Obtained the Kalman state covariance matrix $[P_k]$ the covariance of the innovation can be computed as:

$$E\left[\{e_k\}\{e_k\}^T\right] = [R_0] - [C][P_k][C]^T \tag{84}$$

The presented discussion can not be considered complete and exhaustive, the interested reader is therefore invited to refer to [30, 32, 33, 24, 29] for more details.

2.3 Output-only modal identification

In this section two of the most widely used identification algorithms are presented and discussed:

- *Frequency Domain Decomposition*
- *Stochastic Subspace Identification*

The first is a non-parametric identification method implemented in the frequency domain, as the name suggest; while the second is a parametric (a model is fitted to the experimental data) time domain method.

2.3.1 Frequency domain decomposition

Frequency domain methods, as the name suggest, refers to the analysis of mathematical functions or signals with respect to frequency, rather than time. They have been known and used by engineers since the $1960's$, and were developed mainly to simplify the mathematical analysis. In fact, as explained in the previous sections, converting the description of the system from the time domain to a frequency domain, converts the differential equations to algebraic equations.

The most simple method for output-only modal parameter identification is the basic frequency domain method, also known as the Peak-Picking method (PP). It is based on the computation of auto-spectra and cross-spectra and it has been used in the past also for output-only modal identification purposes [34]. The name of the method comes from the fact that the modes are identified by picking the maxima in the power spectral density (PSD) plots. The frequency-domain decomposition (FDD) (introduced in [35]) takes the classical frequency-domain approach some steps further. The technique is based on the Singular Value Decomposition (SVD) of the Spectral Density matrix and allows to concentrate all information in the plot of singular values of the SD matrix. A way to present the method is from the modal expansion of the structural response:

$$\{y(t)\} = [\Phi]\{\eta(t)\} \tag{85}$$

where $[\Phi]$ is the eigenvectors matrix and $\{\eta(t)\}$ is the vector of modal coordinates. Using the definition of Correlation Function matrix one obtain the following expression:

$$\begin{aligned}[R_{yy}(\tau)] &= E\left[\{y(t+\tau)\}\{y(t)\}^T\right] = \lim_{T\to\infty}\frac{1}{T}\int_0^T \{y(t+\tau)\}\{y(t)\}^T dt \\ &= E\left[[\Phi]\{\eta(t+\tau)\}\{\eta(t)\}^T[\Phi^T]\right] = [\Phi][R_{\eta\eta}(\tau)][\Phi]^T\end{aligned} \tag{86}$$

where $[R_{\eta\eta}(\tau)]$ is the Correlation Function matrix of modal coordinates; $E[\bullet]$ is the expected value operator. Taking the Fourier transform one can obtain the PSD matrix:

$$\{G_{yy}(\omega)\} = [\Phi][G_{\eta\eta}(\omega)][\Phi]^H \tag{87}$$

where $\{G_{yy}(\omega)\}$ is the SD matrix of the modal coordinates, which is both diagonal and positive valued assuming that the modal coordinates are uncorrelated. Applying the Singular Value Decomposition of the PSD matrix at a certain frequency ω leads to the following:

$$\{G_{yy}(\omega)\} = [U][\Sigma][U]^H \tag{88}$$

The comparison between Eq.(87) and Eq.(88) suggests that it is possible to identify a one-to-one relationship between singular vectors and mode shapes; moreover, the singular values are related to the modal responses and they can be used to define the spectra of equivalent SDOF systems characterised by the same modal parameters as the modes contributing to the response of the MDOF system under investigation.

Since the SVD provides the singular values arranged in descending order, near a resonance the first singular value contains the information about the dominant mode at that frequency. Moreover, since the number of nonzero elements in $[\Sigma]$ equals the rank of the PSD matrix at the considered frequency, this property can be used to identify closely spaced or even coincident modes. In fact, the number of dominant singular values (defining the rank of the output PSD matrix) at a certain frequency equals the number of modes that give a significant contribution to the structural response at that particular frequency [24]. Assuming that only one mode is dominant at the frequency ω, and that the selected frequency is associated to the peak of resonance of the k^{th} mode, the PSD matrix approximates to a rank one matrix with only one term on the right side of Eq.(88):

$$[G_{yy}(\omega)] = \sigma_1\{u_1\}\{u_1\}^H, \qquad \omega \to \omega_k \tag{89}$$

In such a case, the first singular vector $\{u_1\}$ represents an estimate of the mode shape of k^{th} mode:

$$\{\hat{\phi}_k\} = \{u_1(\omega_k)\} \tag{90}$$

and the corresponding singular value σ_1 belongs to the auto spectral density function of the equivalent SDOF system corresponding to the mode of interest. An equivalent SDOF PSD function can be identified as the set of singular values around a peak that are characterised by similar singular vectors. Because the SVD given by Eq.(88) does not correspond completely to the theoretical decomposition of the SD matrix, see Eq.(44), the FDD is always an approximate solution.

In the first generation of FDD technique [35] only the natural frequencies and associated mode shapes could be identified. The method was therefore enhanced by [36] so that also damping ratios estimate could be extracted. The basic idea of this enhanced version is to isolate the auto-spectral densities, near a resonance frequency (peak), that can be associated to an equivalent SDOF PSD function. In order to extract this so-called equivalent PSD bell function, the singular vectors associated to the singular values near the resonance peack, are compared with $\{\hat{\phi}_k\}$, through the so-called Modal Assurance Criterion (MAC, [37]), defined as:

$$MAC(\phi_i, \phi_j) = \frac{|\{\phi_i^H\}\{\phi_j\}|^2}{\left(\{\phi_i^H\}\{\phi_i\}\right)\left(\{\phi_j^H\}\{\phi_j\}\right)} \tag{91}$$

The singular values whose singular vectors are above a user-defined MAC rejection level (typically around 0.8) define the equivalent SDOF PSD function. By definition, the MAC is a scalar in the range $[0,1]$; it is equal to zero when the vectors under comparison are orthogonal, and equal to 1 when the vectors differ by a scale factor only. The inverse Fourier transform of the equivalent SDOF PSD function yields an approximated correlation function of the equivalent SDOF system. Thus, an estimate of the modal damping ratio is obtained in the time domain through a linear regression on the logarithmic decrement. In a similar way, an estimate of the natural frequency independent of the frequency resolution can be obtained through a linear regression on the zero crossing times.

A further improvement of the algorithm is due to [38], and is known as Frequency-Spatial Domain Decomposition (FSDD). The idea behind this version of the FDD is to isolate the modal coordinates by modal filtering. An enhanced output PSD $\Delta\hat{G}^e_{yy,m}$ is obtained performing pre- and post-multiplication with a principal vector corresponding to the m^{th} natural frequency. In this way only the contribution from the considered mode, and not from the other modes, defines the estimated modal response for the considered mode.

$$\Delta\hat{G}^e_{yy,m}(\omega_k) = \{u_1^H(\omega_k)\}\{G_{yy}(\omega_k)\}\{u_1^H(\omega_k)\} \tag{92}$$

As for EFDD, the estimated SDOF PSD function can be taken back to time domain, performing the inverse Fourier transform, obtaining the auto-correlation function associated to the SDOF from which the damping ratio and a frequency resolution independent estimate of the natural frequency. An example of a Singular Value plot is shown in Fig.4a, while in Fig.4b the results extracted for a mode using FSDD are shown.

To sum up, the FDD method is a very popular, user friendly, frequency domain based, non-parametric technique. One of the reasons of its popularity is due to the

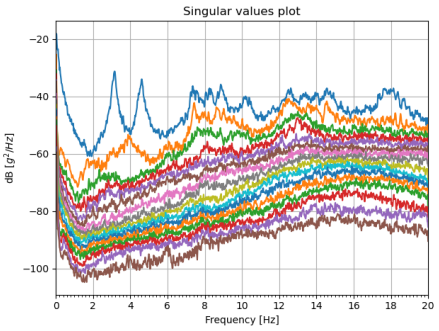

(a) Typical SV plot of the PSD matrix (from real measurement data).

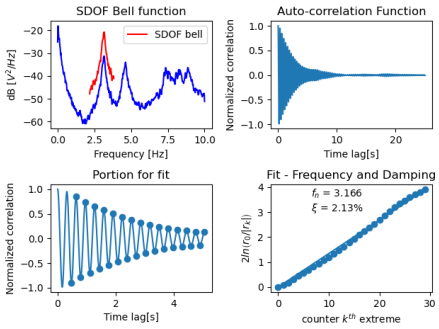

(b) SDOF bell function, associated auto correlation function, portion used for the fit and results of the fit for a mode of the system.

Fig. 4. Typical results of EFDD method

fact that one works directly on spectral densities, which are familiar objects to most engineers. However, the method is more reliant on good quality data compared to SSI methods (the variance of the estimates decrease with increasing length, resolution and signal-to-noise ratio of the data), but can also be affected by close or complex modes of the structure.

2.3.2 Stochastic sub-space identification

The Covariance-driven Stochastic Subspace Identification (SSI-cov) method and the Data-driven Stochastic Subspace Identification (SSI-dat) address the stochastic realisation problem, that is to say the problem of identifying a stochastic state-space model from output-only data [33]. In the following only the version of SSIcov as presented in [24] is reported. In this version of the algorithm all the measured output channels l are used in the calculations, as opposed to the algorithm reported in [33] where the covariances between the outputs and a limited set of reference outputs, $r < l$, are used. The sthocastic sub-space model introduced in Eq.(66) describes the problem. It is repeated here for convenience:

$$\{\dot{s}_{k+1}\} = [A]\{s_k\} + \{w_k\}$$
$$\{y_k\} = [C]\{s_k\} + \{v_k\}$$

The SSI-cov method can be classified as a time-domain, parametric, covariance driven procedure for OMA. It starts from the computation of output correlations:

$$[\hat{R}_i] = \frac{1}{N-i}[Y_{(1:N-i)}][Y_{(i:N)}] \tag{93}$$

where $[Y_{(1:N-i)}]$ is obtained from the data matrix $[Y] \in \mathbb{R}^{l \times N}$ by removal of the last i samples (l is the number of output, N is the number of data points), while $[Y_{(i:N)}]$ is obtained from $[Y]$ by removal of the first i samples; $[\hat{R}_i]$ is the estimate of the correlation matrix at time lag i (also known as number of block row) based on a finite number of data. The estimated correlations at different time lags are gathered into the block Toeplitz matrix $[T_{1|i}]$. A block Toeplitz matrix is a special block matrix, which contains blocks that are repeated down the diagonals of the matrix.

$$[T_{1|i}] = \begin{bmatrix} [\hat{R}_i] & [\hat{R}_{i-1}] & \dots & [\hat{R}_1] \\ [\hat{R}_{i+1}] & [\hat{R}_i] & \dots & [\hat{R}_2] \\ \vdots & \vdots & \ddots & \vdots \\ [\hat{R}_{2i-1}] & [\hat{R}_{2i-2}] & \dots & [\hat{R}_i] \end{bmatrix} \tag{94}$$

Each correlation matrix has dimensions $l \times l$; thus, the block Toeplitz matrix has dimensions $li \times li$. Applying the factorisation property given by Eq.(75) to the block Toeplitz matrix we obtain:

$$[T_{1|i}] = \begin{bmatrix} [C] \\ [C][A] \\ \vdots \\ [C][A]^{i-1} \end{bmatrix} \begin{bmatrix} [A]^{i-1}[G] & \dots & [A][G] & [G] \end{bmatrix} = [O_i][\Gamma_i] \tag{95}$$

$$[O_i] = \begin{bmatrix} [C] \\ [C][A] \\ \vdots \\ [C][A]^{i-1} \end{bmatrix} \tag{96}$$

$$[\Gamma_i] = \begin{bmatrix} [A]^{i-1}[G] & \dots & [A][G] & [G] \end{bmatrix} \tag{97}$$

where $[O_i] \in \mathbb{R}^{li \times n}$ and $[\Gamma_i] \in \mathbb{R}^{n \times li}$ are the *observability matrix* and the *reversed controllability matrix*, respectively. The number of block rows i has to fulfill the condition $li > N_o$, where N_o is the model order, and if the system is observable and controllable, the rank of the $li \times li$ Toeplitz matrix equals N_o, since it is the product of a matrix with N_0 columns, $[O_i]$, and a matrix with N_o rows, $[\Gamma_i]$. Assuming that the order of the system has been estimated and taking into account that the number of outputs l is a constant of the identification problem, a value for i larger than or equal to N_o/l can be set. The adopted value for i is basically a user's choice and it is definitely based on a physical insight of the problem.

The SVD of the block Toeplitz matrix provides its rank, which equals the number of nonzero singular values:

$$[T_{1|i}] = [U][\Sigma][V]^T = \begin{bmatrix}[U_1] & [U_2]\end{bmatrix} \begin{bmatrix}[\Sigma_1] & [0] \\ [0] & [0]\end{bmatrix} \begin{bmatrix}[V_1]^T \\ [V_2]^T\end{bmatrix} \tag{98}$$

If the zero singular values and the corresponding singular vectors are omitted, Eq.(98) yield:

$$[T_{1|i}] = [O_i][\Gamma_i] = [U_1][\Sigma_1][V_1]^T \tag{99}$$

where the matrices $[U_1] \in \mathbb{R}^{li \times N_o}$ and $[V_1]^T \in \mathbb{R}^{N_o \times li}$ and the diagonal matrix $[\Sigma_1] \in \mathbb{R}^{+N_o \times N_o}$ holds the positive singular values arranged in descending order. The matrices $[O_i]$ and $[\Gamma_i]$ can be computed by splitting the SVD in two parts as follows:

$$[O_i] = [U_1][\Sigma_1]^{1/2}[T] \tag{100}$$

$$[\Gamma_i] = [T]^{-1}[\Sigma_1]^{1/2}[V_1]^T \tag{101}$$

where $[T] \in \mathbb{C}^{n \times N_o}$ is a non-singular matrix which plays the role of a similarity transformation applied to the state-space model (see Eq.(59)); $[T]$ can simply be set equal to the identity matrix $[T] = [I]$. Taking into account the definitions of observability matrix (Eq.(96)) and controllability matrix (Eq.(97)), the output influence matrix $[C]$ and the next state-output covariance matrix $[G]$ can be easily obtained as the first l rows of $[O_i]$ and the last l columns of $[\Gamma_i]$, respectively. Written in Python notation:

$$[C] = O_i[:l, :] \tag{102}$$

$$[G] = \Gamma_i[:, l:] \tag{103}$$

The state matrix $[A]$ can be computed according to different approaches. One is based on the decomposition property of the one-lag shifted Toeplitz matrix:

$$[T_{2|i+1}] = \begin{bmatrix} [\hat{R}_{i+1}] & [\hat{R}_i] & \dots & [\hat{R}_2] \\ [\hat{R}_{i+2}] & [\hat{R}_{i+1}] & \dots & [\hat{R}_3] \\ \vdots & \vdots & \ddots & \vdots \\ [\hat{R}_{2i}] & [\hat{R}_{2i-2}] & \dots & [\hat{R}_{i+1}] \end{bmatrix} = [O_i][A][\Gamma_i] \tag{104}$$

Introducing Eq.(100) and (101) into Eq.(104), taking into account that $[T] = [I]$, and solving for $[A]$, the following expression for the state matrix is obtained:

$$[A] = [O_i]^+[T_{2|i+1}][\Gamma_i]^+ = [\Sigma_1]^{-1/2}[U_1]^T[T_{2|i+1}][V_1][\Sigma_1]^{-1/2} \tag{105}$$

where $(\bullet)^+$ denotes the Moore-Penrose pseudo-inverse of a matrix.

As an alternative, the state matrix $[A]$ can be estimated by exploiting the shift structure of the observability matrix [33].

$$[A] = [O_i^{\uparrow}]^{+}[O_i^{\downarrow}] \tag{106}$$

where $[O_i^{\uparrow}]^{+}]$ and $[O_i^{\downarrow}]$ are obtained from the matrix $[O_i]$ by removal of the last and the first l rows, respectively.

Once the matrix $[A]$ is found the identification problem is theoretically solved: the system order N is found as the number of non-zero singular values in Eq.(98) and the system matrices $[A], [G], [C]$ can be computed as in Equations (50), (51) and (53) or (54). The fourth system matrix $[R_0]$ is simply the zero-lag output covariance matrix.

The two matrices $[A]$, $[C]$ are sufficient to compute the modal parameters. As discussed in section 2.2.3), the Eigenvalue Decomposition (EVD) of the matrix $[A]$ provides the modal parameters of the system (see Eq.(58)), in fact, the discrete poles and the observed mode shapes are computed as:

$$[A] = [\Psi][\Lambda][\Psi]^{-1}$$
$$[\Phi] = [C][\Psi]$$

After the conversion from discrete-time to continuous-time, which is found by inserting the eigenvalue decomposition of the continuous state matrix $[A_c]$ into Equation (61):

$$[A] = e^{[A_c]\Delta t} = e^{[\Psi][\Lambda_c][\Psi]^{-1}\Delta t} = [\Psi]e^{[\Lambda_c]\Delta t}[\Psi]^{-1} = [\Psi][\Lambda_d][\Psi]^{-1} = [\Psi]\begin{bmatrix} \ddots & & \\ & \mu_k & \\ & & \ddots \end{bmatrix}[\Psi]^{-1}$$

The discrete eigenvectors are equal to the continuous ones and the discrete eigenvalues, μ_k are related to the continuous eigenvalues by:

$$\mu_k = e^{\lambda_k \Delta t} \quad \Leftrightarrow \quad \lambda_k = \frac{ln(\mu_k)}{\Delta t}$$

The natural frequencies, the damped modal frequencies, and the damping ratios can then be estimated:

$$f_{n,k} = \frac{|\lambda_k|}{2\pi}$$
$$f_{d,k} = \frac{Im(\lambda_k)}{2\pi}$$
$$\xi_k = \frac{Re(\lambda_k)}{|\lambda_k|}$$

As can be seen the method needs the user to specify some parameters for the analysis: the model order N_o, and the time lag i. Theoretically the system order N_o can be determined by inspecting the number of non-zero singular values of Eq.(98). In practice however, the estimated covariance Toeplitz matrix $[T_{1|i}]$ is affected by noise leading to singular values that are all different from zero. As a consequence, even if a minimal realisation of a system of order N_o can be theoretically identified, the determination of the correct order of the system is usually a very complex task. Thus, the rank of $[T_{1|i}]$ is "approximately" N_o, and the truncation of the smallest singular values leads to a certain error in the estimation of the statespace matrices. As explained in [33], various noise sources, such as modeling inaccuracies and measurement noise, leads to the absence of clear gaps in the singular values.

Practical experience with parametric models in modal analysis applications has shown that it is better to over-specify the model order N_o and to eliminate spurious numerical poles afterwards. The use of stabilization diagrams is a great tool to achieve this goal. The poles corresponding to a certain model order are compared to the poles of a one-order lower model. If the eigenfrequency, the damping ratio and the related mode shape differences are within preset limits, the pole is labelled as a stable one.

In case of the SSI-cov method, an efficient construction of the stabilization diagram is achieved by computing the SVD of the covariance Toeplitz matrix, Eq.(98), only once. Models of different order are then obtained by including a different number of singular values and vectors in the computation of O_i and Γ_i, Eq.(96) and Eq.(97), from which the system matrices and the modal parameter are deduced. An example of stabilization diagram is shown in Fig.5.

Typical stability requirements are expressed by the following inequalities:

$$\begin{aligned} \frac{|f(n)-f(n+1)}{f(n)} &< 0.01 \\ \frac{|\xi(n)-\xi(n+1)}{\xi(n)} &< 0.05 \\ 1-MAC(\{\phi(n)\},\{\phi(n+1)\}) &< 0.02 \end{aligned}$$

where (n) and $(n+1)$ are the n^{th} and $n^{th}+1$ model order, f is the natural frequency, ξ is the damping, and ϕ is the mode shape vector. In other words the scatter between the estimates of the modal properties at two subsequent model orders has to be lower than a user defined limit value for a pole to be labelled as stable.

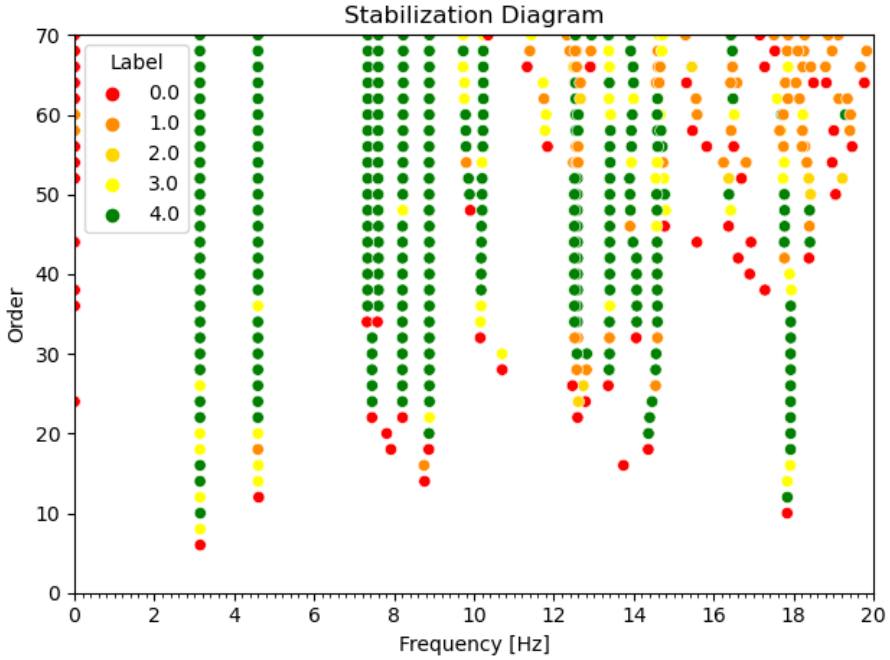

Fig. 5. Typical Stabilisation Diagram. The modes of the system appear as stable lines of poles for increasing model order.

The other parameter that plays an important role in the identification process is the number of block rows, i, (also called time lag or time shift). It has been shown that the estimates of the modal properties (especially damping ratios) are sensitive to variations of the parameter i. As remarked in [39] if a system has a low eigenfrequency compared to the sampling frequency, and if i has a low value, it is possible that only few cycles of the response are included in the block matrix (time lag), and as a consequence the eigenfrequency is not well identified. The authors define a "rule of thumb" to determine a minimum value of i:

$$i \geq max\left(\frac{f_s}{2f_0}; \frac{N_o}{l}\right) \tag{107}$$

where f_s is the sampling frequency, f_0 the lowest frequency of interest, N_o is the maximum model order and l is the number of output.

However Eq.(107) ensures only that the system is identifiable but does not provide a range of values where quality of the fit and clearness of the stabilisation diagram are optimised [40]. In fact, generally, larger values of i are necessary in order to achieve a convergence in terms of damping estimations. Usually, sensitivity analysis are performed

to find optimised modal parameter estimates. For instance, once defined the model order, the effects induced by different choices of i can be analysed, as done in [40]. Other helpful recommendations for finding the best choice for the user defined parameters i and N can be found in the literature [41, 42, 40, 18].

3 Application of ambient-vibration testing

In this chapter the benefits of ambient vibration testing are shown trough some applications. Firstly, to demonstrate the potential and good functioning of the developed module, a benchmark case, where the modal properties of the system are known on beforehand, is analysed. Then three very different applications of ambient vibrations tests are presented and discussed

3.1 PyOMA: a Python module to perform Operational Modal Analysis

As already mentioned, the author developed a set of Python functions that allow for fast analysis of data from ambient vibration tests. These functions have been uploaded and are hosted on a public repository on GitHub (url: `https://github.com/dagghe/PyOMA`) under a GNU General Public License.

GitHub is a popular provider of internet hosting for software development. Its main purpose is to facilitate software development, allowing users to collaborate on projects offering distributed version control, source code management functionalities and other collaboration features. GitHub offers its basic services free of charge, and free accounts are commonly used to host open-source projects.

The code has been made open-source with the hope that other individuals can help in making improvements and expanding its functionalities. A major advantage to open-source code is in fact the ability for a variety of different people to edit, adjust, improve the code, and fix problems and errors that have occurred. Naturally, since there are more people who can edit the material, there are more people who can help make the information more credible and reliable. The open-source mission statement promises better quality, higher reliability, more flexibility and lower cost.

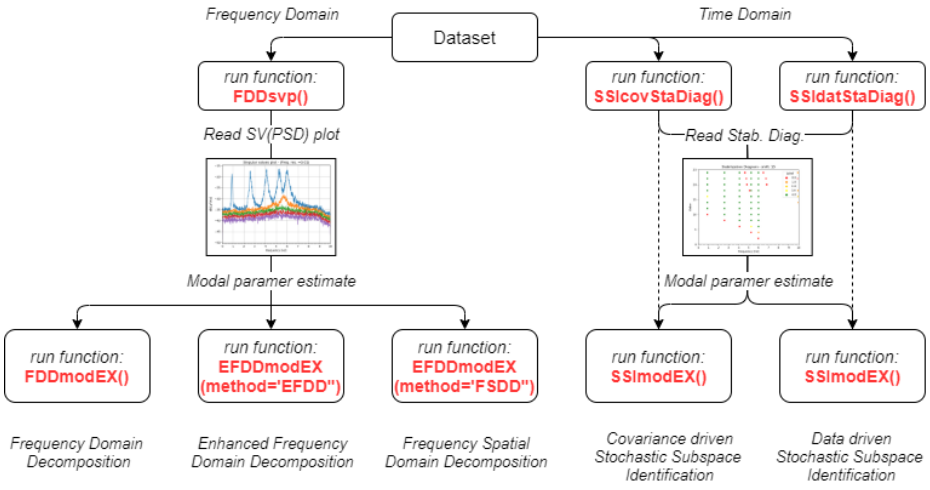

Fig. 6. Flowchart for the use of the module's functions.

For a complete description of the functions (input parameters, returned output) refer to the wiki pages at the provided web page, where all the functionalities of the module are described.

The case study is a simple $5\,DOF$ system, taken from [28]. It is shear type frame (the floor stiffness is assumed significantly larger than the stiffness of the columns) with lumped mass $m = 25.91\,[Ns^2/mm]$ at each floor, and same storey stiffness $k = 10000\,[N/mm]$ to all stories. The mass and stiffness matrix have the structure:

$$[M] = m\begin{bmatrix} 1 & & & & \\ & 1 & & & \\ & & 1 & & \\ & & & 1 & \\ & & & & 1 \end{bmatrix}, \quad [K] = k\begin{bmatrix} 2 & -1 & & & \\ -1 & 2 & -1 & & \\ & -1 & 2 & -1 & \\ & & -1 & 2 & -1 \\ & & & -1 & 2 \end{bmatrix}$$

Solving the eigenvalue problem, $([M] - \lambda[K])[\Phi] = 0$, gives the (undamped) natural frequencies and the mode shapes of the system. The damping is added considering a constant, proportional damping ratio of $\xi_k = 2.0\%$ applied to all modes. Accordingly, the damping matrix is obtained finding first the diagonal entries of the modal damping matrix and then finding the system's damping. In Tab.1 the exact results for the system are reported. Since OMA methods allow to find only un-scaled mode shape (the mass matrix is not known), in this example the mode shapes have been normalised to unity maximum displacement.

Table 1. Exact values of frequencies, damping and mode shapes of the system

$f_k\,[Hz]$	$\xi_k\,[\%]$	ϕ_1	ϕ_2	ϕ_3	ϕ_4	ϕ_5
0.890	2.0%	0.2846	-0.7635	1	0.9190	-0.5462
2.598	2.0%	0.5462	-1	0.2846	-0.7635	0.9190
4.095	2.0%	0.7635	-0.5462	-0.9190	-0.2846	-1
5.261	2.0%	0.9190	0.2846	-0.5462	1	0.7635
6.000	2.0%	1	0.9190	0.7635	-0.5462	-0.2846

The artificial signals, corresponding to the acceleration time history at each floor can be found following multiple approaches. One of the most used methods to solve the equation of motion is Newmark's integration method (see [28]). However, it is also possible to solve the system using state-space models introduced in Section 2.2.3. For instance, PyOma provides a function, $EXdata()$, that generates the simulated data of this system using a state-state approach, and is very computational efficient. In order to satisfy the broadband excitation requirement, all the $5\,DOF$ are excited by a Gaussian white noise input. The results from each response are then polluted with a random noise source (the signal-to-noise ratio is $SNR = 10$). The time histories were generated with a sampling frequency of $f_s = 100\,Hz$, and the duration of the simulation was set to 30 minutes, see Fig.7.

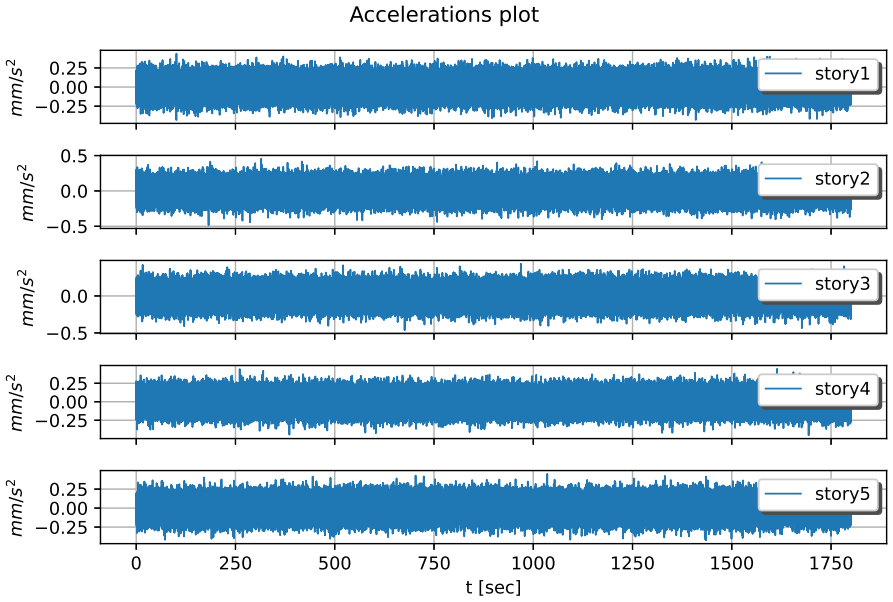

Fig. 7. Time history of the accelerations at each floor

After the dataset has been imported (either using the module's function or importing the txt file), preliminary operations such as detrend, decimation, normalisation may be performed, if needed. For this example the data has been decimated (by a factor of 5), given that the sampling rate is $100\,Hz$ and the highest frequency is $\simeq 6\,Hz$. The pyOMA module's functions can now be used to process and extract the modal information. Firstly the standard FDD algorithm is performed on the artificial data simply by calling the function: *FDDsvp(data, fs, df=0.01, pov=0.5, window='hann')*. The needed parameters by the function are the dataset and the sampling frequency. The optional parameters allow to select the desired frequency resolution (for the PSD) and setting the options for the window. The PSD matrix is estimated using Welch's method, in this case using a Hanning filtering window, with a 50% overlap between the segments.

In the singular values plot, reported in Fig.8a, the five peaks corresponding to the natural frequencies of the system can easily be identified. Using the standard FDD algorithm [35], only frequencies and mode shapes can be extracted. In order to get also damping estimates (and frequencies estimates independent from the frequency resolution of the PSD) the so-called Enhanced Frequency Domain Decomposition [36], and the Frequency Spatial Domain Decomposition, variation of the algorithm may be

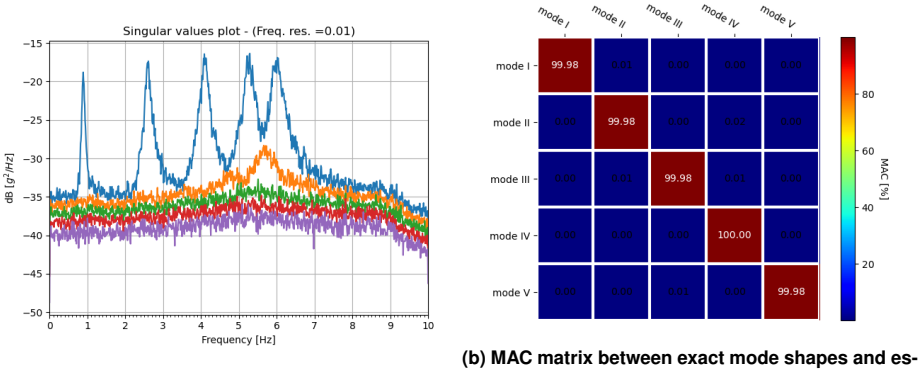

(a) Singular Values plot of the PSD matrix

(b) MAC matrix between exact mode shapes and estimated according to FSDD method

Fig. 8. Results of the identification

used [38]. To run the frequency domain identification algorithms with PyOMA we can simply run the functions:

– *FDDmodEX(freq, FDD[1])* to run FDD
– *EFDDmodEX(freq, FDD[1], method='EFDD', MAClim = 0.95, npmax=25, sppk=3)* to run EFDD
– *EFDDmodEX(freq, FDD[1], method='FSDD', MAClim = 0.95, npmax=25, sppk=3)* to run FSDD

The arguments of the functions $freq$ and $FDD[1]$ are respectively an array containing the frequency values identified in the SV plot, and a dictionary containing the results from the previously called function *FDDsvp()*. The other parameters used for EFDD and FSDD, are the MAC rejection limits (to extract the SDOF bell function), and the number of peaks to consider, $npmax$, and to skip, $sppk$, when calculating the modal properties from the autocorrelation functions.

In Fig.9 the results for the first and second mode extracted according the EFDD and FSDD method are shown for comparison. Tab.2 reports the results of both methods in terms of both natural frequencies and damping ratios, moreover the mode shapes returned by FSDD are also reported. The great accordance between the exact mode shapes of the system and the results extracted from the identification algorithms, is also evidenced by the MAC matrix shown in Fig.8b.

When it comes to Time domain methods, PyOMA allows to perform both SSI-dat [32] and SSI-cov [33] algorithms. To analyse the data with these time domain parametric procedures one can run the following functions:

– *SSIcovStaDiag(data, fs, br, ordmax=None, lim=(0.01,0.05,0.02,0.1))* to run SSI-cov

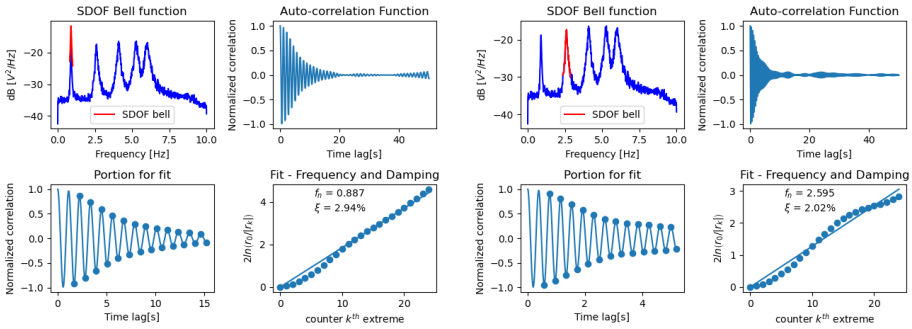

(a) EFDD **(b) FSDD**

Fig. 9. Results of the identification

– *SSIdatStaDiag(data, fs, br, ordmax=None, lim=(0.01,0.05,0.02,0.1))* to run SSI-dat

For these functions the needed parameters are the dataset, the sampling frequency and the number of block rows. The optional parameters permit to define the maximum model order, and the limit values to be used for the stability criteria of the poles in the stabilisation diagram, see Sec. 2.3.2. For this simulated dataset the number of block rows was set to $br = 15$, and the maximum model order was set to 30. Both methods return very clear stabilisation diagrams, where the alignment of the stable poles is very clear and easy to read, see Fig.10.

Once the identified frequencies have been collected in an array, it is possible to extract the estimates of the modal properties. To do so one can run the function *SSIModEX(freq, SSI[1])*, where $freq$ is the array collecting the identified frequency lines in the stabilisation diagram, and $SSI[1]$ is a dictionary containing the results from

Table 2. Results of the identification in the frequency domain

EFDD			*FSDD*	
$f_k\,[Hz]$	$\xi_k\,[\%]$		$f_k\,[Hz]$	$\xi_k\,[\%]$
0.887	2.96%		0.887	2.94%
2.595	2.02%		2.595	2.01%
4.107	1.80%		4.107	1.78%
5.280	1.67%		5.280	1.66%
5.977	1.63%		5.977	1.62%
ϕ_1	ϕ_2	ϕ_3	ϕ_4	ϕ_5
0.287	0.737	1	0.916	0.530
0.546	1	0.283	-0.758	-0.895
0.752	0.558	-0.881	-0.288	1
0.927	-0.291	-0.534	1	-0.795
1	-0.889	0.745	-0.546	0.298

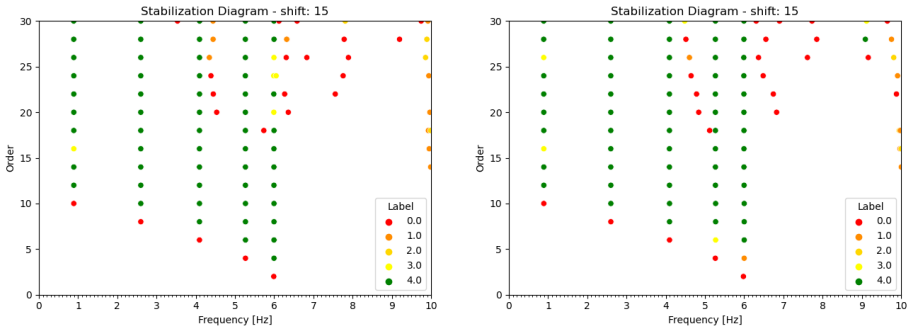

(a) SSI-cov **(b) SSI-dat**

Fig. 10. Stabilisation Diagrams

the previously called functions (*SSIcovStaDiag()* and/or *SSIdatStaDiag()*. The estimated frequencies and damping ratios found with the two methods are reported in Tab.3, moreover the mode shapes estimated with SSI-cov are also reported.

Table 3. Results of the identification in the time domain

$SSI-cov$			$SSI-dat$	
$f_k\,[Hz]$	$\xi_k\,[\%]$		$f_k\,[Hz]$	$\xi_k\,[\%]$
0.889	2.49%		0.889	2.58%
2.598	2.12%		2.598	2.13%
4.095	1.89%		4.094	1.91%
5.266	2.03%		5.267	2.01%
5.996	2.00%		5.994	2.03%
ϕ_1	ϕ_2	ϕ_3	ϕ_4	ϕ_5
0.283	0.750	1	0.908	0.552
0.533	1	0.304	-0.754	-0.937
0.750	0.560	-0.904	-0.284	1
0.926	-0.292	-0.552	1	-0.791
1	-0.901	0.767	-0.546	0.297

From a comparison of the results in Tab.1, Tab.2 and Tab.3, it is clear that both FDD and SSI methods return very good estimates of the natural frequencies. Moreover, the mode shape estimates show also very good agreement with the exact shapes. However, SSI methods stem for the more precise estimates of the damping ratios, whereas FDD methods are more susceptible to frequency resolution, duration of the acquisition, user defined parameters, noise and other issues.

3.2 The A-24 motorway case study

Bridges are a classical example of civil engineering structures that benefit from the advantages of ambient vibration tests (AVT). As already underlined, one of the biggest advantages of OMA methods over EMA methods, is that structures can be tested while in use without the need to interrupt their functions. For instance, the vehicular traffic on a bridge would only have to be limited to permit the safe operations of the technicians at work, without the need of completely closing it off. This is a very attractive feature for infrastructures of strategic importance, where the interruption of the service heavily affects the users, and is usually unwanted by the managing body because of the costs it implies. Furthermore all the logistic hassles and costs related to bringing and operating the massive devices needed to control the input forces given to the structure in forced vibration tests (FVT) are completely avoided. Not to mention the fact that the excitation devices are normally very massive and therefore need to be accounted for when studying the dynamic behaviour. For all these reasons, bridges are probably the most studied kind of structures since the advent and consolidation of the more recent and advanced identifications techniques [18, 43, 20, 41, 44].

After the first pioneering ambient-vibration tests [45, 46, 47, 48], the development of more sophisticated identification algorithms have been of help in spreading the use of modal testing throughout the academic community. Moreover, the incredible technological advancements of the two last decades have contributed to making the installation and operation of temporary or permanent monitoring systems more practical and economical. There is, however, an incongruous discrepancy between the number of academic investigations on the one hand, and the adopted and codified procedures for the inspection of bridges, maintenance, and monitoring by governments and managing bodies on the other hand. The mistrust of governments and managing bodies towards the adoption of non-desctructive examination (NDE) techniques based on dynamic measurements may be related to the absence of codified procedures or publicly available guidelines. The field of academic investigations is still felt hazy, abstract and a waste of money by the government officials when it comes to practical applications. The tragic recent events of Genoa's Morandi bridge collapse have nevertheless contributed in raising the interest towards temporary and permanent ambient-vibration based monitoring solutions. The need of controlling a huge number of structures that are reaching their critical age, and also the necessity of validating the performance of new structures with high levels of complexity, call for a widespread use of dynamic testing and monitoring. In this context researchers should aim at developing straightforward, reliable methods capable of convincing that dynamic-based NDE techniques give useful knowledge,

which surely complete and do not supplant visual inspections.

The appended paper delivers a reliability-based method for the assessment of the MoEs of simply supported concrete girders from dynamic identification. The method is quite simple and exploits the correlation between the natural frequencies of the first bending modes and the MoE in simply supported beam-like structures. Firstly, the concrete MoEs were assessed using both static tests on the whole bridge stock and tests on concrete samples extracted by core drilling. This set of results provides the prior state of knowledge about the considered bridge class. Furthermore, the identified natural frequencies update the prior probability distribution of the MoEs using Bayes inference. The resulting probability of exceeding a specific MoE value expresses the degree of belief of the inspector in the obtained MoE. The posterior probability, compared to a proper threshold, could be used in decision-making processes when prioritising the interventions in the maintenance plans.

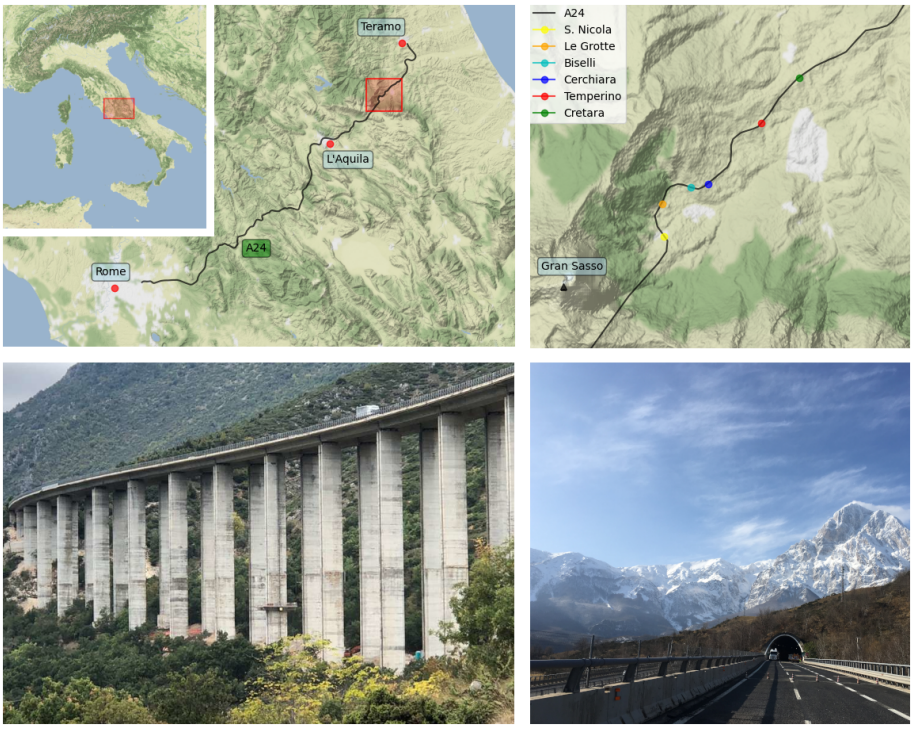

Fig. 11. Location and views of the A24 "Autostrada dei Parchi" motorway

In 2019 the University of L'Aquila carried out a thorough testing campaign on a stock of viaducts belonging to the A24 motorway "Strada dei Parchi" in Italy [49, 50]. The A24 motorway was built during the 70s of last century, it connects Rome to Teramo, crossing the Appennines and passing through "Gran Sasso and Monti della Laga" National Park. The complex morphology of the ground necessitated the construction of a large amount of viaducts, some of which have over 50 spans, see Fig.11. Several of these viaducts are now ageing and are in a non-optimal state of preservation, especially the piers.

Both dynamic and static tests were conducted, and in addition some concrete samples were extracted and tested in the lab. Selected spans, labelled according to the name of the viaduct they belong to, were tested: Biselli, Cerchiara No. 4, Cerchiara No. 7, Cretara, Le Grotte, San Nicola and Temperino. The tested stock belongs to the part of the motorway facing the Adriatic side of the Appenines. All the bridges' spans have the same design and are nominally identical: the concrete girders have a trapezoidal cross-section, 2.3m high with two cantilevered wings 3.85m wide, see Fig. 12, prestressed by bonded post-tensioned tendons. The are two types of bearings supporting the girder: rack and roller supports, or pot rubber bearings. A pair of piers, whose centre distance is about 40 m, sustains each bridge span. The concrete piers have a hollow cross-section, reinforced at their corners.

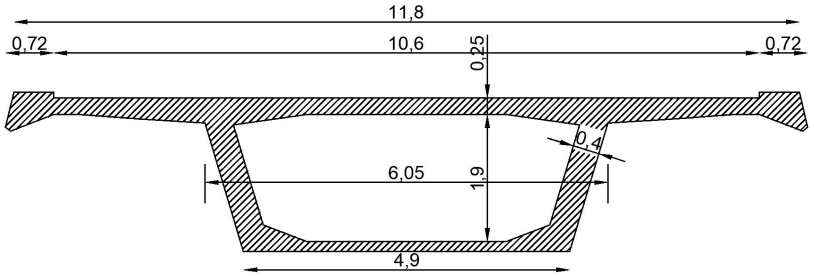

Fig. 12. Cross-section

The notorious L'Aquila earthquake of 2009 caused damages to some girders due to the excessive slipping of the supports. This induced the managing body to install anti-sliding devices, which consist of a steel frame around the original supports 2-5 mm below the underside of the deck, to all girders with rack and roller supports.

The AVT were conducted with ten force balanced accelerometers arranged on two lines in correspondence with the inclined webs of the box girder. The first two and the last two accelerometers were placed close to the expansion joint to investigate the response of the bearings. The tests were carried out under similar environmental

conditions so that the influence of temperature and humidity on modal parameters can be considered negligible. The testing days were sunny and the temperature was on average 15°C. The time series is about 40 minutes long. The processing of the acquired data allowed to identify at least three modes in the bandwidth $0-10Hz$ for all the bridges: a bending mode at nearly $2.5Hz$, a torsional mode at almost $6Hz$ and a second torsional mode at approximately $8.5Hz$.

Even though the bridges are identical in design, they manifested a varied dynamic response, imputable to several factors. Some discrepancies may originate from when the bridges were constructed, due to geometrical irregularities and unlike concrete curing. Others may descend from the time-degradation, soil-substructures interactions and other modifications in the boundary restraints, like the substitution of the original rack and roller bearings with multi-directional pots. The first bending mode shapes are negligibly affected by the specific bearing, and the corresponding natural frequencies have a marked dependence on the values of the MoE, obtained from static load tests and tests on the concrete samples. The Least-Squares fit, see Fig. 13a, between the results from static load tests and the first natural frequency matches with the expression of a simply-supported beam model in Equation (108). Equation (108) presents the expression of the natural frequency of the first bending mode and that of the two torsional frequencies corresponding to the first two torsional modes with extreme rotation prevented.

$$f_{1,theor.} = \frac{\pi}{2l^2}\sqrt{\frac{EI}{m}}\ f_{2,theor.} = \frac{1}{2l}\sqrt{\frac{GJ}{I_\alpha}}\ f_{3,theor.} = \frac{1}{l}\sqrt{\frac{GJ}{I_\alpha}} \tag{108}$$

On the other side, the second mode shape, which is mainly torsional, is likely to be more sensitive to the bearing's state of preservation. This fact induced Aloisio [49] to endeavour to estimate the values of two equivalent torsional springs representative of the actual restraint conditions. He exploited the detected discrepancies between analytical and experimental mode shapes and estimated the equivalent torsional spring yielding the maximum correlation between the modes. The analytical mode shape is the solution of the equation of motion for free torsional vibration, with warping stiffness and warping inertia both neglected. The obtained values reported as the ratio between torsional stiffness of the boundary spring and the torsional stiffness of the beam cross-section yield the estimate of the vertical restraint offered by the two different typologies of bearings [49]. This observation corroborates the fact that an inspection of the mode shapes from a dynamic test can yield very useful information.

Among the bridge population under consideration, Le Grotte and Temperino bridges present higher MoEs, but lower frequencies. The MoEs from static load tests are likely representative of the actual moduli, and other phenomena, not related to the quality of

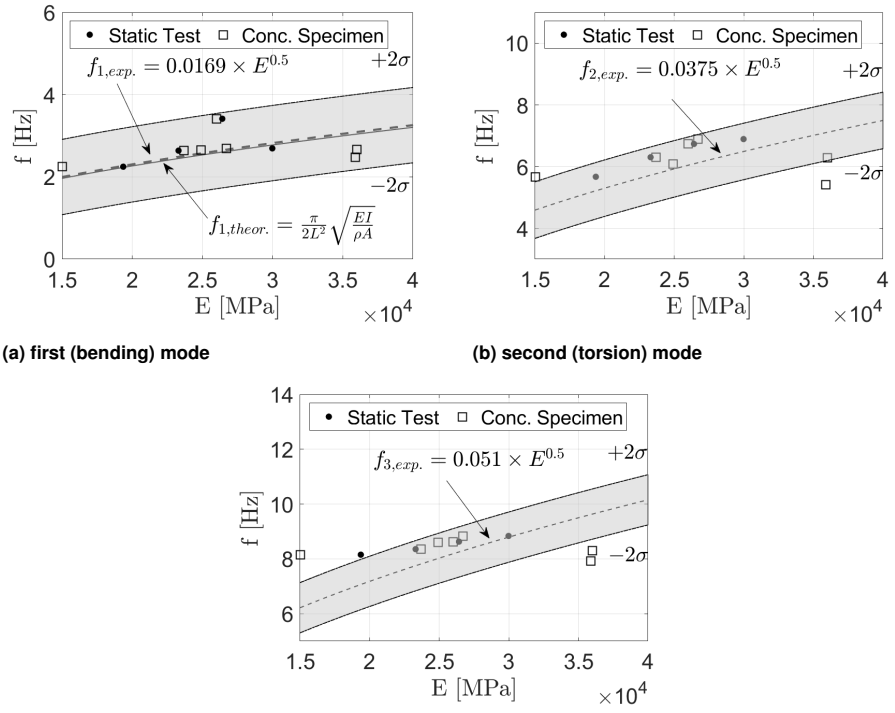

(a) first (bending) mode

(b) second (torsion) mode

(c) third (torsion) mode

Fig. 13. Correlation between the elastic modulus and the natural frequencies of the first three modes. The dashed lines indicate the interpolation curves; The solid lines the theoretical predictions according to Equation (108). The grey region indicates the confidence bounds ($+2\sigma/-2\sigma$) of the Least Squares fit.

concrete, may have lowered the identified natural frequencies. This observation supports the need for probabilistic rather than deterministic models when assessing the MoE from the natural frequencies. The outcomes of dynamic identification can properly drive probabilistic, not deterministic, inferences about the state of the bridge, which could be improved by additional information about the bridge, possibly using Bayesian updating methods. The prediction of the two torsional frequencies is widely inaccurate. For this reason, the authors did not report the curve derived from Equation 108, which stands far beyond the experimental findings. The analytical prediction largely overestimates the natural frequencies: in the considered cases, the bearings are deformable and allow significant rotation, as already discussed [49].

At this point the authors attempted to deliver a Bayesian updating method for the probabilistic assessment of the concrete's MoE values. A common interpretation of

Bayes's theorem is that it gives us a way to update the probability of a hypothesis, H, in light of some body of data, D [51]. Bayes's theorem, in its general form and in the one adopted in this application, can be written as:

$$P(H|D) = \frac{P(D|H)P(H)}{P(D)}; \quad P(E < \hat{E}|f < \hat{f}) = \frac{P(f < \hat{f}|E < \hat{E})}{P(f < \hat{f})} P(E < \hat{E}) \quad (109)$$

where:

- $P(H)$ is the probability of the hypothesis before we see the data, called the prior probability.
- $P(H|D)$ is what we want to compute, the probability of the hypothesis after we see the data, called the posterior.
- $P(D|H)$ is the probability of the data under the hypothesis, called the likelihood.
- $P(D)$ is the probability of the data under any hypothesis, called the normalising constant.

In this application $P(E < \hat{E}|f < \hat{f})$ is the posterior probability, i.e. the probability of observing an MoE below a certain treshold, $E < \hat{E}$, if the expected first natural frequency, f, is below the measured one, $\hat{f}$; $P(f < \hat{f}|E < \hat{E})$ is the likelihood distribution; $P(E < \hat{E})$ is the prior; $P(f < \hat{f})$ is the normalising constant.

The authors assumed a normal distribution to describe the statistics of the MoEs and natural frequencies: $P(E) \approx \mathcal{N}(\mu_E, \sigma_E)$, and $P(f) \approx \mathcal{N}(\mu_f, \sigma_f)$, where μ_E, μ_f and σ_E, σ_f are the mean and variance of E and f respectively. The bivariate Normal distribution describes, instead, the likelihood of observing certain natural frequencies given the MoE values: $P(E, f) \approx \mathcal{N}(\{\mu\}, [\Sigma])$, where $\{\mu\}$ and $[\Sigma]$ are:

$$\{\mu\} = \begin{bmatrix} \mu_E \\ \mu_f \end{bmatrix} = \begin{bmatrix} 26885.714 \\ 2.684 \end{bmatrix} \quad (110)$$

$$[\Sigma] = \begin{bmatrix} \sigma_E^2 & \rho\sigma_E\sigma_f \\ \rho\sigma_E\sigma_f & \sigma_f^2 \end{bmatrix} = \begin{bmatrix} 53418095.238 & -966.540 \\ -966.540 & 0.128 \end{bmatrix} \quad (111)$$

Figure 14 represents the density and cumulative probability distributions (PDF, CDF) of $P(E, f) \approx \mathcal{N}(\{\mu\}, [\Sigma])$. The dots indicate the experimental couples (E-f).

Assuming some threshold values, Equation (109) can then be used to calculate the posterior probability by varying both $\hat{E}$ and $\hat{f}$. The resulting contour plot, derived from the Bayesian updating of the probability distribution in Figure 14b, is displayed in Figure 15a. Figure 15a reveals the probability of observing MoEs lower than the

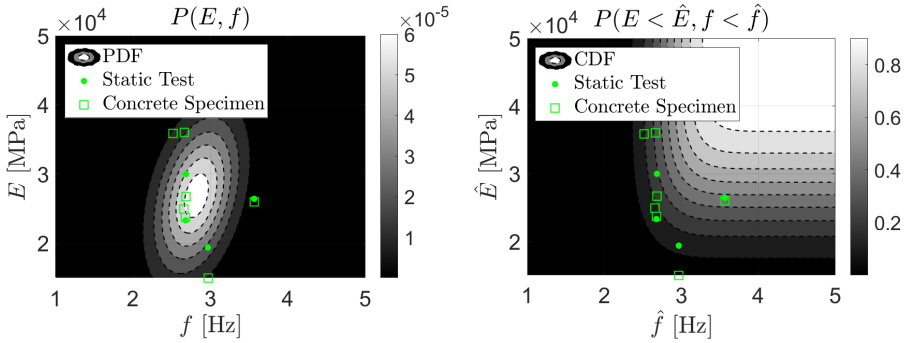

(a) Bivariate normal density distribution **(b) Bivariate cumulative distribution**

Fig. 14. Distributions of the elastic moduli and natural frequencies of the first bending modes.

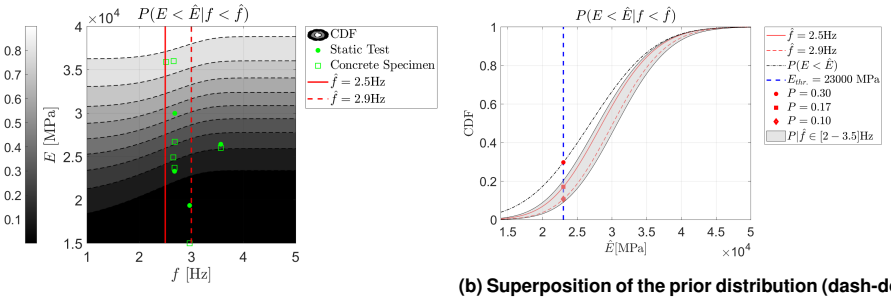

(a) Posterior distribution **(b) Superposition of the prior distribution (dash-dot) and two section cuts of the posterior in (a)**

Fig. 15. Results of the Bayesian updating.

threshold $\hat{E}$, given natural frequencies below a specific threshold $\hat{f}$. Thus, Figure 15a must be interpreted through section-cuts, as shown in Figure 15b. For this reason, the CDF approaches one for every value of the natural frequency, while the CDF in Figure 14b reaches one only when both thresholds of the MoE and natural frequency raise. It is worth to notice in Figure 15a, the stationary behaviour of the posterior probabilities for frequency values below $2Hz$ and exceeding $4Hz$, also depicted in Figure 15b by the grey shaded area. Specifically, the authors represented two sample cases: the probabilities of observing MoE given estimated frequencies, $\hat{f}$, below $2.5Hz$ and $2.9Hz$, indicated by the red solid and dashed line, respectively in Figure 15a. The black dash-dot line, in Figure 15b, on the other hand, represents the CDF of the prior probability $P(E < \hat{E})$. In the considered case, the experimental evidence, given by the estimated frequencies, always yields a probability reduction. Assuming a specific threshold $\hat{E} = 23000\,MPa$, indicated by the blue vertical dashed line in Figure 15b. The probability of observing $E < 23000\,MPa$ is 0.3. The estimation of a natural frequency below $2.5\,Hz$ determines

a decrease to 0.17, i.e. the inspector would obtain a lower probability of observing $E < 23000\,MPa$. If the natural frequency stands below $2.9\,Hz$, the probability would further reduce to 0.10.

In conclusion, dynamic identification provides useful information; Specifically, the case study enlightened two aspects: the inspection of the mode shapes returns knowledge about potential malfunctioning of the bearings, and the natural frequency of the first bending is correlated to the MoE value. This latter evidence drove the authors to develop a reliability-based estimation of the MoE in the context of maintenance plans. The first step involves an experimental campaign: the dynamic identification of the entire bridge stock. The controller must examine the resulting mode shapes to evidence possible anomalies, which would require more in-depth investigations. If no abnormalities emerge, the inspector must define a threshold for the MoE and estimate the posterior probability of observing MoEs higher than the limit, given the estimated frequency value. If the probability surpasses the accepted reliability threshold, the bridge span could be declared as verified. If not, further investigations, like tests on concrete specimens, must guide a careful decision-making process. The presented method might be elementary, but it attempts to comfortably include NDE techniques in the world of maintenance, which lacks the regular presence of dynamic identification in the decision-making process.

Recent years have evidenced a worrying state of deterioration of existing bridges in Italy. There is a widespread lack of knowledge about these structures due to the absence of historical project documentation, the lack of inspections on a timely basis and the need for ordinary and extraordinary maintenance interventions. Currently visual inspection activities are the only assessment methods in most parts of the country. These methods, although essential to estimate a bridge's state of deterioration, could and should be completed by the undoubtedly more objective data coming from systematic dynamic tests. This would guarantee a greater control over the structural materials' durability. Needless to say, the managing bodies need to be more rigorous in the follow-up of the ordinary maintenance interventions, if tragedies like the one in Genoa are to be avoided.

3.3 The Palisaden CLT building case of study

Even though the popularity of timber structures has grown a lot during recent years, the engineering knowledge concerning the dynamic behaviour of tall timber buildings is still limited. In taller, more slender and flexible timber buildings, serviceability considerations associated with lateral movement assume increased importance compared to low-rise buildings, where strength is usually the governing design criterion. For instance, the wind imposed forces on a tall and slender building, while they may not damage any structural element, may cause deformation or vibration in the building which could cause discomfort to occupants, damage non-structural elements, or otherwise prevent the normal operation of the building [52].

Both recent technological developments and increased use of engineered wood products reflect in deficiency of current timber codes and lack of knowledge by professional engineers. As engineers strive to take multi-storey timber buildings to new heights, it is necessary to understand how existing buildings, and current construction systems, are behaving in-service, and how their performance relates to what predicted at the design stage [53].

Probably the first ambient vibration tests (AVT) on a timber-frame building was performed by Ellis and Bougard [54]. The tests were conducted on a full-size, six-storey timber framed structure constructed inside BRE's Cardington laboratory. They performed both Forced Vibration Tests (FVT) and AVT at different stages of construction, which allowed to evaluate the contribution to the global stiffness of the timber frame alone, the contribution of the staircase, and that of the finishing and cladding (bricks). The AVT were performed using a long-range laser interferometer developed for measuring vibrations in-line with the laser beam [54], and the modal properties were extracted through the peak picking (PP) method. The results of their research indicates that the building's non-structural components play a large role in the contribution to the lateral stiffness of the building at service levels.

More recently, some other researcher have attempted to extract the modal properties of mid-rise timber buildings [53, 52, 55, 56] using OMA methods. The research conducted by T. Reynolds and colleagues constitutes probably the largest database of AVT performed on timber structures in Europe to date. They tested different types of timber structural archetype: post and beam, timber-framed, pure CLT and hybrid timber-concrete structures. For most of the buildings tested the random decrement (RD) technique was used to extract the autocorrelation function, then the Ibrahim Time Domain (ITD) method was used to extract modal parameters from the set of random decrement signatures. It is also worth to mention the tests performed in Germany and

Austria on eight timber observation towers (with a height up to 45m), a 100m tall wind turbine and on three multi-storey residential timber buildings (with a height up to 26m) [56]. The findings of all these testing campaigns have allowed to assess the simplified relationship between height and natural frequency for multi-storey buildings given in Eurocode 1 [57]. The 14-storey, 50m tall, Treet building in Bergen, already tested by Reynolds, has also been re-tested by two students from NTNU in their master thesis [58]. Along with Treet they also tested a 9-storey CLT building in Trondheim, where the ground floor is made of concrete and the superstructure of CLT panels.

In North-America, where there is a great tradition in wooden frame housing, efforts have been made to understand the dynamic behaviour of smaller low-rise residential buildings [59, 60]. These researches, which performed both AVT and FVT using shake-table testing, highlighted the highly non-linear response of timber framed shear-walls to the amplitude of the excitation and motion induced by FVT. More recently, in Canada, researchers from FPI innovation [61, 62], and in the U.S., researchers from Oregon University [63], have tested multy-storey residential and commercial timber structures, up to six storey, using OMA methods.

The results of these campaigns have shed some light on the dynamic behaviour of tall timber buildings providing viable information concerning stiffness and damping of the tested structures to designers and stakeholders. However, in order to support the current growing trend of larger, taller and more complex timber buildings, not only an update of the building codes is needed (and of course a higher volume of engineered wood products production), but also skilled carpenters, tradespeople and designers with proper education and training on timber constructions. Thus, also regulation and guidelines in the area of execution and construction supervision of timber buildings should be improved [64]. Interviews, conducted during autumn 2014 by I. Edskar [65], with structural engineers/designers, suppliers, and development managers in Scandinavia, highlighted a need to raise the awareness towards the both the limits and potentials of mid- and high-rise buildings made with engineered wood products, especially in relation to their dynamic behaviour and serviceability limit states.

To help filling this gap in knowledge, the authors present the dynamic identification of an eight-storey CLT building with a CLT core. The estimate of the modal parameters of multi-storey CLT buildings' response under operational conditions from in situ tests is useful to understand the gap between the possibly linear dynamic response to service loading and nonlinear behaviour under seismic excitation. The main objectives of the presented research were: (i) the estimation of the modal parameters of an eight-storey CLT building from Output-Only dynamic identification; (ii) the updating of

an elementary analytical model of the building to the experimental modal parameters; (iii) the assessment of the role of the connection non-linearity on the building's dynamic response in operational conditions; (iv) the derivation of simplified and practice-oriented correlations useful for the assessment of natural frequencies of CLT buildings at a low-level response.

On October 25, 2019, the authors tested a student housing building located in the NMBU campus, in Ås, Norway, Fig.16.

Fig. 16. Location and views of Palisaden building.

The building has eight storeys with a total height of 26.9 m and is rectangular in plan (23.21 m × 15.11 m), with a CLT core at the centre. The structure is built using a platform frame approach, meaning that walls are erected and braced, before floor panels are lowered onto them and fixed. A plan view of the building is shown in Fig. 17. The CLT wall panels are monolithic (doors and windows opening have been cut off in the

factory), with quite high length-to-height ratios. Only the designated shear walls in the longitudinal and transverse directions are connected (to each other and to the floor elements) with hold-down/tie-downs, shear connectors and self-tapping screws, whereas the other panels (both for internal partition and external envelope) are connected only with self-tapping screws. The thickness of the wall panels is reduced with the height of the building, as is commonly done to reduce the total weight of a building. The main characteristics of the building are summed up in Table 4.

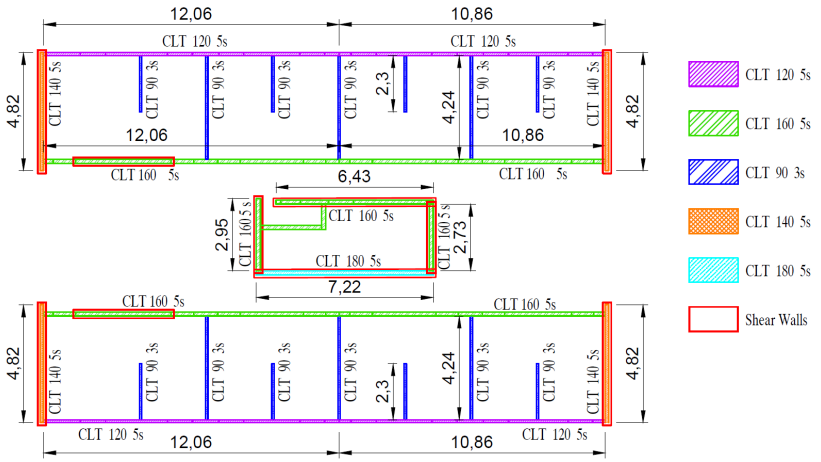

Fig. 17. Plan view of the building.

The processing of the acquired data permitted to clearly identify the first three natural frequencies of the building, as evidenced in Fig. 18, where the Singular Values plot of the PSD matrix is shown beside the stabilisation diagram returned by SSIcov algorithm. The first two modes are translational: the very first, Fig. 19a(a), is a translation parallel to the direction of minor inertia of the building; the second mode is a translation in the orthogonal direction, Fig. 19b(b); the third mode is the first torsional mode, Fig. 19c(c). The results in terms of frequencies and damping ratios are summarised in the caption of Fig. 19.

A simple 3D numerical model of the structure was then built to further investigate the results of the AVT. Given the high values of the experimental eigenfrequencies, and the considerable in-plane stiffness of the CLT floors, it was decided to consider all the walls of the building, not only the designated shear-walls, and to use a shear-type behaviour for the model. The equations of motion of a generic 2D storey were derived, then the resulting mass and stiffness matrices were assembled into the mass and stiffness matrices of the whole structure. The compatibility equations were written assuming the

Table 4. Basic characteristics of the tested building [66].

Parameter	Value	Unit
Lenght	23.21	m
Width	15.11	m
Height	26.9	m
No. of floors	8	
Rooms	127	
Net area /floor	350.55	m^2
Net area /building	2804.4	m^2
CLT wall panels	3 layers-90	mm
	5 layers-100,120,130,	
	140,160,180	mm
CLT floor panels	5 layers-180,220	mm
CLT roof panels	5 layers-200	mm
Wood amount-total	907.62	m^3
Hold-downs steel plates	6225.73	Kg
Shear steel plates	1919	Kg
Self-tapping screws	6124	
Steel brackets	≈390	

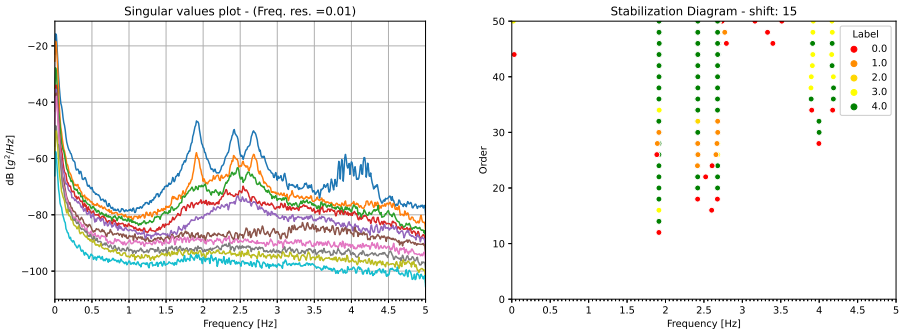

(a) SVP of the PSD matrix **(b) Stabilisation diagram from SSIcov**

Fig. 18. Results of the dynamic identification

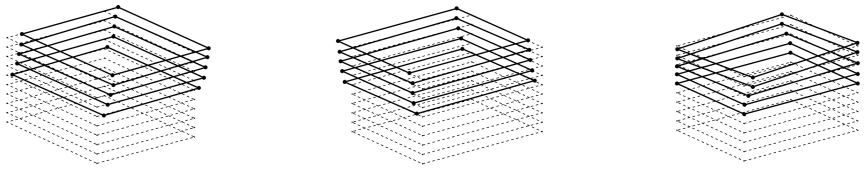

(a) $f_1 = 1.913[Hz]$; $\xi_1 = 1.216\%$ **(b)** $f_2 = 2.414[Hz]$; $\xi_2 = 1.916\%$ **(c)** $f_3 = 2.688[Hz]$; $\xi_3 = 1.921\%$

Fig. 19. Natural frequencies, damping factors and mode shapes of the three stable modes

diaphragm-like behaviour of each floor, while the constitutive equations were based on the estimation of two shear stiffness values in the x and y directions concentrated in the centre of mass of each wall. The computation of the equivalent rigidity of the CLT walls was based on the longitudinal and shear elastic moduli of the CLT, assuming the connections (Hold-downs and angle brackets) as infinitely rigid. The bending stiffness was calculated considering only the vertical layers and an equivalent shear modulus takes into account the torsional deformation of the lamellae. Specifically, both the shear and the bending deformation of the walls were taken into account:

$$k_{CLT} = \left(\frac{h^3}{12\,EI} + \frac{1.2h}{GA} \right)^{-1} \tag{112}$$

where h is the inter-storey height, E the Elastic modulus, G the shear modulus and A the cross sectional area of the wall. The natural frequency and mode shapes were then calculated solving the eigenvalue problem. The complete description of the model, comprising equilibrium, constitutive and compatibility equations, is given in the appended paper.

In order to assess the role of the connections, taking into account the results from the AVT, an updating routine was applied to the model. To find the optimal parameters, a cost function that measures the differences in terms of frequencies and of mode shapes was minimised:

$$C = \sum_{i=1}^{M} \gamma_i \left(\frac{f_i^m - f_i^c}{f_i^m} \right)^2 + \sum_{i=1}^{M} \beta_i \left(1 - MAC(\Phi_i^m, \Phi_i^c)\right) \tag{113}$$

where the apex $()^m$ indicates a measured variable, the apex $(*)^c$ a calculated variable, f_i is the i^{th} natural frequency, Φ_i is the mode shape vector, M is the number of modes, MAC is the Modal Assurance Criterion, while γ_i and β_i are weighting factors.

The optimisation of both stiffness and mass, based on the natural frequencies and unscaled mode shapes, may stand as an undetermined problem since the eigenfrequencies depend on the ratio between rigidity and weight. Theoretically, infinite couples of rigidity and weight values could be possible candidates for the optimisation. To reduce the number of unknowns, the mass of the storeys and of the roof were the assumed unknown variables. The authors estimated the minimum of the objective function by evaluating it on a discretised domain with a 0.1 KN step. The contour plot of the objective function is shown in Fig. 20.

Operating in this way allowed to evaluate the validity of the modelling hypotheses using and indirect approach. The indirect method derives from proving hypothesis through tests. Let us assume a continuum-like behaviour of the building (hypothesis): the connections are neglected in the model updating process (test). If the updated masses

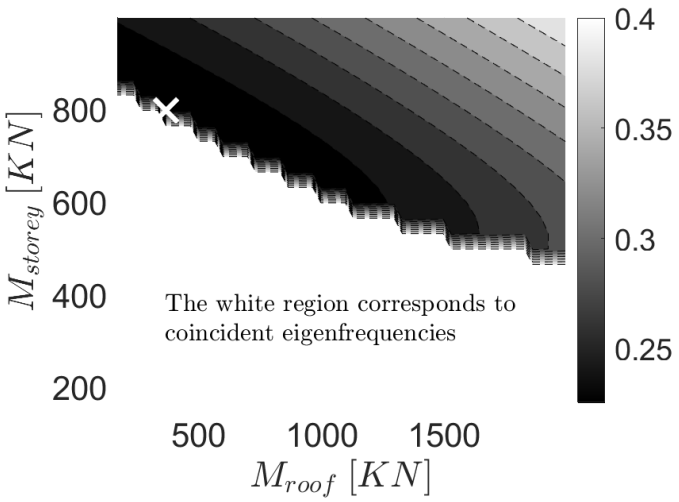

Fig. 20. Contour plot of the objective function.

match with the expected ones, the hypothesis is proven (proof). The results of the updated mass are summarised in Tab. 5, while a comparison between the experimental and the numerical modal parameters are reported in Tab. 6. It should be noted that the diaphragm behaviour of the floor panels (and thus shear-type rather than the cantilevered model) could have been more rigorously assessed taking also measurements in the out-of-plane direction of the floor.

Table 5. Weight values estimated from updating.

Description	*kN*	kN/m^2
Roof	365.6	1.042
j-th storey	797.7	2.275
Self Weight of the j-th storey	350.7	1.000
Variable and permanent of the roof	14.9	0.042
Variable and permanent load of the j-th floor	447.0	1.275

Since the self-weight contribution to the total mass of a storey is known, subtracting this part from the values found by the optimisation should yield the variable and permanent portion of the load. As it is shown in Tab. 5 this yields an estimated variable and permanent load of $1.275 kN/m^2$ to the generic storey and an almost negligible one to the roof. These indeed seem to be reasonable values since, during the tests, the building was fully furnished and in use, and since the only extra load on the roof was coming

Table 6. Comparison between the experimental and numerical modal parameters.

	Experimental		Numerical	
Mode shapes	$f[Hz]$	$\xi[\%]$	$f[Hz]$	*MAC*
1st translational mode	1.913	1.216	1.867	0.99
2nd translational mode	2.414	1.916	2.543	0.98
1st torsional mode	2.693	1.921	2.712	0.92

from the ventilation system. Furthermore, comparing the measured natural frequencies, and mode shapes, with those from the updated numerical model, the good match is pretty evident (see Tab. 6).

The results seem to confirm that the connections do not significantly contribute to the low-amplitude dynamics of mid-rise CLT buildings, and that the panels behave elastically as continuous elements. However, it is possible that a CLT building may exhibit a non-linear behaviour, with possibly important frequency shifts, even at low-level dynamics. This fact could be easily estimated from continuous monitoring under different operational conditions (e.g. wind speed).

Several building codes allow to perform a simplified static seismic analysis if the structure of interest complies with some limitations (e.g. on the maximum height, on the structural regularity in plan or height, etc.); in these cases only the first mode of the structure is considered and the seismic base shear force will be proportional to the ordinate of the design response spectrum (at the specified period), and needless to say to the mass of the building. To estimate the first natural period, T_1 (i.e. $1/f_1$), the following equation is used:

$$T_1 = C_1 H^{\frac{3}{4}} \tag{114}$$

where C_1 is a constant that depends on the typology of the building (e.g. steel framework, RC framework, etc.). The authors therefore compared the results of the measured first natural frequency to the simplified equation (114), available in ASCE 7-16 [67] and in the former Italian building code NTC08 [68]. Interestingly, it turned out that the C_1 found is very close to the one adopted for masonry structures by the two codes, and this might be due to the sharing of a wall-based, box-type structural layout in both typologies.

3.4 Tests in laboratory

Beside the relatively new and barely explored problem of assessing the dynamic behaviour of taller timber buildings, a much more known, dynamic related, issue is the assessment of the vibration performance of timber floors. This serviceability issue is, most of the time, related to the perception of annoying oscillations, caused by the transmission through the floor of walking-induced vibrations, prompted by the users of the building. The "live" feel of timber floors is familiar to many, especially to those living in single family housing with timber framework. However, this problem is not limited to timber-framed residential buildings, since even in those countries where masonry buildings are common, floor systems are very often constructed with timber floor joists. A considerable amount of research works have been carried out concerning the assessment of the dynamical properties of timber floors, especially in northern Europe and North-America, where timber flooring systems are very common. However, new construction practices have had a profound impact on the dynamic characteristic of some timber floors. Unfortunately, the trend of seeking large, open-spaced, architectural layouts, that favour the needs of commercial buildings, obviously does anything but help in enhancing the performance. For these reasons the assessment of the dynamical performance, and ability to predict the behaviour of flooring systems, remains still a particularly topical subject.

As already mentioned, the most common source of excitation on floors is human activities such as walking, running or jumping. Except from the activity, the force from a step also depends on the characteristic of the person (weight and walking style) and the floor characteristics. It has been observed that the range of possible walking frequency is $1.5-2.5\,Hz$ [69]. The dynamic force from walking has been found to excite frequencies up to the fourth harmonic of the walking frequency, and sometimes even higher [70, 71, 72]. The shape of force-time history of a single step presents two peaks that correspond to the contact force caused by the heel impact and the push-off by the toes, respectively. A very thorough review on experimental identification and analytical modelling of human walking forces can be found in [73]. Evidence has shown that depending on the value of the fundamental natural frequency of a floor, the response to forces from walking will differ. Low-frequency floors with natural frequencies below $8-10\,Hz$, that coincide with the harmonics of walking frequency, have been found to respond to walking excitation with resonant vibrations. The amplitudes will build up and the resulting vibration will be dominated by the natural frequency of the floor that is excited the most by the walking frequency and its harmonics [74]. On the other hand, in high-frequency floors, with natural frequencies above $8-10\,Hz$, the response is not

influenced by the walking frequency and its harmonics, but is dominated by a train of impulses, which correspond to the heel impacts of the walker [74].

Another important aspect is the human sensitivity to vibrations, numerous efforts have been made to identify factors affecting human response to vibrations, which are reflected in several international standards [75, 76, 77, 78]. Besides the vibrations felt by our body, vibrations may also be perceived as visual effects or audible sounds made by moving objects [79]. Moreover the degree of annoyance depends on the activity carried out by the person that is disturbed and his or her relation to the source of disturbance e.g. if the person is moving, resting or reading, or if the disturbance is caused by a known source or by an unknown source.

For many years, limiting static deflection to a proportion of the span has been a spread safeguard against most of serviceability aspects of floors, including vibration serviceability. However, predicting the behaviour of a timber floor is not an easy task, and using prescriptive construction practices or simple engineering design methods often yields inaccurate result. Over the years several studies have investigated the correlation of satisfaction ratings to quantitative measurements, that can be estimated with simple formulations, such as static deflection under gravity load and first natural frequency [80, 81, 82, 79]. For instance the vibration performance design of timber floors according to EC5 is largely based on the results of the findings of Ohlsson [83, 84, 85]. The guidelines applies for floors that have a fundamental natural frequency higher than $8\,Hz$, to avoid resonant situations. The designer must first check the instantaneous vertical deflection caused by a vertical concentrated force, and then check the impulse velocity response corresponding to the maximum initial value of the vertical floor vibration velocity caused by a unit impulse of $1Ns$. The impulse velocity response also takes into account the presence of higher order modes in the bandwidth of interest (i.e $< 40\,Hz$) [84, 86]. However, numerous different national application rules for the EC5 exist [87].

More advanced guidelines are the one published by The Concrete Center and developed by Arup [88], and the one from the Steel Construction Institute [74]. The guidelines present refined methods for evaluating the walking induced vibrations caused by pedestrians where the design parameters are the (frequency weighted) root mean square (rms) acceleration and the Vibration Dose Value (VDV). The latter parameter is based on the fourth power of the acceleration and accounts for the duration of vibration and how often it occurs. Both methods are based on modal analysis and have been calibrated and refined with verification measurements taken on completed structures over several years.

Unfortunately, an universal agreement on acceptance levels and design procedures has not been achieved, and there is still need for appropriate engineering code and

standard provisions. Moreover, vibration serviceability of timber floors continues to be a very relevant topic and efforts are in progress within the European Committee for Normalisation (CEN) to update code methods and testing standards. Modal testing has been a popular approach to assess the modal properties of timber floors over the years, and recently a new document that specifies test methods for the determination of natural frequencies, damping, unit point load deflection and acceleration of timber floors has been released in Europe [89]. Forced vibration tests are the only ones referenced in the standard, however the refinement and consolidation of OMA methods, suggests that AVT could also be used with confidence by engineers both for laboratory tests and in situ tests.

Even if some application of AVT to timber floors can be found in the literature [90, 91, 92], FVT and EMA methods remain the most known and used procedures to estimate modal properties through testing. In order to demonstrate the potential of OMA methods also in laboratory experiments, in the appended paper the authors present the results of a testing campaign on a timber floor. AVT were performed on each of the floor components and on the assembled floor, the results were used as basis for a sensitivity analysis so as to find the best modelling choices. High fidelity FE models were then obtained tuning the numerical models to the experimental results through automated updating procedures suitably programmed by the authors. The research aims at clarifying and discussing the issues related to dynamic testing of timber elements under operational loads in laboratory environment. Furthermore it is shown how the use of "black box" automated optimisation algorithms can yield FE models that better represent the data obtained through testing.

The authors tested a timber floor made by two beams and decking above, see Fig. 21. Firstly, each one of the floor components were tested separately, then the floor was assembled and tested. The two beams are made of Glulam GL30c, they are $5\,m$ long and have a $115\,x\,315\,mm$ cross-section. Both beams presented some defect at delivery: one had two cracks, approximately $15\,cm$ and $20\,cm$ wide, on both faces at one end; while the other had a hole on one face that was filled with silicone. The decking consists of $1.5x1.5m$ sheets, $21\,mm$ thick, made of plywood veneers. The beams were tested both as simply supported and as freely suspended, but due to the laboratory conditions, the free boundary conditions were achieved using a small piece of Rockwool insulation placed under the beams at mid-span. The plywood decking was tested only as freely suspended using the same technique of placing a small piece of Rockwool to support the board at the centre. The floor system was only tested as simply supported. Two metal cylinders, spaced $4.8\,m$, supported each beam, with a $600\,mm$ centre-to-centre distance. The decking of the floor was made of the three square boards, placed one

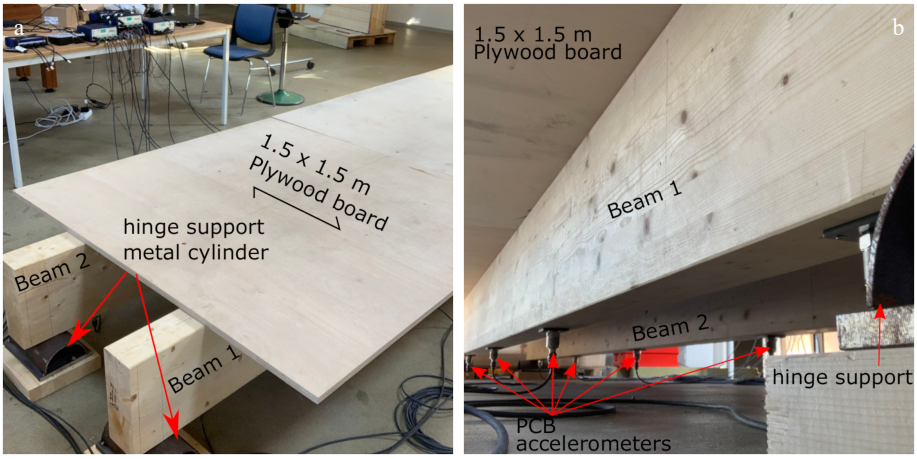

Fig. 21

next to the other. The insertion of connectors, to fix the boards to the beams, would have altered/damaged each component, thus undermining the efforts to identify the dynamics of each of them accurately. Therefore, the authors devised an alternative solution to study the entire structural arrangement without the need for connectors. They placed a reusable putty-like pressure-sensitive adhesive, which guarantees the joint response of the beams and the decking in the vertical direction. Even if in a real building the decking would be fixed to the beams, thus enhancing the composite interaction and the overall stiffness, the floor would also be much thicker and heavier, due to the finishing. The structural assembly does not represent a realistic situation, it is a structural archetype useful for the accurate calibration of simplified models for the prediction of walked-induced vibrations.

Before the testing the authors developed a set of numerical models, with the FE program SAP2000, for each sub-assembly using standardised values for the material properties. These models provided an expected response, which was useful to derive a proper setup and instrumentation plan. Two models reproduced the dynamics of the beams. The former derived from the one-dimensional "Frame elements" based on the Timoshenko beam theory, the latter originated from the use of "Solid elements", which are eight-node elements for modelling three-dimensional structures. The material property was defined as orthotropic to model the glulam. Thin "shell elements" modelled the decking, with the plywood of the boards idealised as an orthotropic material.

The measurement chain was composed by ten seismic ceramic shear piezoelectric accelerometers, an HBM QuantumX data acquisition unit (24-bit analogue-to-digital converter) and a laptop pc. Shielded polyurethane coaxial cables made the connection

between the sensors and the acquisition unit. More information on the measuring chain and on the different test set-up are given in enclosed the paper. The ambient vibrations measurements were then processed and the modal properties extracted using the EFDD and the SSI-cov algorithms. A slight and random brushing was applied to the tested structures using a wooden stick in order to improve the signal-to-noise ratio of the measurements [23]. Interestingly, it was found that exciting the tested structure did undoubtedly help to increase the signal to noise ratio, but it also partially masked the presence of spurious harmonics. As already explained in the background chapter, the structure under test may show dominant frequency components which do not represent natural frequencies but derive from deterministic signals superimposed to the stochastic response (e.g., rotating equipment) and particular attention must be paid in order to identify them.

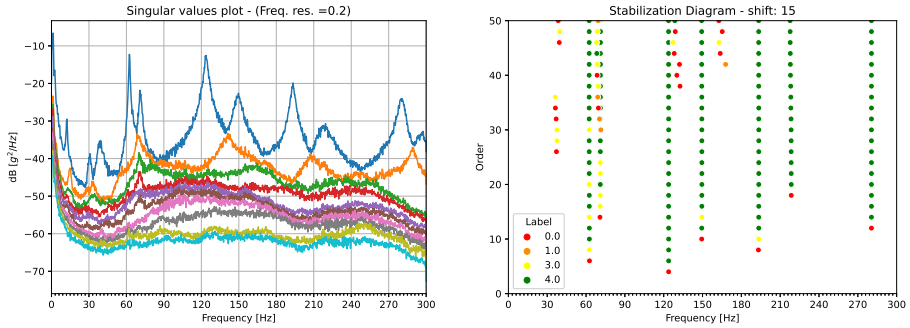

(a) SVP Beam 1 Torsional set-up

(b) Stabilisation diagram Beam 1 Torsional set-up

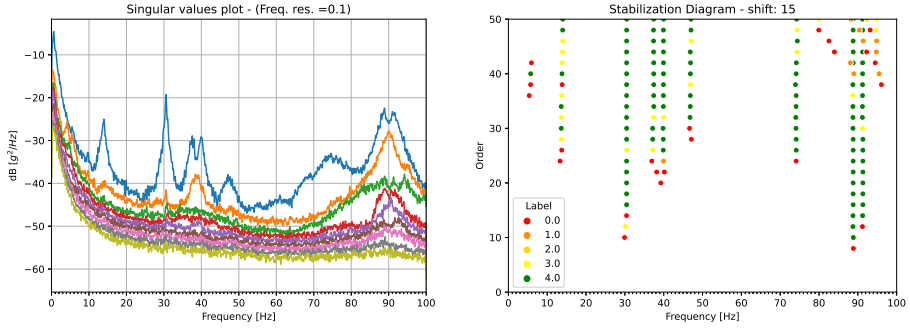

(c) SVP Plywood plate

(d) Stabilisation diagram Plywood plate

Fig. 22. Results of the dynamic identification

The processing of the data yielded very clear PSD plot and stabilisation diagrams, see Fig. 22, and allowed to extract useful information regarding the modal properties of

both the single components and the floor assembly. Namely: ten modes were identified with the free-free test of the beams, and three with the pin-pin test; seven modes from the testing of the plywood board; and two modes (in the bandwidth $0-40\,Hz$) from the floor assembly. More information regarding the estimated results can be found in the enclosed paper. It is worthwhile to point out that the higher bending mode shape were increasingly sensitive to damages, only when the beams were tested as simply supported. The damage locations are quite evident, especially in the third bending mode shape of the simply supported beam. On the other hand the effects of the damages were not detectable when the beams were tested under free-free boundary conditions. The results of the simply supported beam and those of the floor system were also compared with the results of the analytical solution of the Euler-Bernoulli beam model, which constitutes the basis for the simplified calculation formulas of building codes.

After the identification phase, the authors used SAP2000 Open Application Programming Interface (OAPI) in combination with the open-source programming language Python to develop the routines for the automatic sensitivity analysis and model updating. The OAPI allows third-party products, like Python, to interact with SAP2000, allowing the users to create custom applications. Firstly, a Sobol sensitivity analysis [93] evidenced the role of each term of the flexibility matrix of an orthotropic finite element. Namely, the analysis returned the sensitivity indices of the three MoE, E_X E_Y E_Z, the three Shear Moduli, G_{XY} G_{XZ} G_{YZ}, and three Poisson's ratios, ν_{YX} ν_{ZX} ν_{ZY} on the output (modal properties). Then, the FE models were tuned to better reflect the measured data using two global optimization algorithms for "black box" functions, the Differential Evolution (DE) [94] and the Particle Swarm Optimization (PSO)[95]. The script for the model updating process was written in Python using SAP2000 OAPI along with the Python module PySwarms [96] (to run PSO), and the popular Python toolkit SciPy [97](to run DE). The same cost function as the one used in Paper III is used to find the optimal parameters 113.

Both the sensitivity analysis and the model updating process confirm that the simple beam model predicts very well the dynamic behaviour of slender elements such as glulam beams. Moreover, the sensitivity analysis shows that the most significant material properties for such structural elements are the MoE along the fiber direction and the shear modulus for the strong axis of the cross-section. Even though numerical models should be as representative of the real structure as possible, in this case the use of solid elements has proved not to be worth the much greater computational time. Once all the single structural elements had been updated, the model of the assembled floor was built. It was quickly found that to get modal properties comparable with those from the tests, the model detailing needed to be high: for example, the decking's boards were modelled

separately with a little gap in between them, and their plane was "lifted" with respect to the one identified by the beams' axes. The final model of the floor was obtained by also updating the stiffness of the springs representing the metal cylinder support.

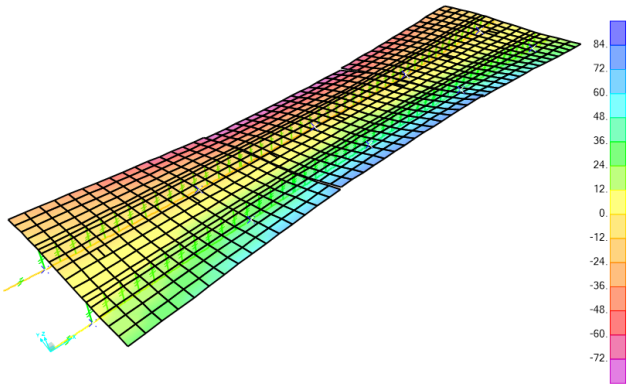

(a) Floor Mode I

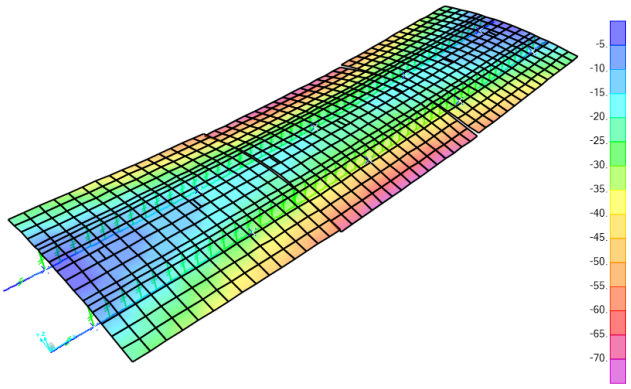

(b) Floor Mode II

Fig. 23. Finite element mode shapes

As shown by other researchers [98] predicting the dynamic response of complicated substructures as floor systems is often beyond the capabilities of traditional engineering

approaches. Also in this case the discussed findings weigh against the applicability of simplified design practices reported in building codes. Only very detailed FE models seem able to predict fairly well the behaviour of their real counterparts. Even though simplified approaches are very useful at preliminary project phases, they become unreliable if a higher performance of the floor is desired. Today's engineers have however "new weapons" in their repertoire: modal testing based on ambient vibrations, automatic model updating algorithms, sensitivity analysis methods, and other techniques, are all valuable aids in the difficult task of creating representative models of the studied structure.

4 Conclusions

This thesis discusses and reports various methods of Operational Modal Analysis. It presents an open-source Python module that allows to perform two of the most widely used output-only dynamic identification techniques. Furthermore it presents and discusses the application of OMA methods to three case studies, highlighting the usefulness and potential of such methods.

The Python module consists of a set of functions that allows to quickly and easily perform OMA on output-only data. The programming language Python was chosen because of its high versatility, ease of use and because it is a free-software license. The module is hosted on a public repository on the popular provider GitHub, under a GNU license. The author hopes in this way to attract other individuals interested in the topic and willing to help in further developing the module. The ambition is to provide a comprehensive set of tools to help researchers analysing ambient vibration data sets. The author has already started to implement two other identification procedures: poly-reference least square complex frequency algorithm (p-LSCF, also known under the commercial name PolyMAX) and second order blind identification algorithm (SOBI). Furthermore, he wishes to achieve a natural development of the module, extending its capabilities to continuous monitoring applications. The very first step to reach this goal has already been taken, with the implementation of an automated version of the SSI-cov algorithm, however there is still a long way to go.

When it comes to the findings of the research, the studied cases prove that AVT and OMA are effective tools for the identification of the dynamic characteristics of the tested object, provided that an appropriate (capable of capturing the "interesting" dynamics embedded in the noise) acquisition chain is used in the tests. In addition, the work shows that the results of such tests may be used in multiple useful ways.

Specifically, the A24 motorway case study reveals two aspects: the inspection of the mode shapes may be used as an indicator for potential malfunctioning of the bearings, and the natural frequency of the first bending is correlated to the modulus of elasticity. This latter evidence encouraged the authors to develop a reliability-based procedure to estimate the module of elasticity of short span pre-stressed concrete bridges, in the context of maintenance plans. The presented method might be elementary, but it attempts to include non-destructive techniques in maintenance procedures, which currently lack the regular presence of dynamic identification in the decision-making process. In

fact, visual inspection activities are the only assessment methods adopted currently in most parts of Italy. These methods, although essential to estimate a bridge's state of deterioration, could and should be completed with the undoubtedly more objective data coming from systematic dynamic tests. This would guarantee a greater control over the structural materials' durability.

Dynamic tests were also performed on an eight-storey CLT building in Norway. To this date very few research works treating AVT and OMA applied to mid- and high-rise timber buildings can be found in the literature, thus the presented work proposes to add some knowledge to this subject. A simplified analytical model was constructed to test different modelling assumptions. The research found that, at least for low amplitude of vibrations, the connections between the panels do not show a significant influence on the response of the building, so that the panels can be considered as continuous elements; furthermore, a shear-type behaviour of the building, with the floor panels acting as rigid diaphragms, describes in a better way the obtained results from the output-only tests than a cantilever behaviour. In order to test the hypotheses on the stiffness, an indirect approach was followed: the conclusions were drawn from an updating procedure on the building's masses instead of the stiffness. However, to better understand the contribution of the connections to the global dynamics, a continuous monitoring of a CLT building would be of great help. In this way the response of the building to different levels of excitation will allow to ascertain if higher amplitude vibrations result in an activation of the connections, with a consequent frequency shift of the modes. Moreover, the research found that the first eigenfrequency matches well with that estimated from empirical relations tuned to masonry structures: this may be due to the shear wall-based construction typology, recurring in both masonry and CLT structures.

Finally, some AVT were conducted in a laboratory controlled environment, on smaller timber structural components, to investigate the potential of OMA methods as a cheaper replacement to traditional input-output techniques. Two glulam beams and a plywood board were tested first separately and then assembled into a lightweight floor system. Furthermore, the influence of the boundary condition was also studied. The results from the ambient vibration testing were used to perform a sensitivity analysis on the numerical models. Not surprisingly, it was found that for the beams the longitudinal module of elasticity is the most important parameter, followed by the shear modulus along the strong axis. Since all the other parameters are almost negligible, there is no point in using other elements than the standard "frame element" to model glulam beams, despite wood's orthotropic nature. The numerical models were then updated (tuned to the experimental data) using two automated optimisation algorithms. This allowed to build high fidelity numerical models much more representative compared to the "starting

ones". Simplified analytical approaches were also compared to the test results and to the numerical models. Unfortunately, predicting the dynamic response of complicated substructures such as floor systems is often beyond the capabilities of traditional engineering approaches. The discussed findings weigh against the applicability of simplified design practices reported in building codes. Only very detailed FE models were found able to predict well the behaviour of their real counterparts. Even though simplified approaches are very useful at preliminary project phases, they become unreliable if a higher performance of the floor is desired.

To conclude, the results achieved by this research confirm the high quality OMA methods applied to simple and complex structures, to traditional constructions in reinforced concrete and to that innovative generation of sustainable and technological buildings made of timber. The methods, increasingly widespread in the academic community, have proven reliable and flexible and should be more often used by practitioners. They are not completely mature, but they open new horizons to the sector both for the design of new buildings and for the monitoring and maintenance of pre-existing structures.

References

[1] J. L. Skullestad, R. A. Bohne, and J. Lohne, "High-rise timber buildings as a climate change mitigation measure–a comparative lca of structural system alternatives," *Energy Procedia*, vol. 96, pp. 112–123, 2016.

[2] D. Peñaloza, M. Erlandsson, and A. Falk, "Exploring the climate impact effects of increased use of bio-based materials in buildings," *Construction and Building Materials*, vol. 125, pp. 219–226, 2016.

[3] P. Börjesson and L. Gustavsson, "Greenhouse gas balances in building construction: wood versus concrete from life-cycle and forest land-use perspectives," *Energy policy*, vol. 28, no. 9, pp. 575–588, 2000.

[4] B. Upton, R. Miner, M. Spinney, and L. S. Heath, "The greenhouse gas and energy impacts of using wood instead of alternatives in residential construction in the united states," *Biomass and Bioenergy*, vol. 32, no. 1, pp. 1–10, 2008.

[5] S. Hameury and T. Lundström, "Contribution of indoor exposed massive wood to a good indoor climate: in situ measurement campaign," *Energy and buildings*, vol. 36, no. 3, pp. 281–292, 2004.

[6] S. Hameury, "Moisture buffering capacity of heavy timber structures directly exposed to an indoor climate: a numerical study," *Building and environment*, vol. 40, no. 10, pp. 1400–1412, 2005.

[7] K. Nore, A. Q. Nyrud, D. Kraniotis, K. R. Skulberg, F. Englund, and T. Aurlien, "Moisture buffering, energy potential, and volatile organic compound emissions of wood exposed to indoor environments," *Science and Technology for the Built Environment*, vol. 23, no. 3, pp. 512–521, 2017.

[8] J. Rice, R. A. Kozak, M. J. Meitner, and D. H. Cohen, "Appearance wood products and psychological well-being," *Wood and Fiber Science*, vol. 38, no. 4, pp. 644–659, 2007.

[9] A. Q. Nyrud and T. Bringslimark, "Is interior wood use psychologically beneficial? a review of psychological responses toward wood," *Wood and Fiber Science*, vol. 42, no. 2, pp. 202–218, 2010.

[10] M. D. Burnard and A. Kutnar, "Wood and human stress in the built indoor environment: a review," *Wood science and technology*, vol. 49, no. 5, pp. 969–986, 2015.

[11] K. A. Malo, R. B. Abrahamsen, and M. Bjertnæs, "Some structural design issues of the 14-storey timber framed building "treet" in norway," *European Journal of Wood and Wood Products*, vol. 74, no. 3, pp. 407–424, 2016.

[12] R. Abrahamsen, "Mjøstårnet-construction of an 81 m tall timber building," in *International House Forum*, 2017.

[13] E. Poirier, M. Moudgil, A. Fallahi, S. Staub-French, and T. Tannert, "Design and construction of a 53-meter-tall timber building at the university of british columbia," *Proceedings of WCTE*, 2016.

[14] W. Winter, K. Tavoussi, A. Fadai, F. Riola-Parada, and I. Prašnjak, "Development of prefabricated timbersteel-concrete ribbed decks," in *Wold Conference on Timber Engineering*, 2016.

[15] B. Peeters, H. Van der Auweraer, F. Vanhollebeke, and P. Guillaume, "Operational modal analysis for estimating the dynamic properties of a stadium structure during a football game," *Shock and Vibration*, vol. 14, no. 4, pp. 283–303, 2007.

[16] E. Reynders, R. Pintelon, and G. De Roeck, "Uncertainty bounds on modal parameters obtained from stochastic subspace identification," *Mechanical systems and signal processing*, vol. 22, no. 4, pp. 948–969, 2008.
[17] E. Reynders, J. Houbrechts, and G. De Roeck, "Fully automated (operational) modal analysis," *Mechanical Systems and Signal Processing*, vol. 29, pp. 228–250, 2012.
[18] F. Ubertini, C. Gentile, and A. L. Materazzi, "Automated modal identification in operational conditions and its application to bridges," *Engineering Structures*, vol. 46, pp. 264–278, 2013.
[19] M. Döhler, X.-B. Lam, and L. Mevel, "Uncertainty quantification for modal parameters from stochastic subspace identification on multi-setup measurements," *Mechanical Systems and Signal Processing*, vol. 36, no. 2, pp. 562–581, 2013.
[20] F. Magalhaes, A. Cunha, and E. Caetano, "Online automatic identification of the modal parameters of a long span arch bridge," *Mechanical Systems and Signal Processing*, vol. 23, no. 2, pp. 316–329, 2009.
[21] C. Gentile, A. Ruccolo, and F. Canali, "Long-term monitoring for the condition-based structural maintenance of the milan cathedral," *Construction and Building Materials*, vol. 228, p. 117101, 2019.
[22] A. Kita, N. Cavalagli, and F. Ubertini, "Temperature effects on static and dynamic behavior of consoli palace in gubbio, italy," *Mechanical Systems and Signal Processing*, vol. 120, pp. 180–202, 2019.
[23] R. Brincker and C. Ventura, *Introduction to operational modal analysis*. John Wiley & Sons, 2015.
[24] C. Rainieri and G. Fabbrocino, "Operational modal analysis of civil engineering structures," *Springer, New York*, vol. 142, p. 143, 2014.
[25] S. Ibrahim, J. Asmussen, and R. Brincker, *Modal Parameter Identification from Responses of General Unknown Random Inputs*, ser. Fracture and Dynamics. Denmark: Dept. of Building Technology and Structural Engineering, Aalborg University, 1995, no. 72, presented at the 14th International Modal Analysis Conference, Dearborn, Michigan, USA, February 12-15, 1996 PDF for print: 12 pp.
[26] J. S. Bendat and A. G. Piersol, *Random data: analysis and measurement procedures*. John Wiley & Sons, 2011, vol. 729.
[27] J. W. Cooley and J. W. Tukey, "An algorithm for the machine calculation of complex fourier series," *Mathematics of computation*, vol. 19, no. 90, pp. 297–301, 1965.
[28] A. Chopra, *Dynamics of Structures: International Edition*. Pearson Education Limited, 2015. [Online]. Available: https://books.google.it/books?id=ysajCwAAQBAJ
[29] D. J. Ewins, *Modal testing: theory, practice and application*. John Wiley & Sons, 2009.
[30] J.-N. Juang, *Applied system identification*. Prentice-Hall, Inc., 1994.
[31] P. Avitabile, *Modal testing: a practitioner's guide*. John Wiley & Sons, 2017.
[32] P. Van Overschee and B. De Moor, *Subspace identification for linear systems: Theory—Implementation—Applications*. Springer Science & Business Media, 2012.
[33] B. Peeters, *System identification and damage detection in civil engeneering*. Katholieke Universiteit te Leuven (1970-), 2000.
[34] A. J. Felber, "Development of a hybrid bridge evaluation system," Ph.D. dissertation, University of British Columbia, 1994.
[35] R. Brincker, L. Zhang, and P. Andersen, "Modal identification of output-only systems using frequency domain decomposition," *Smart materials and structures*, vol. 10, no. 3, p. 441, 2001.
[36] R. Brincker, C. E. Ventura, and P. Andersen, "Damping estimation by frequency domain decomposition," in *Proceedings of IMAC 19: A Conference on Structural Dynamics: februar*

5-8, 2001, Hyatt Orlando, Kissimmee, Florida, 2001. Society for Experimental Mechanics, 2001, pp. 698–703.

[37] R. J. Allemang, "A correlation coefficient for modal vector analysis," in *Proc. 1st Int. Modal Analysis Conference*, 1982, pp. 110–116.

[38] L. Zhang, T. Wang, and Y. Tamura, "A frequency–spatial domain decomposition (fsdd) method for operational modal analysis," *Mechanical systems and signal processing*, vol. 24, no. 5, pp. 1227–1239, 2010.

[39] E. Reynders and G. De Roeck, "Reference-based combined deterministic–stochastic subspace identification for experimental and operational modal analysis," *Mechanical Systems and Signal Processing*, vol. 22, no. 3, pp. 617–637, 2008.

[40] C. Rainieri and G. Fabbrocino, "Influence of model order and number of block rows on accuracy and precision of modal parameter estimates in stochastic subspace identification," *International Journal of Lifecycle Performance Engineering 10*, vol. 1, no. 4, pp. 317–334, 2014.

[41] A. Cabboi, F. Magalhães, C. Gentile, and Á. Cunha, "Automated modal identification and tracking: Application to an iron arch bridge," *Structural Control and Health Monitoring*, vol. 24, no. 1, p. e1854, 2017.

[42] C. Rainieri and G. Fabbrocino, "Automated output-only dynamic identification of civil engineering structures," *Mechanical Systems and Signal Processing*, vol. 24, no. 3, pp. 678–695, 2010.

[43] W.-H. Hu, C. Moutinho, E. Caetano, F. Magalhães, and A. Cunha, "Continuous dynamic monitoring of a lively footbridge for serviceability assessment and damage detection," *Mechanical Systems and Signal Processing*, vol. 33, pp. 38–55, 2012.

[44] J. Brownjohn, F. Magalhaes, E. Caetano, and A. Cunha, "Ambient vibration re-testing and operational modal analysis of the humber bridge," *Engineering Structures*, vol. 32, no. 8, pp. 2003–2018, 2010.

[45] V. R. McLamore, G. C. Hart, and I. R. Stubbs, "Ambient vibration of two suspension bridges," *Journal of the Structural Division*, vol. 97, no. 10, pp. 2567–2582, 1971.

[46] M. D. Trifunac, "Comparisons between ambient and forced vibration experiments," *Earthquake Engineering & Structural Dynamics*, vol. 1, no. 2, pp. 133–150, 1972.

[47] A. M. Abdel-Ghaffar and R. H. Scanlan, "Ambient vibration studies of golden gate bridge: I. suspended structure," *Journal of Engineering Mechanics*, vol. 111, no. 4, pp. 463–482, 1985.

[48] J. Brownjohn, A. Dumanoglu, R. Severn, and C. Taylor, "Ambient vibration survey of the humber suspension bridge," *University of Bristol*, 1986.

[49] A. Aloisio, R. Alaggio, and M. Fragiacomo, "Dynamic identification and model updating of full-scale concrete box girders based on the experimental torsional response," *Construction and Building Materials*, 2020.

[50] ——, "Time-domain identification of the elastic modulus of simply supported box girders under moving loads: Method and full-scale validation," *Engineering Structures*, vol. 215, p. 110619, 2020.

[51] J. Joyce, "Bayes' theorem," 2003.

[52] T. Reynolds, R. Harris, W.-S. Chang, J. Bregulla, and J. Bawcombe, "Ambient vibration tests of a cross-laminated timber building," *Proceedings of the Institution of Civil Engineers-Construction Materials*, vol. 168, no. 3, pp. 121–131, 2015.

[53] T. Reynolds, Å. Bolmsvik, J. Vessby, W.-S. Chang, R. Harris, J. Bawcombe, and J. Bregulla, "Ambient vibration testing and modal analysis of multi-storey cross-laminated timber buildings," in *World Conference on Timber Engineering*, 2014.

[54] B. Ellis and A. Bougard, "Dynamic testing and stiffness evaluation of a six-storey timber framed building during construction," *Engineering Structures*, vol. 23, no. 10, pp. 1232–1242, 2001.

[55] T. Reynolds, D. Casagrande, and R. Tomasi, "Comparison of multi-storey cross-laminated timber and timber frame buildings by in situ modal analysis," *Construction and building materials*, vol. 102, pp. 1009–1017, 2016.

[56] A. Feldmann, H. Huang, W. Chang, R. Harris, P. Dietsch, M. Gräfe, and C. Hein, "Dynamic properties of tall timber structures under wind-induced vibration," in *World Conference on Timber Engineering (WCTE 2016)*, 2016.

[57] T. Reynolds, A. Feldmann, M. Ramage, W. Chang, R. Harris, and P. Dietsch, "Design parameters for lateral vibration of multi-storey timber buildings," in *International Network on Timber Engineering Research Proceedings (INTER 2016)*, 2016.

[58] O. Hansen and M. Fjeld Olsen, "Measuring vibrations and assessing dynamic properties of tall timber buildings-måling av vibrasjoner og kartlegging av dynamiske egenskaper i høye trehus," Master's thesis, NTNU, 2016.

[59] M. H. Kharrazi and C. E. Ventura, "Vibration frequencies of woodframe residential construction," *Earthquake spectra*, vol. 22, no. 4, pp. 1015–1034, 2006.

[60] D. Fischer, A. Filiatrault, B. Folz, C. Uang, and F. Seible, "Shake table tests of a two-story woodframe house, curee publication no," *W-06, Consortium of Universities for Research in Earthquake Engineering, Richmond, CA*, 2001.

[61] L. Hu, A. Omeranovic, S. Gagnon, and M. Mohammad, "Wind-induced vibration of tall wood buildings-is it an issue," in *World Conference on Timber Engineering*, 2014.

[62] L. Hu, E. Karsh, S. Gagnon, C. Dagenais, and R. Ramzi, "Dynamic performance measured on two 6-storey buildings made from wood structures before and after their completion and occupancy," in *Proceedings of the WCTE 2016 World Conference on Timber Engineering (Vienna)*, 2016.

[63] I. Mugabo, A. R. Barbosa, and M. Riggio, "Dynamic characterization and vibration analysis of a four-story mass timber building," *Frontiers in Built Environment*, vol. 5, p. 86, 2019.

[64] M. Stepinac, I. Šušteršič, I. Gavrić, and V. Rajčić, "Seismic design of timber buildings: Highlighted challenges and future trends," *Applied Sciences*, vol. 10, no. 4, p. 1380, 2020.

[65] I. Edskär, "Modal analysis, dynamic properties and horizontal stabilisation of timber buildings," Ph.D. dissertation, Luleå tekniska universitet, 2019.

[66] I. Lukacs, A. Björnfot, T. Tsalkatidis, and R. Tomasi, "Structural redundancy in cross-laminated timber buildings," *Proceedings of the World Conference on Timber Engineering WCTE2016*, 2016.

[67] A. S. of Civil Engineers, *Minimum design loads and associated criteria for buildings and other structures*. American Society of Civil Engineers, 2017.

[68] NTC08, *Decreto Ministeriale 14 gennaio 2008, Norme tecniche per le costruzioni*. Ministero delle infrastrutture, Gazzetta Ufficiale, 2008.

[69] T. Ji and A. Pachi, "Frequency and velocity of people walking," *Structural Engineer*, vol. 84, no. 3, pp. 36–40, 2005.

[70] J. Rainer and G. Pernica, "Vertical dynamic forces from footsteps," *Canadian Acoustics*, vol. 14, no. 2, pp. 12–21, 1986.

[71] G. Pernica, "Dynamic load factors for pedestrian movements and rhythmic exercises," *Canadian Acoustics*, vol. 18, no. 2, pp. 3–3, 1990.

[72] B. Ellis, "On the response of long-span floors to walking loads generated by individuals and crowds," *Structural Engineer*, vol. 78, no. 10, pp. 17–25, 2000.

[73] V. Racic, A. Pavic, and J. Brownjohn, "Experimental identification and analytical modelling of human walking forces: Literature review," *Journal of Sound and Vibration*, vol. 326, no. 1-2, pp. 1–49, 2009.

[74] A. L. Smith, S. J. Hicks, and P. J. Devine, *Design of floors for vibration: A new approach*. Steel Construction Institute Ascot, Berkshire, UK, 2007.

[75] I. O. for Standardization, *10137: Bases for Design of Structures–serviceability of Buildings and Walkways Against Vibrations*. ISO, 2007.

[76] B. Standard, *6472: Guide to Evaluation of human exposure to vibration in buildings (1 Hz to 80 Hz)*. BSI, 1992.

[77] I. O. for Standardization, *2631-2: Mechanical vibration and shock-evaluation of human exposure to whole body vibration; Part2: Continuous and shock induced vibration in buildings (1—80 Hz)*. ISO, 1989.

[78] ——, *2631-1: Mechanical vibration and shock; evaluation of human exposure to whole body vibration in the working environment; Part 1 General requirements*. ISO, 1997.

[79] T. Toratti and A. Talja, "Classification of human induced floor vibrations," *Building acoustics*, vol. 13, no. 3, pp. 211–221, 2006.

[80] I. Smith and Y. H. Chui, "Design of lightweight wooden floors to avoid human discomfort," *Canadian Journal of Civil Engineering*, vol. 15, no. 2, pp. 254–262, 1988.

[81] J. Dolan, T. Murray, J. Johnson, D. Runte, and B. Shue, "Preventing annoying wood floor vibrations," *Journal of structural engineering*, vol. 125, no. 1, pp. 19–24, 1999.

[82] L. J. Hu, Y. H. Chui, and D. M. Onysko, "Vibration serviceability of timber floors in residential construction," *Progress in Structural Engineering and Materials*, vol. 3, no. 3, pp. 228–237, 2001.

[83] S. V. Ohlsson, *Floor vibrations and human discomfort*. Chalmers University of Technology, Division of Steel and Timber Structures, 1982.

[84] S. Ohlsson, *Springiness and human-induced floor vibrations: a design guide*. Swedish Council for Building Research, 1988, no. 1988.

[85] ——, "Ten years of floor vibration research—a review of aspects and some results," in *Proceedings of the Symposium/Workshop on Serviceability of Buildings (Movements, Deformations, Vibrations)*, vol. 1, 1988, pp. 419–434.

[86] J. Weckendorf, T. Toratti, I. Smith, and T. Tannert, "Vibration serviceability performance of timber floors," *European Journal of Wood and Wood Products*, vol. 74, no. 3, pp. 353–367, 2016.

[87] B. Zhang, B. Rasmussen, A. Jorissen, and A. Harte, "Comparison of vibrational comfort assessment criteria for design of timber floors among the european countries," *Engineering Structures*, vol. 52, pp. 592–607, 2013.

[88] M. R. Willford, P. Young, and M. CEng, *A design guide for footfall induced vibration of structures*. Concrete Society for The Concrete Centre, 2006.

[89] E. C. for Standardization, *16929: Test methods; Timber floors; Determination of vibration properties*. CEN, 2018.

[90] J. Weckendorf and I. Smith, "Dynamic characteristics of shallow floors with cross-laminated-timber spines," *World*, vol. 15, p. 19, 2012.

[91] J. Weckendorf, G. Hafeez, G. Doudak, and I. Smith, "Floor vibration serviceability problems in wood light-frame buildings," *Journal of Performance of Constructed Facilities*, vol. 28, no. 6, p. A4014003, 2014.

[92] J. Weckendorf, E. Ussher, and I. Smith, "Dynamic response of clt plate systems in the context of timber and hybrid construction," *Composite Structures*, vol. 157, pp. 412–423, 2016.

[93] I. M. Sobol, "Sensitivity estimates for nonlinear mathematical models," *Mathematical modelling and computational experiments*, vol. 1, no. 4, pp. 407–414, 1993.

[94] R. Storn and K. Price, "Differential evolution–a simple and efficient heuristic for global optimization over continuous spaces," *Journal of global optimization*, vol. 11, no. 4, pp. 341–359, 1997.

[95] J. Kennedy and R. Eberhart, "Particle swarm optimization," in *Proceedings of ICNN'95-International Conference on Neural Networks*, vol. 4. IEEE, 1995, pp. 1942–1948.

[96] L. J. V. Miranda, "PySwarms, a research-toolkit for Particle Swarm Optimization in Python," *Journal of Open Source Software*, vol. 3, 2018. [Online]. Available: https://doi.org/10.21105/joss.00433

[97] P. Virtanen, R. Gommers, T. E. Oliphant, M. Haberland, T. Reddy, D. Cournapeau, E. Burovski, P. Peterson, W. Weckesser, J. Bright, S. J. van der Walt, M. Brett, J. Wilson, K. Jarrod Millman, N. Mayorov, A. R. J. Nelson, E. Jones, R. Kern, E. Larson, C. Carey, İ. Polat, Y. Feng, E. W. Moore, J. Vand erPlas, D. Laxalde, J. Perktold, R. Cimrman, I. Henriksen, E. A. Quintero, C. R. Harris, A. M. Archibald, A. H. Ribeiro, F. Pedregosa, P. van Mulbregt, and S. . . Contributors, "SciPy 1.0: Fundamental Algorithms for Scientific Computing in Python," *Nature Methods*, vol. 17, pp. 261–272, 2020.

[98] M. M. Ebadi, G. Doudak, and I. Smith, "Finite-element modeling and parametric study of glulam beam-and-deck floors," *Journal of Structural Engineering*, vol. 143, no. 9, p. 04017106, 2017.

Paper I

I D. Pasca, A. Aloisio, L. De Lauretis (2021) PyOMA A Python module to perform Operational Modal Analysis. *(Submitted to Journal of Open Source Software, March 2021)*.

url: `https://github.com/dagghe/PyOMA`

Paper II

II A. Aloisio, D. P. Pasca, R. Alaggio, M. Fragiacomo (2020) Bayesian estimate of the elastic modulus of concrete box girders from dynamic identification: a statistical framework for the A24 motorway in Italy, Structure and Infrastructure Engineering, DOI: 10.1080/15732479.2020.1819343

Bayesian estimate of the elastic modulus of concrete box girders from dynamic identification: a statistical framework for the A24 motorway in Italy

Angelo Aloisio*[a], Dag Pasca[b], Rocco Alaggio[a], Massimo Fragiacomo[a]

[a] *Department of Civil, Construction-Architectural and Environmental Engineering, Università degli Studi dell'Aquila, Via G. Gronchi, 18, L'Aquila, 67100, Abruzzo, Italy*
[b] *Faculty of Science and Technology, Norwegian University of Life Sciences, Oslo, Norway*

Abstract

This paper delivers a reliability-based method for the assessment of the elastic modulus (EM) of concrete in simply supported girders from dynamic identification. The correlation between the natural frequencies of the first bending modes and the concrete EM supports the use of the first natural frequency as a predictor of the EM value, which is a well-acknowledged indicator of the concrete state. In the current application, the EMs of seven girders provide the prior state of knowledge about the considered bridge class, possibly to be obtained by more samples in working applications. The identified natural frequencies update the prior probability distribution of the EMs using Bayes inference. The resulting probability of exceeding a specific EM value expresses the degree of belief of the inspector in the obtained EM. The posterior probability, compared to a proper threshold, could be used in decision-making processes when prioritizing the interventions in the maintenance plans.

Keywords: Reliability and Risk analysis; Concrete structures; Bridge maintenance; Beams and girders; Concrete elastic modulus; Bayesian inference; Dynamic Tests.

1. Introduction

According to the UNI EN 13306 (2018), maintenance encompasses all technical, administrative actions, including supervisions, aiming at maintaining or taking an object in a state suitable for its right functioning. Most of the Italian maintenance plans descend from the outcomes of periodical visual inspections, which yield the

*Corresponding author.
Email addresses: angelo.aloisio1@graduate.univaq.it (Angelo Aloisio*), dag.pasquale.pasca@nmbu.no (Dag Pasca), rocco.alaggio@univaq.it (Rocco Alaggio), massimo.fragiacomo@univaq.it (Massimo Fragiacomo)

so-called defect cards, well explained in the CIAS[1] manual (Ceccotti et al.,2002).

The defect cards attempt to numerically express the severity (i), extension (ii) and intensity (iii) of a defect using the following expression:

$$D_R = \sum_i (G_i \cdot K_{i,1} \cdot K_{i,2}) \tag{1}$$

where D_R is the relative defectivity, G_i the severity of the ith defect, $K_{i,1}$ and $K_{i,2}$ the corresponding extension and intensity coefficients respectively. The G_i values span in the range 1-5 depending on the associated risk: actual, potential, induced or economical. The $K_{i,1}$ and $K_{i,2}$ coefficients can assume the following discretized values: 0.2, 0.5 and 1.

Particularly risky defects require further investigations and, if additional pieces of evidence confirm their inherent risk, they are considered "non-conformities" and the Managing Body will adopt the needed precautionary actions. There are as many defect cards as the number of structural components (piers, abutments, e.g.), further classified according to the constituent material (steel, concrete, timber, e.g.).

This method endeavours to deliver an objective and straightforward procedure for the arrangement of maintenance plans. However, it has weaknesses which may deserve enhancements: namely, the prevalence of visual inspections over non-destructive damage evaluation (NDE) techniques (i), the absence of a probability-based reliability framework (ii), the potential unobjective choice of the K_1 and K_2 coefficients (iii). (i) NDE techniques attempt to enlighten defects hidden to the human eye.

Specifically, dynamic-based NDE techniques, which find extensive use in academic investigations, do not have a meaningful role in the actual maintenance plans. (ii) There are exceptions: since 2004, the Autonomous Province of Trento, Italy, has adopted a Bridge Management System entirely based on reliability concepts (Zonta et al., 2007). However, most of Italy bridge stock lacks a reliability-based maintenance plan. (iii) The choice of the intensity and extension coefficients mostly depends on the experience and interpretation of the inspector.

This paper shows a possible and quite-straightforward application of dynamic-based NDE techniques. The scientific literature soundly proved the potentialities of finite element analysis with on-site measurement through finite element model updating. Several researchers developed diverse model updating methods to esti-

[1]CIAS (Centro Sperimentale Aggiornamento Sperimentale-Scientifico) a is non-profit organization that carries out a scientific dissemination activity and development of experimentation in the structural and geotechnical field of civil engineering.

mate the model parameters reliably (model-driven estimation) (Schlune et al.,2009; Aloisio et al., 2020d). Oppositely, other researchers endeavoured to determine the structural parameters via sole experimental investigations (data-driven estimation) (Aloisio et al., 2020b; Aloisio et al., 2019a; Aloisio et al., 2019b; Di Egidio et al., 2019).

In this paper, the authors implemented a data-driven probabilistic framework for the assessment of the EM values, calibrated on the results of the dynamic identification of seven simply supported Prestressed Concrete (PSC) girders of the A24 motorway. The A24 motorway crosses the Apennines range in Central Italy; Many girders were poured on-site in harsh environmental conditions, resulting in scattered qualities of the concrete pastes. Improper curing conditions, especially in frozen times, yield shallow EMs. In a few cases, the consequences of creep and low EMs required the installation of external prestressing cables. Hence, EM is a significant control parameter in the current application.The method of core drilling is the principal method for accurate, quick and economical identification of the EM of concrete. Though, the estimate affects a specific specimen extracted in a limited location of the structure. The mechanical properties of concrete may not be uniform within the structure. Nevertheless, the extraction of multiple specimens to achieve satisfactory statistics may be complicated in Prestressed Concrete Structures, where extreme prudence must be needed to avoid interference with the prestressing cables. Dynamic identification provides a sort of homogenized EM of the entire structure directly, without relying on multiple concrete specimens.The natural frequency of the first bending mode evidences a significant correlation with the EM, almost coinciding with the theoretical prediction for a simply supported beam. The relationship between the first natural frequency and EM validates the use of the first natural frequency as a predictor of the EM value, which is an essential control parameter. However, the dispersion of the results requires the use of a reliability-based procedure.

The paper is organized as follows: the second and third sections present the case study and the results of the dynamic identification. The fourth section discusses the correlation between EM and the first natural frequency. The fifth and sixth sections present and discuss the Bayesian framework for the assessment of the EM from the first natural frequency.

2. Case study: the A24 motorway

The University of L'Aquila carried out static and dynamic tests on the A24 motorway. The entire experimental campaign lasted from February to June 2019. The

Autostrada A24 or "Parks Motorway", in Abruzzo (Italy), connects Rome to the Adriatic Sea. Starting from GRA[2] and ending to Teramo, the A24 created a new historical linkage between Rome and the Apennines mountains. The A24 motorway has a consistent number of viaducts due to the complex orography. Many of them consist of single-span simply supported PSC beams.

The girders have a trapezoidal cross-section, depicted in Figure 1(a), 2.3m high

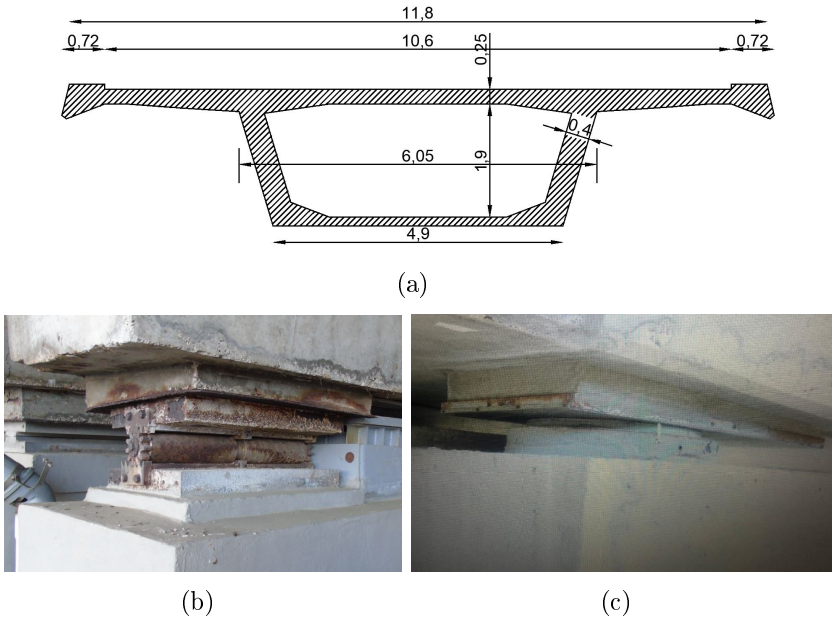

(a)

(b) (c)

Figure 1: (a) Cross-section; (b) Detail of the rack and roller (RR) bearing; (c) Multidirectional Pot (MP) bearing.

with two cantilevered wings 3.85m wide, prestressed by bonded post-tensioned tendons. A pair of piers, whose centre distance is about 40 m, sustains each bridge span. The concrete piers have a hollow cross-section, reinforced at their corners.

In the last decade, the managing body of the A24 motorway in Italy replaced several worn rack and rollers bearings with pot ones. Since 2009, the demand for seismic safety arose as an almost emotional tide after the 2009 earthquake in L'Aquila (Aloisio et al., 2019d; Aloisio et al., 2019c; Aloisio, 2020), which caused damages to some girders: they slid more than the length's support. This event induced the managing body to install an anti-sliding device to all girders with rack and rollers supports: it consists of a steel frame around the original supports 2-5 mm below the underside of the deck.

Figure (2) details the experimental setup. Ten Force Balance Accelerometers (FBA) measured the deck's response to ambient excitation. The accelerometers

[2]Grande Raccordo Anulare (GRA):is a toll-free, ring-shaped 68.2 kilometres (42.4 mi) long orbital motorway that encircles Rome.

were arranged into two measurement chains, each one driven by a master recording unit connected to a Wi-Fi access point and synchronized by GPS[3] sensors. The

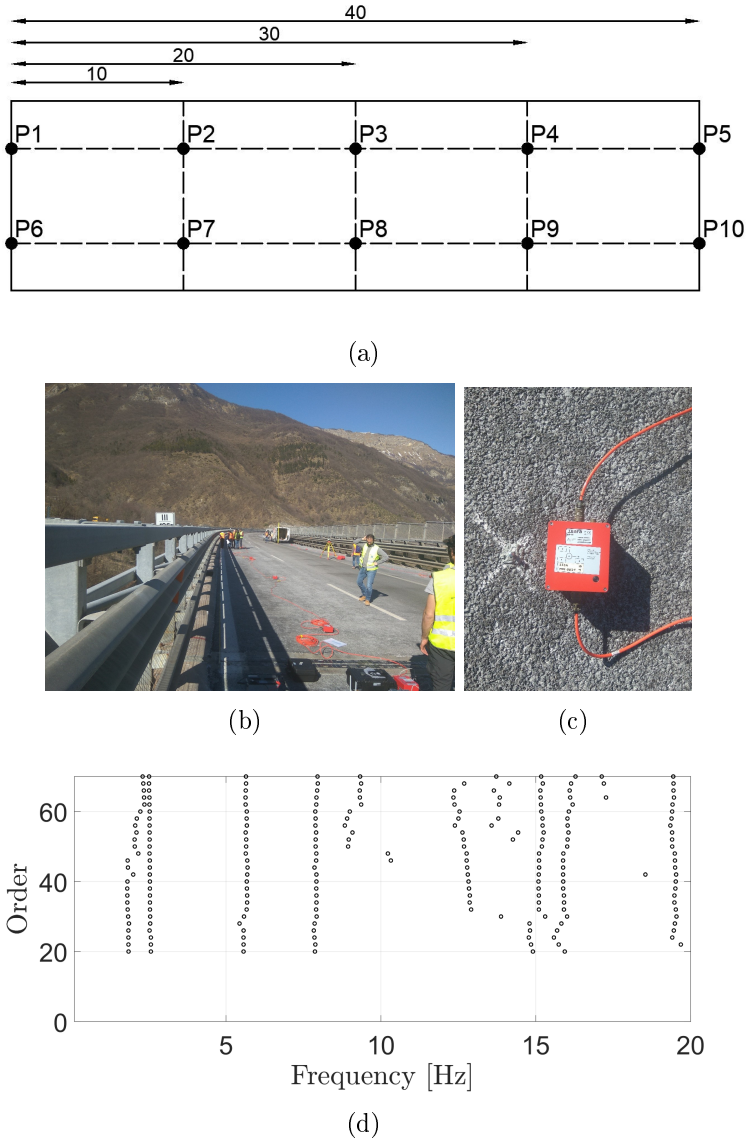

Figure 2: (a) Layout of the experimental setup, where P_i indicates the positions of the accelerometer; (b) Experimental setup; (c) Force-Balance accelerometer used in the current experimental campaign; (d) Sample of a stabilization diagram.

dynamic tests were carried out under similar environmental and weather conditions so that the influence of temperature and humidity on modal parameters can be considered negligible.The time series is about 40 minutes long.

The modal parameters are estimated from Output-Only Experimental Modal Analysis (EMA) using the Covariance-driven Stochastic Subspace Identification (Peeters and De Roeck, 2001). The data were sampled at a rate of 200 Hz. The

[3]Global Positioning System.

cut-off frequency of the anti-aliasing filter was set to 40 Hz. The Stochastic Subspace Identification (Reynders et al., 2008; Antonacci et al., 2020) method yields eigenfrequencies, damping ratios and mode shapes for each setup (Figure 2). The parameters used for the identification are $i = 7$, $n = 20$ and $n_b = 70$ (Reynders et al., 2008).

3. Results: dynamic identification

The authors tested the following bridge spans, labelled according to the viaduct they belong to: namely, Biselli, Cerchiara No 4, Cerchiara No 7, Cretara, Le Grotte, San Nicola, Temperino. The pictures of the first three mode shapes follow henceforth, where f indicates the natural frequency and ξ the modal damping.

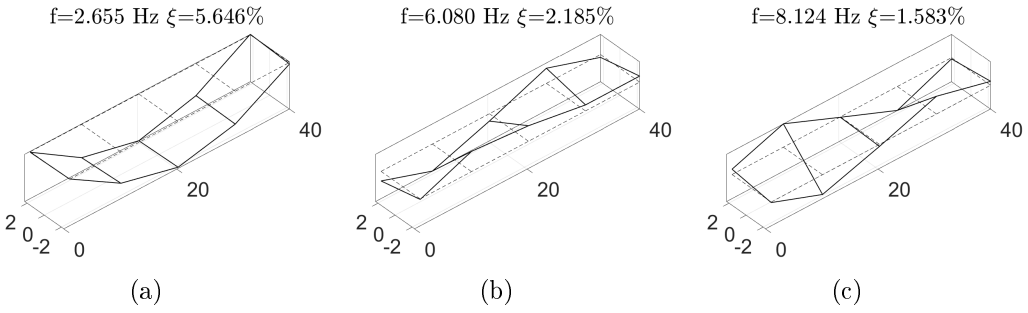

Figure 3: Mode shapes representation of the first three stable modes of the Biselli bridge span.

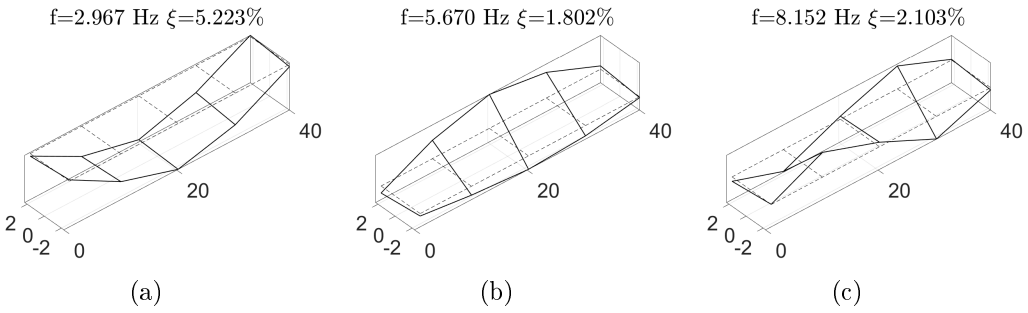

Figure 4: Mode shapes representation of the first three stable modes of the Cerchiara 4 bridge span.

Three mode shapes arise from the stabilization diagrams (Figure 2(d)): a bending mode at nearly 2.5Hz, a torsional mode at almost 6Hz and a second torsional mode at approximately 8.5Hz. The three modes are detectable in all tested configurations.

The authors extracted, for each mode, the torsional angle and the vertical displacement of five fictitious points, equidistant from the two rows P_1-P_5 and P_6-P_{10}

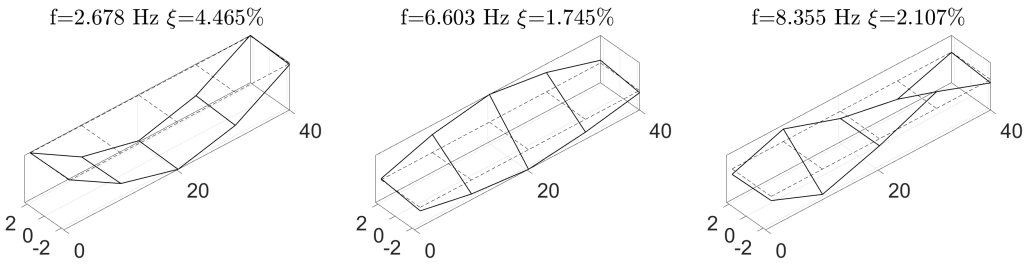

Figure 5: Mode shapes representation of the first three stable modes of the Cerchiara 7 bridge span.

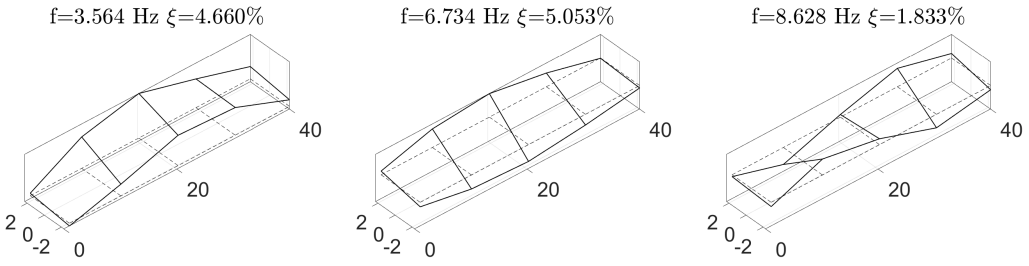

Figure 6: Mode shapes representation of the first three stable modes of the Cretara bridge span.

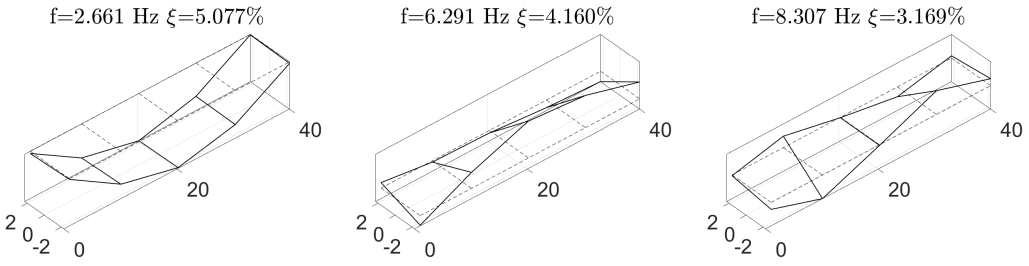

Figure 7: Mode shapes representation of the first three stable modes of the Le Grotte bridge span.

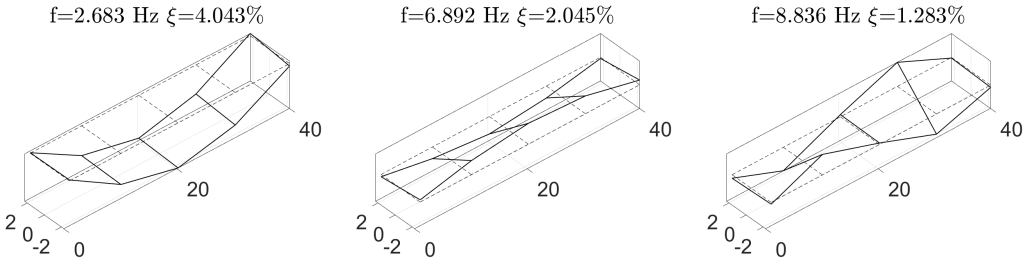

Figure 8: Mode shapes representation of the first three stable modes of the San Nicola bridge span.

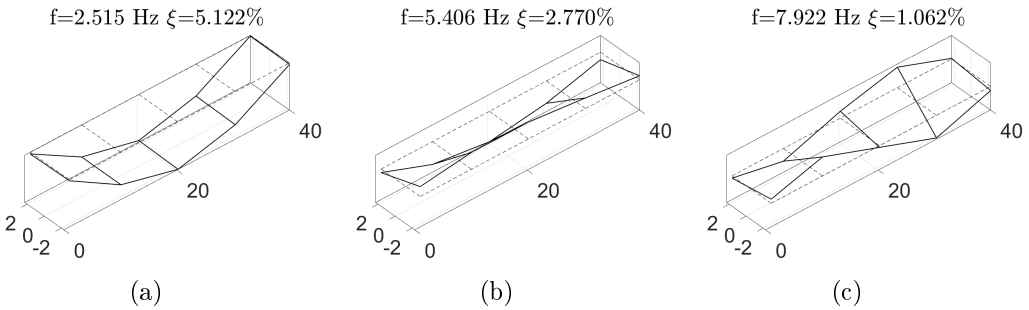

Figure 9: Mode shapes representation of the first three stable modes of the Temperino bridge span.

(Fig.2(a)). The considered points belong to an equivalent 3d beam possibly representative of the actual spatial structure. The following measures enable to shortly evaluate the torsional and bending fractions of the modal response.

$$v_0 = \frac{v_{P_i} + v_{P_j}}{2}; \quad v_r = \frac{v_{P_i} - v_{P_j}}{2} \rightarrow \psi = \frac{v_r}{L} \tag{2}$$

The Bending (B) and Torsional (T) fractions for the ith point are:

$$B = \frac{v_0}{v_0 + v_r}; \quad T = \frac{v_r}{v_0 + v_r} \tag{3}$$

The first mode is, on average, more than 95% bending, while the two torsional

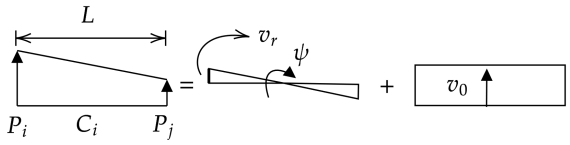

Figure 10: Decomposition od the response into a translational and rotational component.

modes have a significant bending component, see the Appendix. The torsional-bending coupling generally derives from the discrepancy between the elastic and mass axis (Banerjee and Williams, 1992; Di Nino and Luongo, 2020). The cross-section is symmetric, and the four bearings are nominally identical. Except for the influence of substructures (piers and soil), two reasons may lay behind the detected coupling: (i) the eccentricity of the load distribution due to the presence of a row of Jersey barriers along one side of the deck; (ii) asymmetry of the boundary conditions due to possible installation faults, like micro-metric levelling defects.

Specifically, the Biselli, Cerchiara No 4, Cerchiara No 7, Le Grotte, San Nicola and Temperino bridge spans have an almost pure bending mode. The Cretara bridge span has a coupled first mode, with a nearly 30% torsional component. Such coupling may derive from the reason mentioned above: a possible asymmetry of

the boundary condition. In the considered cases, there is more difference in terms of natural frequencies than mode shapes. Concerning the damping ratios, the first mode has a damping ratio approximately close to 5%, which is consistent with the intrinsic concrete damping. The higher modes have damping lower than 5%. Still, although modal frequencies and mode shapes can be measured confidently and quite easily using dynamic tests, accurate identification of damping ratios requires further development (Rainieri et al., 2010; Aloisio et al., 2020e; Aloisio et al., 2020a). For this reason, the authors will entrust to future investigations a valid damping identification.

4. Discussion: Correlation between the elastic modulus and the first natural frequency

The similarity between mode shapes conflicts with the scattered values of the natural frequencies. Concerning the first modes, the bearings show a negligible influence over the mode shapes, which induce to believe the same irrelevant effect over the natural frequencies. Conversely, the EM significantly varies between girders, see Tab.1. The discrepancy of the EM may originate from the construction time when different curing and environmental conditions affected the concrete hardening.

Tab.1 collects the EM estimated from static load tests and the outcomes of concrete samples. Figure 11 reports the correlations between the EM and the natural

Table 1: Correlation between the elastic modulus obtained from static load tests and concrete samples and the natural frequencies of the first three modes.

Viaduct	**Span**	**elastic modulus [MPa]**		**Natural Frequencies [Hz]**		
		Static Tests	**Concr. Samp.**	**1st Mode**	**2nd Mode**	**3rd Mode**
Biselli	12	24900	/	2.652	6.080	8.610
Cerchiara	4	15000	19361	2.247	5.670	8.152
Cerchiara	7	23700	23299	2.638	6.303	8.355
Cretara	9	26000	26416	3.413	6.734	8.628
Le Grotte	5	36000	/	2.661	6.291	8.307
San Nicola	10	26700	29978	2.693	6.892	8.836
Temperino	6	35900	/	2.483	5.406	7.922

frequencies of the first three modes. The values of the EM derive from static load tests and experimental tests on concrete specimens, indicated in Table 1 by "Static Tests" and "Concr. Samp" respectively. Static load testing is used to assess if the mechanical performance and carrying capacity of the tested structure agrees with design criteria. The adopted test load arrangement followed the recommendations of the Italian technical provisions [15]. Table 1 reports the outcomes of static load tests compared to the EM identification from concrete specimens, carried out

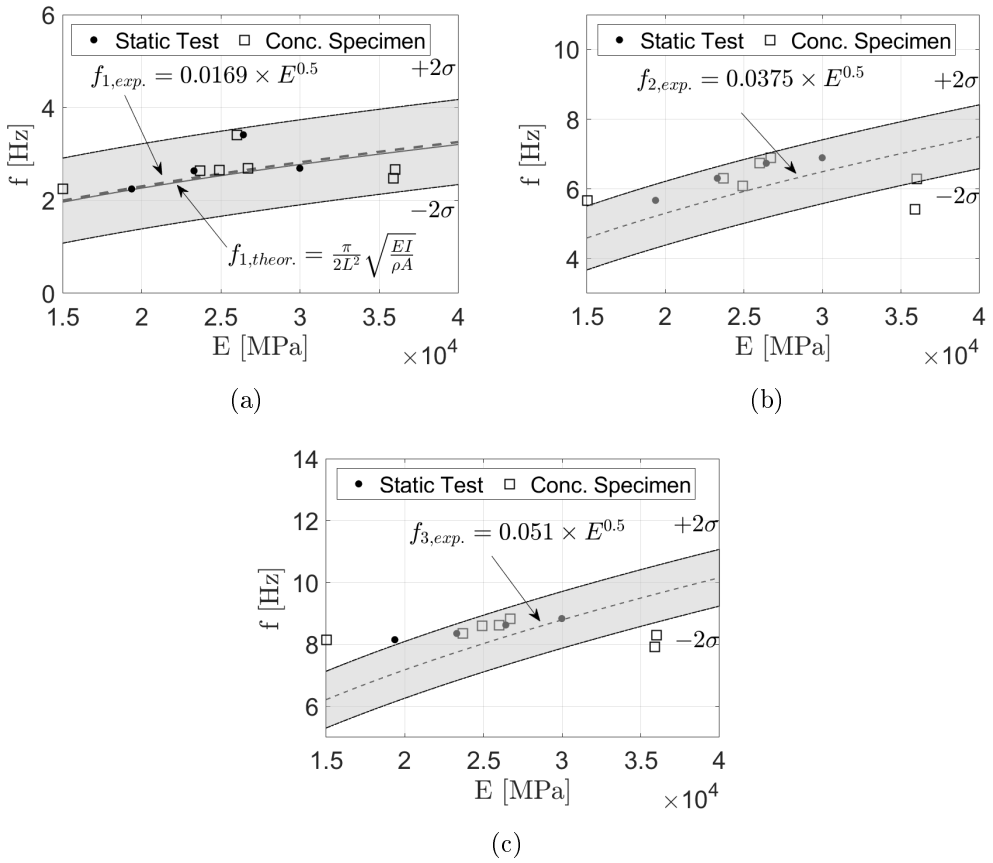

Figure 11: Correlation between the elastic modulus obtained from static load tests and concrete samples and the natural frequencies of the first three modes. The dotted lines indicate the interpolation curves; The solid lines the theoretical predictions according to Equation (4). The grey region indicates the confidence bounds ($+2\sigma/-2\sigma$) of the Least Squares fitting.

following the UNI EN 12504-1 [24] and averaged over three specimens.The values are quite dispersed, but an evident increasing trend descends from the relationships with the first mode. The authors adopted the following polynomial: $f = k \times E^{0.5}$, where k is the unknown coefficient obtained from Ordinary Least Squares, f and E are expressed in Hz and MPa respectively.

The curves confirm the expected trend; higher EM yield higher natural frequencies. Specifically, the first correlation in Figure 11(a) closely follows the expected curve for a simply supported beam in Equation (4). Equation (4) presents the expression of the natural frequency of the first bending mode and that of the two torsional frequencies corresponding to the first two torsional modes with extreme rotation prevented.

$$f_{1,theor.} = \frac{\pi}{2l^2}\sqrt{\frac{EI}{m}} \quad f_{2,theor.} = \frac{1}{2l}\sqrt{\frac{GJ}{I_\alpha}} \quad f_{3,theor.} = \frac{1}{l}\sqrt{\frac{GJ}{I_\alpha}} \tag{4}$$

The theoretical curve of the first bending mode closely matches with the experimental fitting.

Among the considered bridge population, Le Grotte and Temperino bridges present higher EMs, but lower frequencies. The EMs from static load tests are likely representative of the actual EM and other phenomena, not related to the quality of concrete, may have lowered the identified natural frequencies. This observation supports the need for probabilistic rather than deterministic models when assessing the EM from the natural frequencies. The outcomes of dynamic identification can properly drive probabilistic, not deterministic, inferences about the bridge state, which could be improved by additional information about the bridge, possibly using Bayesian updating methods.

The prediction of the two torsional frequencies is widely inaccurate. For this reason, the authors did not report the curve derived from Equation (4), which stands far beyond the experimental findings. The analytical prediction largely overestimates the natural frequencies: in the considered cases, the bearings are deformable and allow significant rotation.

5. Bayesian framework for the assessment of the elastic modulus

This section delivers a Bayesian updating method for the probabilistic assessment of the EM values from dynamic tests.

5.1. Background

Bayes' theorem describes the probability of an event, based on prior knowledge of conditions possibly related to the event (Gelman et al., 2013; Aloisio et al., 2020c). The probability of having the EM below a given value $\hat{E}$, indicated as $P(E < \hat{E})$, updated to the experimental evidence from dynamic tests can be written as:

$$P(E < \hat{E} | f < \hat{f}) = \frac{P(f < \hat{f} | E < \hat{E})}{P(f < \hat{f})} P(E < \hat{E}) \tag{5}$$

where $P(E < \hat{E} | f < \hat{f})$ is the posterior probability, i.e. the probability of observing $E < \hat{E}$ if the expected first natural frequency f is below the measured one $\hat{f}$; $P(f < \hat{f} | E < \hat{E})$ is the likelihood distribution, i.e. the probability of observing natural frequencies f below $\hat{f}$; $P(E < \hat{E})$ is the prior distribution, i.e. the probability of observing E below $\hat{E}$; $P(f < \hat{f})$ is the marginal likelihood.

5.2. Application

The authors attempted to choose suitable probability distributions to represent the statistical correlation between EM and natural frequencies. A reliability-oriented

method would require the use of Weibull distributions for the EM (Xie and Lai, 1996). Nevertheless, the Normal distributions of the natural frequency and the EM mostly agree with the associated Weibull probability distributions, see Figure 12.

Consequently, the authors assumed Normal distributions to describe the statistics of the EM and natural frequencies:

$$P(E) \approx \mathcal{N}(\mu_E, \sigma_E) \tag{6}$$

$$P(f) \approx \mathcal{N}(\mu_f, \sigma_f) \tag{7}$$

where μ_E, μ_f and σ_E, σ_f are the mean and variance of E and f respectively. The

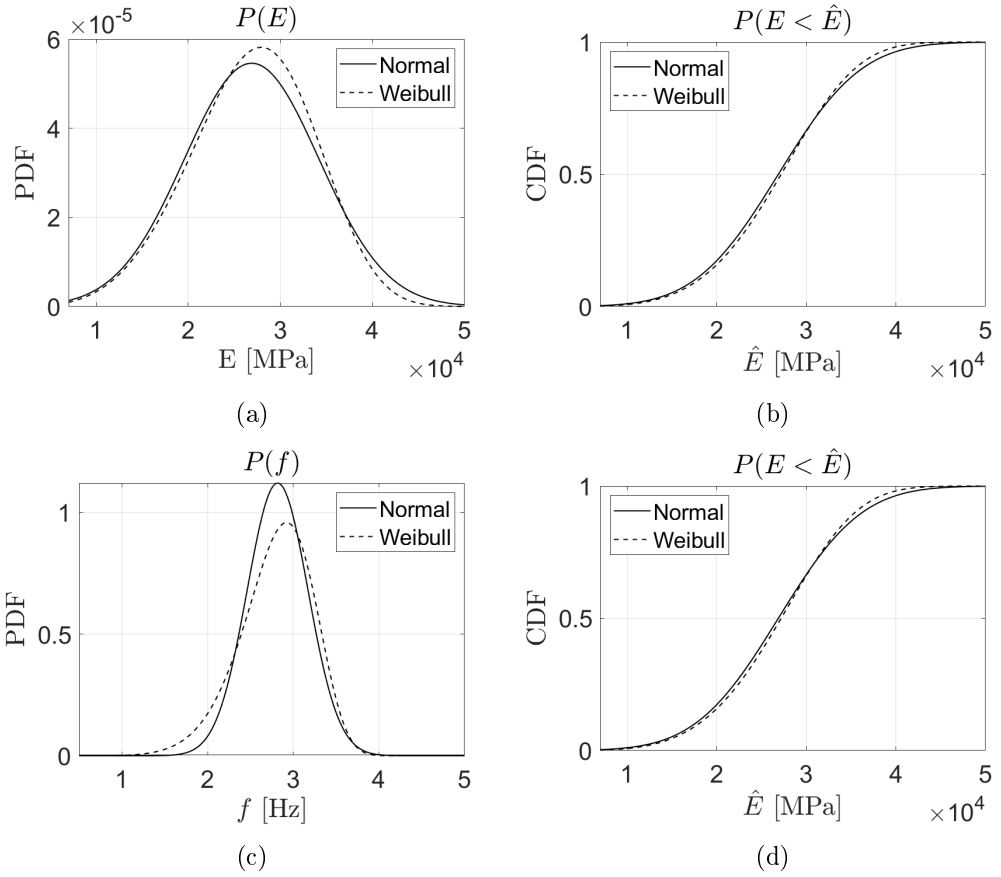

Figure 12: (a)-(b) Probability Density Functions (PDF) and Cumulative Density Functions (CDF) of the elastic Moduli in terms of Gaussian and Weibull statistics; (c)-(d) PDF and CDF of the natural frequencies of the first bending modes in terms of Gaussian and Weibull statistics;

parameters of the marginal probabilities in Equations (6)-(7) derive from a scarce statistical sample: the number of data (seven) may be inadequate for a sound statistical population. Yet, the authors used all accessible experimental data. The bivariate Normal distribution describes the likelihood of observing certain natural

frequencies given the EM values.

$$P(E, f) \approx \mathcal{N}(\boldsymbol{\mu}, \boldsymbol{\Sigma}) \tag{8}$$

The parameters of Equation (8) are the following:

$$\boldsymbol{\mu} = \begin{bmatrix} \mu_E \\ \mu_f \end{bmatrix} = \begin{bmatrix} 26885.714 \\ 2.684 \end{bmatrix} \tag{9}$$

$$\boldsymbol{\Sigma} = \begin{bmatrix} \sigma_E^2 & \rho\sigma_E\sigma_f \\ \rho\sigma_E\sigma_f & \sigma_f^2 \end{bmatrix} = \begin{bmatrix} 53418095.238 & -966.540 \\ -966.540 & 0.128 \end{bmatrix} \tag{10}$$

where $\boldsymbol{\mu}$ is the mean vector and $\boldsymbol{\Sigma}$ the covariance matrix. Figure 13 represents the density and cumulative probability distributions in Equation (8). The dots indicate the experimental couples (E-f). The joint density distribution leads to

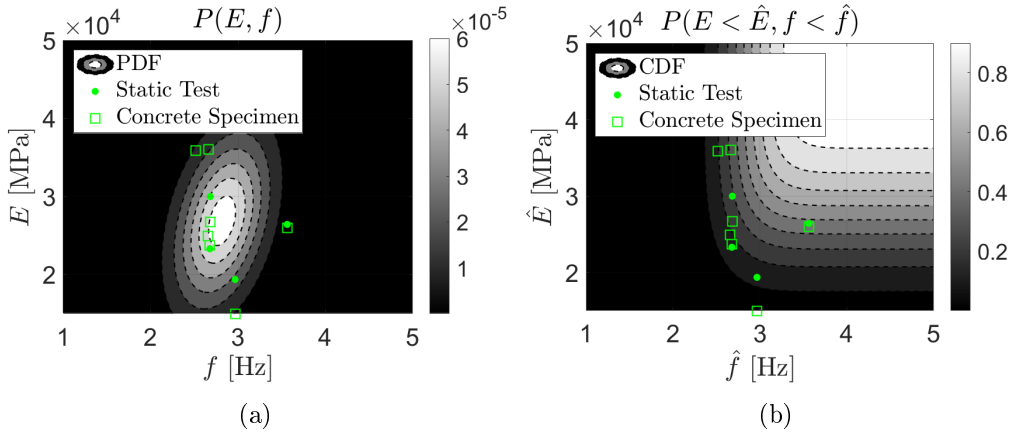

Figure 13: Bivariate normal density (a) and cumulative (b) distribution of the elastic Moduli and natural frequencies of the first bending modes.

the likelihood function in Equation (8). Figure 14(a) represents the contour plot of the posterior distribution in Equation (5), obtained by varying both $\hat{E}$ and $\hat{f}$. Figure 14(a) illustrates the Bayesian updating of the probability distribution in Figure 13(b). Figure 13(b) expresses the increment in probability when increasing both the ranges of EM and natural frequency. Probabilities close to 1 correspond to values of the natural frequency and the EM approximately higher than 40000 MPa and 3 Hz respectively. Conversely, the Bayesian updating in Figure 14(a) carries a piece of different information: it reveals the probability of observing EMs lower than the threshold $\hat{E}$, given natural frequencies below a specific threshold $\hat{f}$. Hence, Figure 14(a) must be read by section-cuts, as Figure 14(b), by assuming frequency values. As a consequence, the Cumulative Density Functions (CDF) approaches one for each value of the natural frequency, while the CDF in Figure 14(b) reaches one only when

both thresholds of the EM and natural frequency raise.The posterior CDF has a peculiar pattern: the probabilities below 2Hz and exceeding 4Hz are stationary along the frequency axis, though increasing for higher $\hat{E}$ values. Conversely, estimated frequencies $\hat{f}$ in the range 2-4Hz yield diverse probability values: the probability of observing an EM underneath a given value $\hat{E}$ decreases for growing values of the first natural frequency. This fact is consistent with the expected behaviour: higher natural frequencies descend from higher EM. Still, the meaning of the Bayesian updating attains the section cuts along the frequency axis.

Figure 14(b) shows the grey region of CDF between the two asymptotic distributions below 2Hz and beyond 4Hz. All possible posterior distributions stand in the grey region. Specifically, the authors represented two sample cases: the probabilities of observing EM given estimated frequencies below 2.5 and 2.9, indicated by the solid and dashed line, respectively. The dash-dot line represents the CDF of the prior probability $P(E < \hat{E})$. In the considered case, the experimental evidence, given by the estimated frequencies, always yields a probability reduction.

Let us assume a specific EM threshold $\hat{E}$=23000MPa, indicated by a vertical dashed line in Figure 14(a). The probability of observing EM below 23000MPa is 0.3. The estimation of a natural frequency below 2.5Hz determines a decrease to 0.17, i.e. the inspector would obtain a lower probability of observing EM below 23000MPa. If the natural frequency stands below 2.9Hz, the probability would further reduce to 0.10.

Figure 15 depicts the complement to 1 of Equation (5). It expresses a complementary concept: the probability of exceeding a given EM value $\hat{E}$ if the estimated natural frequency exceeds $\hat{f}$.

The same threshold at $\hat{E}$=23000MPa intersects the prior distribution and the two posterior distributions at 2.5Hz and 2.9Hz. The prior probability of observing EM exceeding 23000MPa is 0.7. Supposed frequencies higher than 2.5 and 2.9Hz determine an increment up to 0.83 and 0.9 individually. Figure 14(b) and Figure 15 reveals the same idea: the estimated natural frequency raise the degree of belief of the inspector in the EM values. The procedure, shown for a 23000MPa threshold, can be extended to any EM value and could represent a relatively simple reliability-based method for the assessment of the EM using the outcomes of dynamic tests. In the next section, the authors provide a simplified flow chart of the procedure.

6. Discussion

Dynamic identification provides useful information; Specifically, the case study enlightened two aspects: the inspection of the mode shapes returns knowledge about

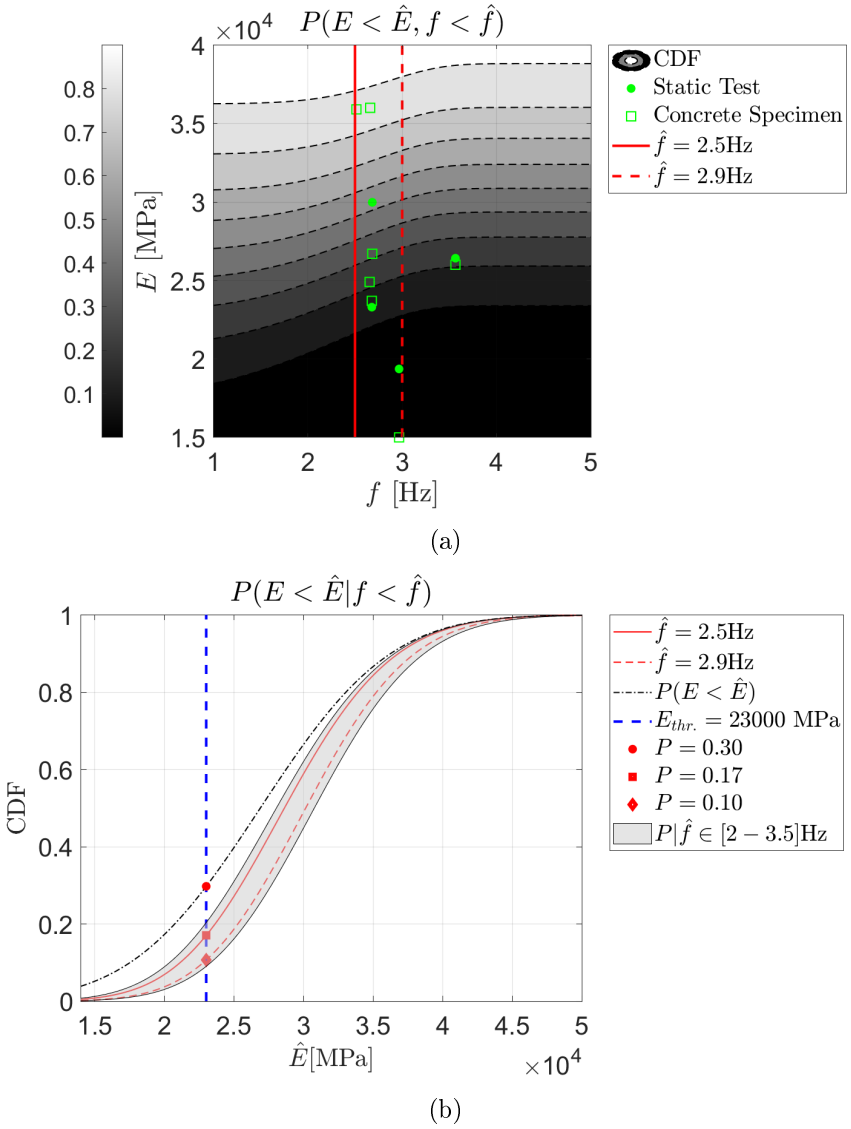

Figure 14: (a) Posterior bivariate cumulative distribution in Equation (5); (b) Superposition of the prior distribution (dash-dot) and two section cuts of the posterior in (a).

potential bearing malfunctioning (see the Cretara bridge span in Figure 6(a)), and the natural frequency of the first bending is correlated with the EM value.

Hence, the implementation of a reliability-based assessment of the bridge state would need the definition of a proper threshold for the EM, below which the bridge is estimated unreliable and the selection of an adequate reliability threshold, which represents the admitted uncertainty in the decision-making process. Figure 16 outlines the logical development of a possible reliability-based estimation. The first step involves an experimental campaign: the dynamic identification of the entire bridge stock.

The controller must examine the resulting mode shapes to evidence possible anomalies, which would require more in-depth investigations. If no abnormalities

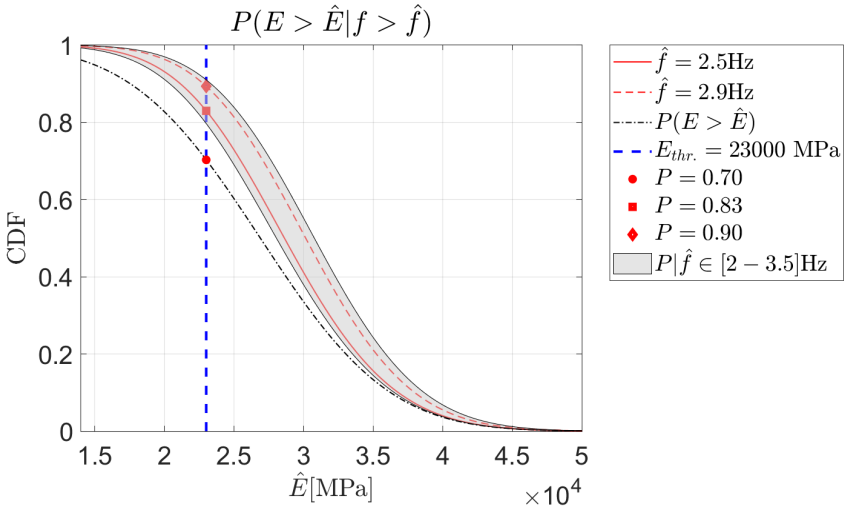

Figure 15: Superposition of the prior distribution (dash-dot) and two section cuts of the posterior in terms of exceeding probability.

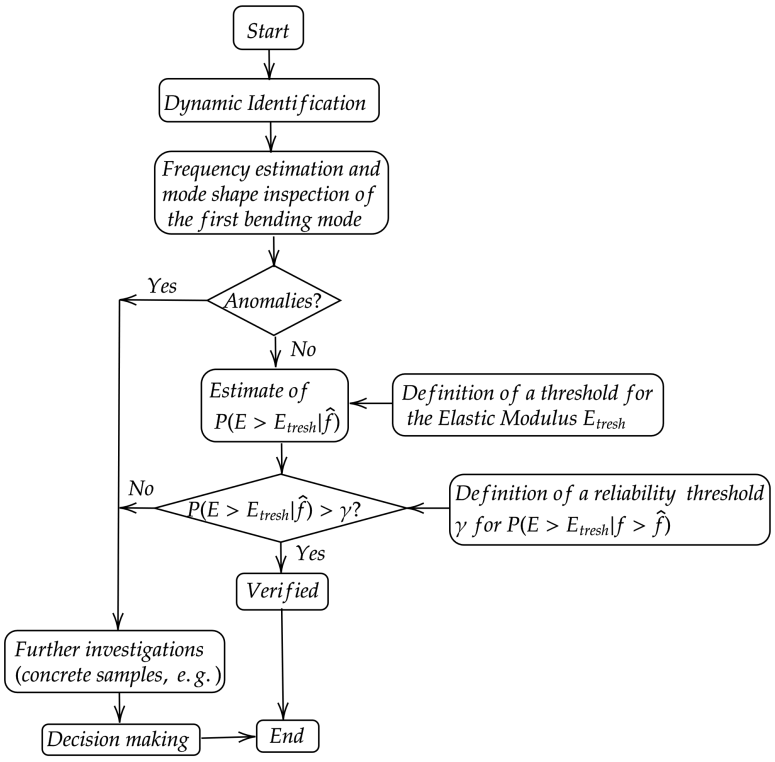

Figure 16: Flow chart of the proposed reliability-based procedure.

emerge, the inspector must define a threshold for the EM and estimate the posterior probability of observing EM higher than the limit, given the estimated frequency value. If the probability surpasses the accepted confidence level, the bridge span could be declared as verified. If not, further investigations, like tests on concrete specimens, must drive a careful decision-making process. The presented flowchart might be elementary, but it attempts to comfortably include NDE techniques in the world of Mantainace, which still lacks the regular presence of dynamic identification in the decision-making process. The Managing Bodies regularly report on the state of the infrastructures via annual and trimestral reports. A check on the EM via dynamic identification could be an additional parameter included in the technical report. The technical reports founds the decision-making process and the drafting on maintenance plans. If the inspector observes suspectingly low EM, further confirmed by additional investigations (concrete samples, e.g.), the bridge under investigation must be object of maintenance plan.

7. Conclusions

The paper presents a reliability-based method for the probabilistic assessment of the elastic modulus values from the natural frequencies of the first bending mode. The procedure is calibrated over the seven simply supported girders of the A24 motorway. The results of the performed dynamic identification evidenced a significant empirical correlation between the EM values, obtained from static tests and the first natural frequency. The correlation agrees with the expected theoretical relationship between frequency and EM for a simply supported beam. This evidence supports the use of the first natural frequency as a predictor of the EM within a Bayesian updating framework.

The first natural frequency could be used as a predictor of the EM of low/mid-span bridges, like the ones which were the object of this investigation. However, the extension of this method to more complex or larger bridges is not straightforward. The dynamics of long-span bridges generally affects the fields of nonlinear dynamics, and the framework of linear dynamics could be inadequate to derive direct and meaningful correlations between material properties and modal parameters.

The procedure enables to assess the probability of exceeding given EM thresholds by estimating the natural frequency of the first mode. The probability value, compared to a proper reliability threshold, possibly drive a decision-making process concerning the choice of more in-depth investigations. The authors discussed the method by examining two section-cuts of the cumulative posterior probability, which represent two possible situations. A flow-chart of the procedure further explain the

logical sequence of actions required for the reliability-bases assessment.

The Managing Bodies of the Italian motorways, except for a few exceptions, lack an organic, systematic use of dynamic identification in the arrangement of maintenance plans. The prioritization of interventions would benefit from the proposed method, which attempts to balance saving and the need for more reliable infrastructures. The current proposal precedes an accurate fragility estimate based on experimental observations. The authors will aim at developing probabilistic capacity models (Gardoni et al., 2002) of the considered concrete girders based on the estimate of the first natural frequency. The current application relies on a limited data set, which does not provide a genuinely statistical sample. However, the paper delivers a method, which, in working applications, should be based on a considerably higher number of samples.

8. Acknowledgments

The authors would like to acknowledge Strada dei PARCHI S.p.A. for the research funding which allowed the authors to undertake this research, and Prof. Angelo Luongo, Head of the Civil and Environmental Engineering Department (DICEEA) of the University of L'Aquila, for the support provided.

References

[1] 13306, U. E. (2018). Uni en 13306. *Manutenzione—Terminologia di manutenzione*.

[2] Aloisio, A. (2020). The timber-framed (tf) masonries in l'aquila: The baraccato aquilano. *Heritage*.

[3] Aloisio, A., Alaggio, R., and Fragiacomo, M. (2019a). Dynamic identification of a masonry façade from seismic response data based on an elementary ordinary least squares approach. *Engineering Structures*, 197:109415.

[4] Aloisio, A., Alaggio, R., and Fragiacomo, M. (2020a). Time-domain identification of elastic modulus of simply supported box girders under moving loads: method and full-scale validation. *Engineering Structures*.

[5] Aloisio, A., Alaggio, R., Köhler, J., and Fragiacomo, M. (2020b). Extension of generalized bouc-wen hysteresis modeling of wood joints and structural systems. *Journal of Engineering Mechanics*, 146(3):04020001.

[6] Aloisio, A., Battista, L. D., Alaggio, R., Antonacci, E., and Fragiacomo, M. (2020c). Assessment of structural interventions using bayesian updating and subspace-based fault detection methods: the case study of s. maria di collemaggio basilica, l'aquila, italy. *Structure and Infrastructure Engineering*, pages 1–15.

[7] Aloisio, A., Di Battista, L., Alaggio, R., and Fragiacomo, M. (2019b). Analysis of the forced dynamics of a masonry facade by means of input-output techniques and a linear regression model. In *COMPDYN, 2019, 7th International Conference on Computational Methods in Structural Dynamics and Earthquake Engineering*.

[8] Aloisio, A., Di Battista, L., Alaggio, R., and Fragiacomo, M. (2020d). Sensitivity analysis of subspace-based damage indicators under changes in ambient excitation covariance, severity and location of damage. *Engineering Structures*, 208:110235.

[9] Aloisio, A., Fragiacomo, M., and D'Alò, G. (2019c). The 18th-century baraccato of l'aquila. *International Journal of Architectural Heritage*, pages 1–15.

[10] Aloisio, A., Fragiacomo, M., and D'Alò, G. (2019d). Traditional tf masonries in the city centre of l'aquila–the baraccato aquilano. *International Journal of Architectural Heritage*, pages 1–18.

[11] Aloisio, A., Pasca, D., Tomasi, R., and Fragiacomo, M. (2020e). Dynamic identification and model updating of an eight-storey clt building. *Engineering Structures*, 213:110593.

[12] Antonacci, E., Aloisio, A., Galeota, D., and Alaggio, R. (2020). The s. maria di collemaggio basilica: from vulnerability assessment to first results of shm. *Journal of Architectural Engineering*, In press.

[13] Banerjee, J. and Williams, F. (1992). Coupled bending-torsional dynamic stiffness matrix for timoshenko beam elements. *Computers & Structures*, 42(3):301–310.

[14] Ceccotti, A., Giangreco, E., Jurina, L., Martinello, S., Siviero, E., Tattoni, S., Bruson, R., Caramel, G., Maliardi, L., Papaleo, A., et al. (2002). Manuale per la valutazione sullo stato dei ponti.

[15] delle Infrastrutture e Trasporti, M. (2018). Norme tecniche per le costruzioni.

[16] Di Egidio, A., Alaggio, R., Aloisio, A., De Leo, A. M., Contento, A., and Tursini, M. (2019). Analytical and experimental investigation into the effectiveness of a pendulum dynamic absorber to protect rigid blocks from overturning. *International Journal of Non-Linear Mechanics*, 115:1–10.

[17] Di Nino, S. and Luongo, A. (2020). Nonlinear aeroelastic behavior of a base-isolated beam under steady wind flow. *International Journal of Non-Linear Mechanics*, 119:103340.

[18] Gardoni, P., Der Kiureghian, A., and Mosalam, K. M. (2002). Probabilistic capacity models and fragility estimates for reinforced concrete columns based on experimental observations. *Journal of Engineering Mechanics*, 128(10):1024–1038.

[19] Gelman, A., Stern, H. S., Carlin, J. B., Dunson, D. B., Vehtari, A., and Rubin, D. B. (2013). *Bayesian data analysis*. Chapman and Hall/CRC.

[20] Peeters, B. and De Roeck, G. (2001). Stochastic system identification for operational modal analysis: a review. *Journal of Dynamic Systems, Measurement, and Control*, 123(4):659–667.

[21] Rainieri, C., Fabbrocino, G., and Cosenza, E. (2010). Some remarks on experimental estimation of damping for seismic design of civil constructions. *Shock and Vibration*, 17(4-5):383–395.

[22] Reynders, E., Pintelon, R., and De Roeck, G. (2008). Uncertainty bounds on modal parameters obtained from stochastic subspace identification. *Mechanical systems and signal processing*, 22(4):948–969.

[23] Schlune, H., Plos, M., and Gylltoft, K. (2009). Improved bridge evaluation through finite element model updating using static and dynamic measurements. *Engineering structures*, 31(7):1477–1485.

[24] UNI, E. (2002). Uni en 12504–1. *Prove sul calcestruzzo nelle strutture–Carote–Prelievo, esame e prove di compressione*.

[25] Xie, M. and Lai, C. D. (1996). Reliability analysis using an additive weibull model with bathtub-shaped failure rate function. *Reliability Engineering & System Safety*, 52(1):87–93.

[26] Zonta, D., Zandonini, R., and Bortot, F. (2007). A reliability-based bridge management concept. *Structures & Infrastructure Engineering*, 3(3):215–235.

9. Appendix

Table 2: Components of the identified mode shapes. The last columns indicate the torsional and bending fraction of the total displacement.

Biselli

First mode f=2.655Hz								
Position	v[m]	Position	v[m]	Position	v_0[m]	v_r[m]	Bending [%]	Torsion [%]
P1	0.006	P10	-0.003	C1	0.011	-0.005	68.18%	31.82%
P2	0.362	P9	0.340	C2	0.359	0.003	99.27%	0.73%
P3	0.507	P8	0.495	C3	0.501	0.006	98.83%	1.17%
P4	0.346	P7	0.356	C4	0.343	0.003	99.06%	0.94%
P5	-0.006	P6	0.016	C5	-0.005	-0.002	73.95%	26.05%
Second mode f=6.080Hz								
P1	0.077	P10	0.004	C1	0.014	0.063	18.64%	81.36%
P2	0.219	P9	-0.164	C2	0.085	0.134	38.87%	61.13%
P3	0.06	P8	-0.126	C3	-0.033	0.093	26.18%	73.82%
P4	-0.12	P7	-0.049	C4	-0.143	0.021	87.38%	12.62%
P5	0.023	P6	-0.049	C5	0.013	0.009	58.75%	41.25%
Third mode f=8.61Hz								
P1	-0.12	P6	0.012	C1	-0.106	-0.016	86.65%	13.35%
P2	-0.54	P7	0.455	C2	-0.474	-0.064	88.09%	11.91%
P3	0.01	P8	0.045	C3	0.028	-0.018	61.24%	38.76%
P4	0.551	P9	-0.410	C4	0.503	0.048	91.29%	8.71%
P5	0.028	P10	-0.090	C5	0.020	0.008	71.63%	28.37%

List of Figures

1 (a) Cross-section; (b) Detail of the rack and roller (RR) bearing; (c) Multidirectional Pot (MP) bearing. 4

2 (a) Layout of the experimental setup, where P_i indicates the positions of the accelerometer; (b) Experimental setup; (c) Force-Balance accelerometer used in the current experimental campaign; (d) Sample of a stabilization diagram. 5

3 Mode shapes representation of the first three stable modes of the Biselli bridge span. 6

4 Mode shapes representation of the first three stable modes of the Cerchiara 4 bridge span. 6

5 Mode shapes representation of the first three stable modes of the Cerchiara 7 bridge span. 7

6 Mode shapes representation of the first three stable modes of the Cretara bridge span. 7

Table 3: Components of the identified mode shapes. The last columns indicate the torsional and bending fraction of the total displacement.

Cerchiara No 4

Position	v[m]	Position	v[m]	Position	v_0[m]	v_r[m]	Bending [%]	Torsion [%]
First mode f=2.967Hz								
P1	0.030	P10	-0.015	C1	0.029	0.001	96.75%	3.25%
P2	0.350	P9	0.323	C2	0.358	-0.008	97.84%	2.16%
P3	0.506	P8	0.530	C3	0.518	-0.012	97.73%	2.27%
P4	0.312	P7	0.366	C4	0.317	-0.005	98.41%	1.59%
P5	-0.017	P6	0.028	C5	-0.016	-0.001	93.46%	6.54%
Second mode f=5.670Hz								
P1	0.128	P10	0.045	C1	0.072	0.056	56.32%	43.68%
P2	-0.337	P9	0.163	C2	-0.074	-0.263	21.97%	78.03%
P3	-0.621	P8	0.246	C3	-0.188	-0.433	30.22%	69.78%
P4	-0.470	P7	0.189	C4	-0.153	-0.316	32.67%	67.33%
P5	-0.060	P6	0.016	C5	-0.008	-0.053	12.57%	87.43%
Third mode f=8.152Hz								
P1	0.091	P6	-0.003	C1	0.069	0.022	75.95%	24.05%
P2	0.454	P7	-0.516	C2	0.462	-0.007	98.47%	1.53%
P3	-0.064	P8	-0.095	C3	-0.080	0.016	83.68%	16.32%
P4	-0.477	P9	0.469	C4	-0.497	0.019	96.27%	3.73%
P5	-0.017	P10	0.047	C5	-0.010	-0.007	59.40%	40.60%

Table 4: Components of the identified mode shapes. The last columns indicate the torsional and bending fraction of the total displacement.

Cecrchiara No 7

Position	v[m]	Position	v[m]	Position	v_0[m]	v_r[m]	Bending [%]	Torsion [%]
First mode f=2.678Hz								
P1	0.001	P10	-0.006	C1	0.006	-0.006	53.19%	46.81%
P2	0.347	P9	0.336	C2	0.355	-0.009	97.64%	2.36%
P3	0.502	P8	0.514	C3	0.508	-0.006	98.86%	1.14%
P4	0.340	P7	0.364	C4	0.338	0.002	99.42%	0.58%
P5	-0.008	P6	0.012	C5	-0.007	-0.001	90.51%	9.49%
Second mode f=6.303Hz								
P1	-0.022	P10	0.067	C1	0.010	-0.032	23.66%	76.34%
P2	-0.343	P9	0.266	C2	-0.050	-0.293	14.47%	85.53%
P3	-0.528	P8	0.374	C3	-0.077	-0.451	14.55%	85.45%
P4	-0.368	P7	0.244	C4	-0.051	-0.317	13.89%	86.11%
P5	-0.051	P6	0.042	C5	0.008	-0.059	11.69%	88.31%
Third mode f=8.355Hz								
P1	0.090	P6	0.068	C1	0.072	0.018	80.05%	19.95%
P2	-0.206	P7	0.414	C2	-0.240	0.034	87.46%	12.54%
P3	0.119	P8	0.115	C3	0.117	0.002	98.08%	1.92%
P4	0.302	P9	-0.274	C4	0.358	-0.056	86.49%	13.51%
P5	0.005	P10	0.054	C5	0.036	-0.031	53.76%	46.24%

Table 5: Components of the identified mode shapes. The last columns indicate the torsional and bending fraction of the total displacement.

Cretara

Position	v[m]	Position	v[m]	Position	v_0[m]	v_r[m]	Bending [%]	Torsion [%]
First mode f=3.564Hz								
P1	-0.022	P10	0.025	C1	-0.041	0.019	68.16%	31.84%
P2	-0.287	P9	-0.108	C2	-0.270	-0.017	94.05%	5.95%
P3	-0.407	P8	-0.277	C3	-0.342	-0.065	83.99%	16.01%
P4	-0.263	P7	-0.253	C4	-0.185	-0.078	70.47%	29.53%
P5	-0.112	P6	-0.060	C5	-0.044	-0.069	38.86%	61.14%
Second mode f=6.734Hz								
P1	-0.078	P10	0.095	C1	-0.012	-0.065	16.06%	83.94%
P2	-0.392	P9	0.295	C2	-0.083	-0.309	21.13%	78.87%
P3	-0.497	P8	0.355	C3	-0.071	-0.426	14.28%	85.72%
P4	-0.290	P7	0.226	C4	0.002	-0.293	0.84%	99.16%
P5	0.007	P6	0.053	C5	0.051	-0.044	53.50%	46.50%
Third mode f=8.628Hz								
P1	0.039	P6	0.090	C1	0.065	-0.025	71.76%	28.24%
P2	0.360	P7	-0.338	C2	0.323	0.037	89.66%	10.34%
P3	-0.054	P8	-0.124	C3	-0.089	0.035	71.82%	28.18%
P4	-0.390	P9	0.285	C4	-0.364	-0.026	93.38%	6.62%
P5	-0.094	P10	0.090	C5	-0.002	-0.092	1.92%	98.08%

Table 6: Components of the identified mode shapes. The last columns indicate the torsional and bending fraction of the total displacement.

Le Grotte

Position	v[m]	Position	v[m]	Position	v_0[m]	v_r[m]	Bending [%]	Torsion [%]
First mode f=2.661Hz								
P1	0.025	P10	0.007	C1	0.021	0.004	83.87%	16.13%
P2	0.361	P9	0.347	C2	0.360	0.002	99.56%	0.44%
P3	0.500	P8	0.493	C3	0.496	0.004	99.29%	0.71%
P4	0.351	P7	0.358	C4	0.349	0.002	99.47%	0.53%
P5	0.006	P6	0.017	C5	0.007	-0.001	87.14%	12.86%
Second mode f=6.291Hz								
P1	-0.037	P10	0.064	C1	-0.075	0.038	66.30%	33.70%
P2	0.009	P9	-0.107	C2	-0.103	0.112	47.90%	52.10%
P3	0.017	P8	-0.247	C3	-0.115	0.132	46.51%	53.49%
P4	0.051	P7	-0.215	C4	-0.028	0.079	26.14%	73.86%
P5	0.069	P6	-0.113	C5	0.067	0.002	96.47%	3.53%
Third mode f=8.307Hz								
P1	0.019	P6	0.167	C1	-0.074	0.093	44.30%	55.70%
P2	-0.275	P7	0.567	C2	-0.425	0.149	73.98%	26.02%
P3	0.011	P8	0.014	C3	0.013	-0.002	88.10%	11.90%
P4	0.237	P9	-0.574	C4	0.402	-0.165	70.92%	29.08%
P5	-0.054	P10	-0.167	C5	0.057	-0.110	33.90%	66.10%

7 Mode shapes representation of the first three stable modes of the Le Grotte bridge span. 7
8 Mode shapes representation of the first three stable modes of the San Nicola bridge span. 7
9 Mode shapes representation of the first three stable modes of the Temperino bridge span. 8
10 Decomposition od the response into a translational and rotational component. 8
11 Correlation between the elastic modulus obtained from static load tests and concrete samples and the natural frequencies of the first three modes. The dotted lines indicate the interpolation curves; The solid lines the theoretical predictions according to Equation (4). The grey region indicates the confidence bounds ($+2\sigma/-2\sigma$) of the Least Squares fitting. 10
12 (a)-(b) Probability Density Functions (PDF) and Cumulative Density Functions (CDF) of the elastic Moduli in terms of Gaussian and Weibull statistics; (c)-(d) PDF and CDF of the natural frequencies of the first bending modes in terms of Gaussian and Weibull statistics; 12
13 Bivariate normal density (a) and cumulative (b) distribution of the elastic Moduli and natural frequencies of the first bending modes. . . 13
14 (a) Posterior bivariate cumulative distribution in Equation (5); (b) Superposition of the prior distribution (dash-dot) and two section cuts of the posterior in (a). 15
15 Superposition of the prior distribution (dash-dot) and two section cuts of the posterior in terms of exceeding probability. 16
16 Flow chart of the proposed reliability-based procedure. 16

List of Tables

1 Correlation between the elastic modulus obtained from static load tests and concrete samples and the natural frequencies of the first three modes. 9
2 Components of the identified mode shapes. The last columns indicate the torsional and bending fraction of the total displacement. 20
3 Components of the identified mode shapes. The last columns indicate the torsional and bending fraction of the total displacement. 21
4 Components of the identified mode shapes. The last columns indicate the torsional and bending fraction of the total displacement. 21

5 Components of the identified mode shapes. The last columns indicate the torsional and bending fraction of the total displacement. 22
6 Components of the identified mode shapes. The last columns indicate the torsional and bending fraction of the total displacement. 22

Paper III

III A. Aloisio, D. Pasca, R. Tomasi, M. Fragiacomo (2020) Dynamic identification and model updating of an eight-storey CLT building. https://doi.org/10.1016/j.engstruct.2020.110593

Dynamic identification and model updating of an eight-storey CLT building

Angelo Aloisio[a,*], Dag Pasca[b,*], Roberto Tomasi[b], Massimo Fragiacomo[a]

[a] *Department of Civil, Construction-Architectural and Environmental Engineering, Università degli Studi dell'Aquila, Via G. Gronchi, 18, L'Aquila, 67100, Abruzzo, Italy*
[b] *Faculty of Science and Technology, Norwegian University of Life Sciences, Oslo, Norway*

Abstract

So far, few in situ tests have been carried out to estimate the modal parameters of multi-storey Cross-Laminated-Timber (CLT) buildings: the understanding of their dynamic behaviour under operational conditions is still an open issue. In this paper, the results of the dynamic identification of an eight-storey CLT building are reported and interpreted in the light of a simplified shear-type analytical model. The structural model is calibrated on the experimental modal parameters, which are assessed using the Stochastic Subspace Identification (SSI). The SSI provides mode shapes, natural frequencies and damping factors of the structures in its first linear response range; The minimum of a modal-based objective function gives an estimation of the unknown parameters of the structural model. Given the results of the dynamic identification, the storey-masses are the chosen optimization parameters: the values of the experimental eigenfrequencies likely reveal a continuum-like behaviour of the building without connections. The identified storey masses are indeed realistic and confirm the negligible role of the connections in the low-amplitude dynamic response. The nonlinear effects of connections over the building response to higher displacements are discussed, providing simplified and practice-oriented correlations for the first natural frequency estimation.

Keywords: Dynamic Identification; Model Updating; CLT buildings; Nonlinear response

1. Introduction

Developments at the beginning of the 20th century made it possible to use reinforced concrete economically, and traditional timber constructions [1, 2] (log or stave

*Corresponding author.
Email addresses: angelo.aloisio1@graduate.univaq.it (Angelo Aloisio), dag.pasquale.pasca@nmbu.no (Dag Pasca), roberto.tomasi@nmbu.no (Roberto Tomasi), massimo.fragiacomo@univaq.it (Massimo Fragiacomo)

construction or lattice work) were successively superseded by the mineral-based solid construction materials concrete and brick, at least in Europe [3]. However, over the last 10 years or so, timber has recaptured market shares from the mineral-based solid construction materials, in particular in the fields of residential buildings, office buildings and schools but also other fields of construction. One reason for this development is the increasing interest in high-rise structures: the so-called "tall buildings". They require a higher level of seismic performance, leading to the use of massive and more effective systems, such as Cross-Laminated Timber (CLT) [4]. However, for the construction of larger and taller CLT buildings, it is necessary to understand their dynamic behaviour: movements, which may be acceptable for small heights and spans, are magnified in large structures, and may cause discomfort to building occupants, damage to non-structural elements, or increased loads on elements [5].

Aside from a few studies [5–8], the majority of research into the dynamic response of multi-storey CLT buildings has been under seismic loading: experiments and numerical modelling of CLT have been deeply investigated [4, 9–12], but the response to small-amplitude vibration is still an open issue. Reynolds et al. [5] obtained the modal parameters of a five-storey CLT building with an internal RC core. To fill a gap in knowledge, the authors present the dynamic identification of an eight-storey CLT building with a CLT core.

The estimate of the modal parameters of multi-storey CLT buildings' response under operational conditions from *in situ* tests is useful to understand the gap between the possibly linear dynamic response to service loading and nonlinear behaviour under seismic excitation. This gap is much wider for CLT buildings rather than concrete or steel buildings since the bearing resistance to lateral loads is concentrated in the connections (hold-downs and angle brackets e.g.), which are used for the building assemblage. The main objectives of this paper are: (i) the estimation of the modal parameters of an eight-storey CLT building from Output-Only dynamic identification; (ii) the updating of an elementary analytical model of the building to the experimental modal parameters; (iii) the assessment of the role of the connection nonlinearities on the building's dynamic response in operational conditions; (iv) the derivation of simplified and practice-oriented correlations useful for the assessment of natural frequencies and damping factors of CLT buildings at a low-level response.

2. Test building description

The eight-story case study building (Fig.1(a)) is in the NMBU campus (Norwegian University of Life Science), located in Ås, Norway. It has eight storeys with a total height of 26.9 m and is rectangular in plan (23.21 m × 15.11 m), with a CLT core at the centre. A plan of the building, indicating its structure, is shown in Fig.1(c), and an elevation showing the floor levels is given in Fig.1(b).

The tested building is made of large monolithic walls with high length-to-height ratios, assembled by tie-downs and shear connectors.

Table 1: Basic characteristics of the tested building [13].

Parameter	**Value**	**Unit**
Lenght	23.21	m
Width	15.11	m
Height	26.9	m
No. of floors	8	
Rooms	127	
Net area /floor	350.55	m^2
Net area /building	2804.4	m^2
CLT wall panels	3 layers-90 mm 5 layers-100,120,130, 140,160,180 mm	
CLT floor panels	5 layers-180,220 mm	
CLT roof panels	5 layers-200 mm	
Wood amount-total	907.62	m^3
Hold-downs steel plates	6225.73	Kg
Shear steel plates	1919	Kg
Self-tapping screws	6124	
Steel brackets	≈390	

The total lengths of the designated shear walls in the longitudinal and transverse directions are approximately 21,5m and 25m, respectively, excluding the partition walls, see Fig.1(d) [13]. Shear forces are being distributed using shear plates and brackets while long steel plates, ranging from the foundation to the roof, are placed at each end of the shear walls [13]. The main characteristics of the building are reported in Tab.1. The building currently houses student apartments in eight floors of similar layout.

3. Dynamic identification

The Stochastic Subspace identification method is used for the estimate of modal parameters from Output Only measurements [14–16].

(a)

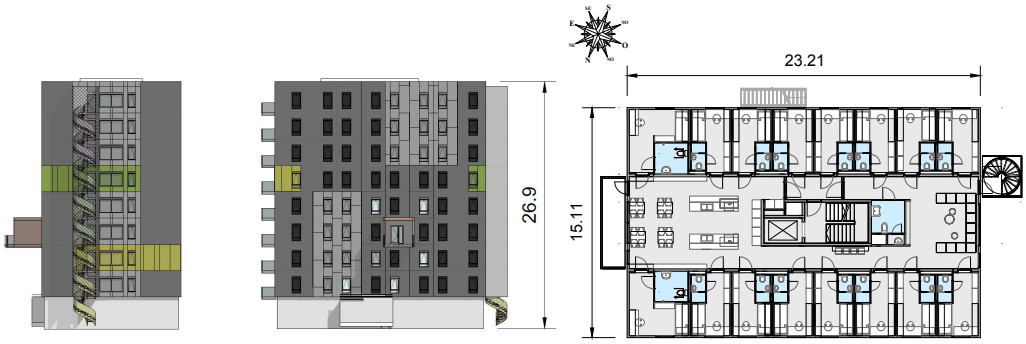

(b) (c)

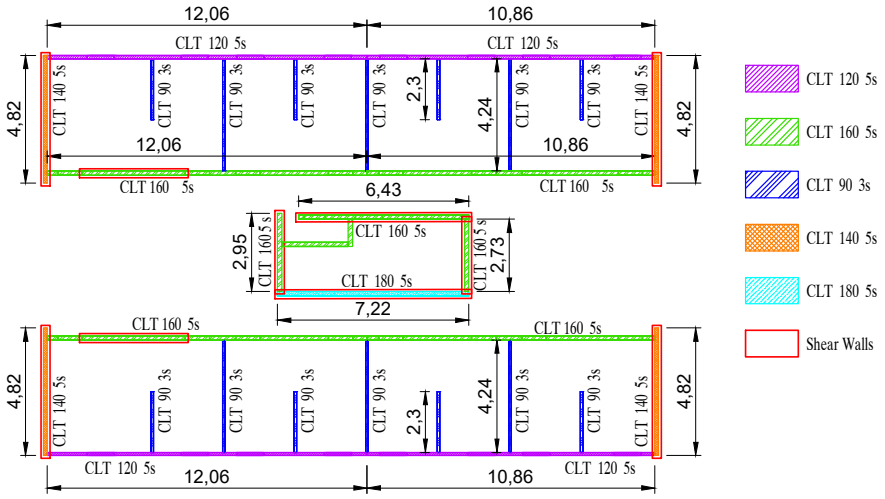

(d)

Figure 1: (a) North view of the building; (b) Prospects and plan (c)-(d) of the building.

3.1. Theoretical background

The SSI technique is a classical covariance-driven stochastic realization algorithm, namely the Principal Component algorithm [17, 18], also known as the covariance-driven SSI algorithm (SSIcov), that was generalized to a reference-based version (SSI-cov/ref) by Peeters and De Roeck [19–22].

State-space representation of output-only vibration-based structural monitoring corresponds to the following discrete time model

$$\begin{aligned} x_{k+1} &= Ax_k + v_k \\ y_k &= Cx_k + w_k \end{aligned} \tag{1}$$

with the states $x_k \in \mathbb{R}^n$, the outputs $y_k \in \mathbb{R}^r$, the state transition matrix $A \in \mathbb{R}^{n\times n}$ and the observation matrix $C \in \mathbb{R}^{r\times n}$, where r is the number of sensors and n is the system order. The excitation v_k is an unmeasured Gaussian white noise sequence with zero mean and constant covariance matrix $Q = \boldsymbol{E}(v_k v_k^T) \stackrel{\text{def}}{=} Q\delta(k-k')$, where $\boldsymbol{E}(\cdot)$ denotes the expectation operator and w_k is the measurement noise.

The algorithm starts with the construction of a block Toeplitz matrix of output covariance matrices, constructed with the l measured outputs and the r reference outputs:

$$L_{l,i}^{\text{ref}} \stackrel{\text{def}}{=} \begin{bmatrix} \Lambda_i^{\text{ref}} & \Lambda_{i-1}^{\text{ref}} & \dots & \Lambda_1^{\text{ref}} \\ \Lambda_{i+1}^{\text{ref}} & \Lambda_i^{\text{ref}} & \dots & \Lambda_2^{\text{ref}} \\ \vdots & \vdots & \ddots & \vdots \\ \Lambda_{2i-1}^{\text{ref}} & \Lambda_{2i-2}^{\text{ref}} & \dots & \Lambda_i^{\text{ref}} \end{bmatrix}, L_{l,i}^{\text{ref}} \in \mathbb{R}^{il\times ir} \tag{2}$$

where $\Lambda_j^{\text{ref}} = \boldsymbol{E}(y_k y_k^{\text{ref}\,T})$ is the covariances between all outputs y_k and some reference outputs. This matrix decomposes as

$$L_{l,i}^{\text{ref}} \stackrel{\text{def}}{=} \begin{bmatrix} C \\ CA \\ \vdots \\ CA^{i-1} \end{bmatrix} \begin{bmatrix} A^{i-1}G^{\text{ref}} & A^{i-2}G^{\text{ref}} & \dots & G^{\text{ref}} \end{bmatrix} \stackrel{\text{def}}{=} O_i C_i^{\text{ref}} \tag{3}$$

where $O_i \in \mathbb{R}^{il\times n}$ is called the extended observability matrix, $C_i^{\text{ref}} \in \mathbb{R}^{n\times ir}$ the reference-based stochastic controllability matrix, $G^{\text{ref}} = A\Sigma C^{\text{ref}T}$, $\Sigma = \boldsymbol{E}[x_k x_k^T]$ and n is the system order. The system matrices $A \in \mathbb{R}^{n\times n}$ and $C \in \mathbb{R}^{n\times l}$ can be derived as follows:

$$\begin{aligned} A &= (S_2 O_i)^{\dagger}(S_1 O_i) \\ C &= S_3 O_i \end{aligned} \tag{4}$$

where S_1, S_2 and S_3 are selection matrices:

$$S_1 = [0_{(i-1)l\times l} I_{(i-1)l}]; S_2 = [I_{(i-1)l} 0_{(i-1)l\times l}]; S_3 = [I_l 0_{l\times(i-1)l}] \tag{5}$$

The system's modal parameters (eigenfrequencies, damping ratios and mode shapes) can be calculated from the identified system description A, C.

$$A = \Psi\Lambda\Psi^{-1},\ A\psi_i = \lambda\psi_i \tag{6}$$

The undamped eigenfrequencies f_i and damping ratios ξ_i in % can be calculated from the dicrete-time poles λ_{ci}:

$$\lambda_{ci} = \frac{ln(\lambda_i)}{\Delta T},\ f_i = \frac{|\lambda_{ci}|}{2\pi},\ \xi_i = -100\frac{\lambda_{ci}^R}{|\lambda_{ci}} \tag{7}$$

where $|\cdot|$ denotes the complex modulus and $\lambda_{ci} = \lambda_{ci}^R + i\lambda_{ci}^I$. The observed part of the eigenvectors ψ_i leads to the experimental mode shapes ϕ_i:

$$\Phi = C\Psi,\ \phi_i = C\psi_i \tag{8}$$

3.2. Experimental setup

On October 25, 2019, the structure was subject to ambient vibration measurements. A set of 10 piezoelectric accelerometers was used Fig.2(a): 6 accelerometers, which provided a reference location [23], were placed on the rooftop, see Fig.2(c), while the other 4 were placed in the inferior floors in the 1 and 2 measurement points, Fig.2(c). Specifically, four tests were then carried out and five floors were tested, from the roof to the 5th elevation. The accelerometers were arranged to measure acceleration in two orthogonal directions, Fig.2(b). In order to confirm the

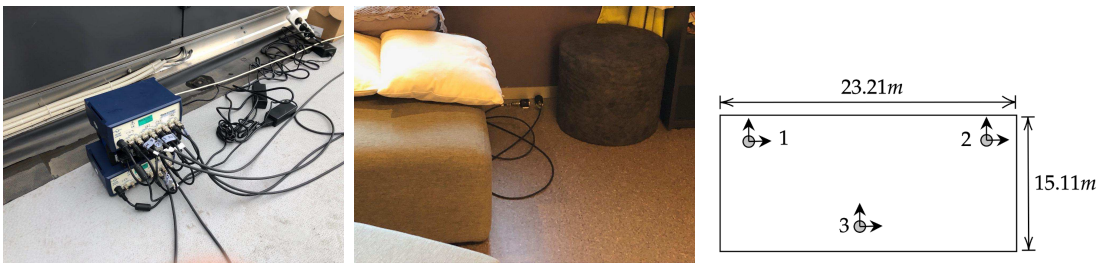

(a) (b) (c)

Figure 2: (a) Signal conditioner and DAQ system of the 10 IEPE piezoelectric accelerometers; (b) View of a couple of accelerometers measuring in two orthogonal directions; (c) Schematic view of the experimental setup of the rooftop.

assumption of horizontal rigid diaphragms, a redundant number of measurements

points on each floor was used.
The accelerometers PCB model 393B12 have a sensitivity of approximately 10000 mV/g, a frequency range from 0.15 Hz to 1000 Hz and a measurement range up to 10 m/s^2. The data were sampled at a rate of 100 Hz. The cut-off frequency of the anti-aliasing filter was set to 10 Hz. The number of samples was set to N=360000, which resulted in a measurement time of 1 hour. Data from multi-setup measurements (4 setups) were then merged following the approach recalled in. [24].

3.3. Results

Three stable frequencies clearly arise from the stabilization diagram [19] in the frequency range 0-10 Hz, Fig.3(d). The first three modes are evidenced by the peaks of the FFT of the signals in two orthogonal sensors, Fig.3(b)-(c). The variance of the acquired signal is approximately equal to $1.4 \times 10^{-5}\ m/s^2$ Fig.3(a): the low excitation is due to the wind, which blew at an approximate speed of $6\,Km/h$ with a NNE direction. The first two modes are translational: the very first at $1.913\,Hz$,

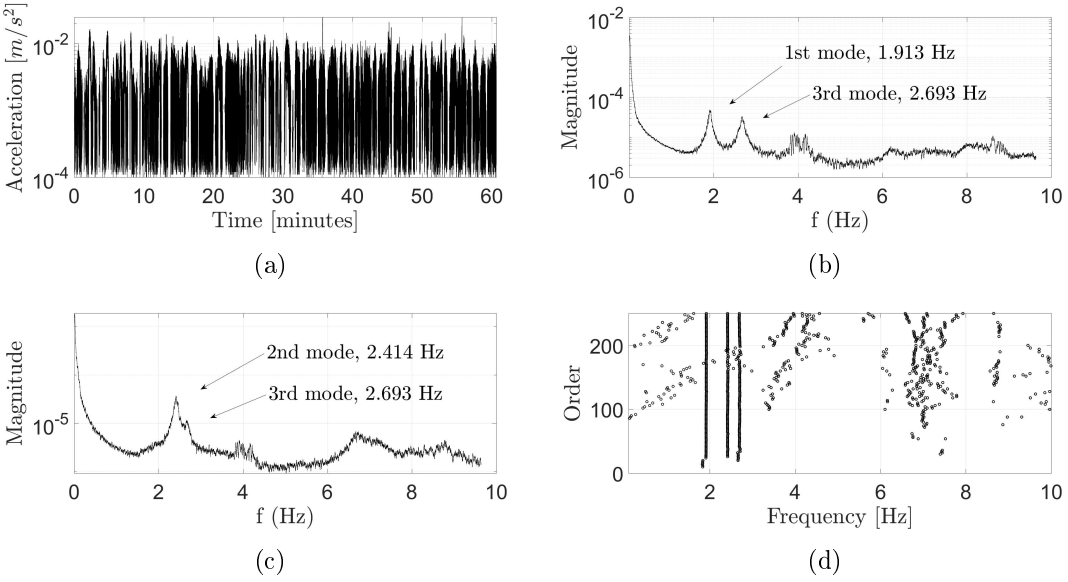

Figure 3: (a) Acceleration time-history of a reference accelerometer placed on the rooftop; (b)-(c) FFT of the signals in two orthogonal directions; (d) Stabilization diagram of the merged signals. The stabilization criteria are: $\delta f_i \leq 1\%$, $\delta \xi_i \leq 1\%$, MAC<1% [25].

Fig.4(a), is a translation parallel to the direction of minor inertia of the building; The second mode at $2.414\,Hz$ is a translation in the orthogonal direction, Fig.4(b). The third mode at $2.688\,Hz$ can be regarded as the first torsional mode, Fig.4(c). The damping factors range between 1.2-1.9%: the first modes are less damped than the other two, whose damping is almost close to 2%. Besides, a 2% damping can be considered in accordance with the standards predictions [26]. Two relevant aspects should be remarked:

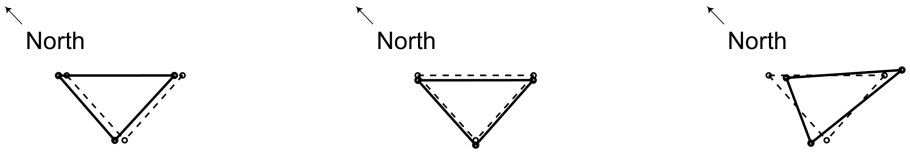

(a) 1st mode1.913 Hz; ξ = 1.216% (b) 2nd mode 2.414 Hz; ξ = 1.916% (c) 3rd mode 2.688 Hz; ξ = 1.921%

Figure 4: Natural frequencies, damping factors and mode shapes of the three stable modes in the frequency range $0 - 10\,Hz$ corresponding to the roof setup.

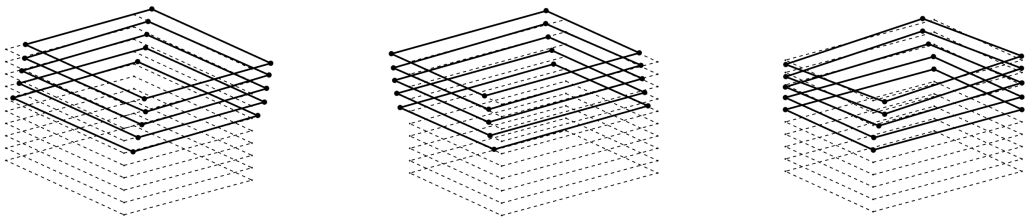

(a) 1st mode (b) 2nd mode (c) 3rd mode

Figure 5: Natural frequencies, damping factors and mode shapes of the three stable modes in the frequency range $0 - 10\,Hz$ corresponding to merged data sets.

- The CLT floors behave like rigid diaphragms;
- As later evidenced by the model updating, the natural frequencies are very high, as if the global stiffness of the building was due to the in-plane deformability of the sole CLT panels, without the contribution of the connections. At a very low vibration level, the building may behave like a rigid "box-like" structure: the amplitude of the excitation might not be enough to activate the uplift of the tie-downs nor to overcome the initial slip of the shear connectors.

The behaviour of timber structural systems and their connections is substantially nonlinear at low loads as well as high [6], as evidenced by experimental cyclic tests on CLT panels; However, very low excitation levels, like the ones of the current tests, are not considered in experimental cyclic tests [9]: below a certain displacement threshold, the CLT building may behave almost linearly, like a continuum.
However, the assessment of the nonlinear or possibly non-stationary behaviour of CLT buildings in operational conditions cannot be derived from dynamic identification tests. A continuous monitoring would be needed to appreciate the actual behaviour at low vibration levels under different values of the excitation (wind, e.g.). So far, there is a lack of knowledge on the Structural Health Monitoring

(SHM) of high-rise CLT buildings and more researches on this topic are needed.

Given the diaphragm-like behaviour of the CLT floors, a linear analytical model is used to interpret the experimental results and better understand the aspects remarked in this section. Detailed modelling of the CLT building is an important issue to be investigated in future researches, but it is not the purpose of this paper.

4. Model updating

An elementary shear-type 3-D building model [27] is presented and then calibrated to the experimental results by minimizing a proper objective function. The values of the experimental eigenfrequencies and the considerable in-plane stiffness of the CLT floors drove the choice towards the stiffest structural model: the shear-type one. However, the availability of accelerometers in the out-of-plane floor direction would have let to rigorously assess the approximation in using the shear-type rather than the cantilevered model. In practical situations, the selection of the structural model can profoundly affect the prediction of dynamic properties [28, 29], yielding a wide range of natural frequencies. For this reason, the designer should carefully ponder the choice of the model based on the expected structural response in relation with the considered limit state and the type of excitation (wind, seismic load, e.g.).

4.1. Model description

The equations of motion of a generic 2D storey are derived, then the resulting mass and stiffness matrices are assembled into the mass and stiffness matrices of the whole structure.
It is assumed that a generic storey is supported by N structural elements. The

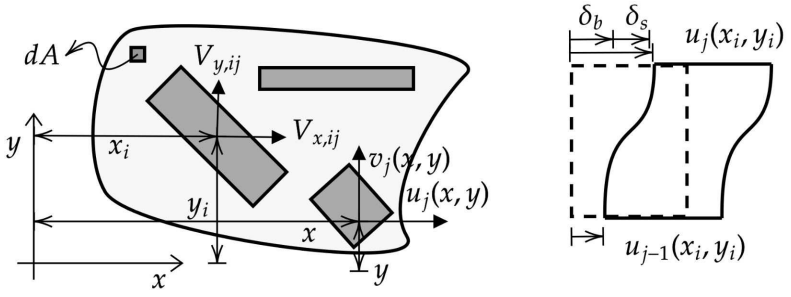

Figure 6: Plan view of a general configuration of the bearing walls of the j-th storey.

equilibrium (Eq.9), compatibility (Eq.10) and constitutive (Eq.11) equations of a

j-th storey can be written as:

$$\begin{gathered}\sum_{i=1}^{N} V_{x,ij} + \int_{A_j} \rho_j(x,y)\, \ddot{u}_j(x,y)\, dA = 0 \\ \sum_{i=1}^{N} V_{y,ij} + \int_{A_j} \rho_j(x,y)\, \ddot{v}_j(x,y)\, dA = 0 \\ -\sum_{i=1}^{N} V_{x,ij} y_i + \sum_{i=1}^{N} V_{y,ij} x_i + \int_{A_j} \rho_j(x,y)\, y\, \ddot{u}_j(x,y)\, dA - \int_{A_j} \rho_j(x,y)\, x\, \ddot{v}_j(x,y)\, dA = 0\end{gathered} \tag{9}$$

$$\begin{aligned} u_j(x,y) &= u_{0j} - \theta_j y \\ v_j(x,y) &= v_{0j} + \theta_j x \end{aligned} \tag{10}$$

$$\begin{aligned} V_{x,ij} &= k_{x,ij}\left(u_j(x_i,y_i) - u_{j-1}(x_i,y_i)\right) \\ V_{y,ij} &= k_{y,ij}\left(v_j(x_i,y_i) - v_{j-1}(x_i,y_i)\right) \end{aligned} \tag{11}$$

where $V_{x,ij}$ and $V_{y,ij}$ are the shear components in the x and y direction of the i-th wall of the j-th storey, $\rho_j(x,y)$ is the mass per unit square, $u_j(x,y)$ and $v_j(x,y)$ are the displacement components in the x and y direction, dA is the infinitesimal element area and A_j the total area of the storey, Fig.(6).
The compatibility equations are written assuming the diaphragm-like behaviour of each floor, while the constitutive equations are based on the estimation of two shear stiffness values in the x and y directions, $k_{x,ij}$ and $k_{y,ij}$ respectively, concentrated in the centre of mass of each wall. The undamped equilibrium equations of the j-th storey in terms of displacements can be then written as follows:

$$M_j \ddot{v}_j + K_j v_j = 0 \tag{12}$$

$$v_j = \begin{bmatrix} u_{0,j} \\ v_{0,j} \\ \theta_j \end{bmatrix}^{\mathrm{T}} \quad M_j = \begin{bmatrix} M_{xx,j} & 0 & -M_{xy,j} \\ 0 & M_{yy,j} & M_{yx,j} \\ -M_{xy,j} & M_{yx,j} & I_{M,j} \end{bmatrix} \quad K_j = \begin{bmatrix} K_{xx,j} & 0 & -K_{xy,j} \\ 0 & K_{yy,j} & K_{yx,j} \\ -K_{xy,j} & K_{yx,j} & I_{K,j} \end{bmatrix} \tag{13}$$

where $M_{xx,j} = M_{yy,j} = \int_{A_j} \rho_j(x,y) dA$, $M_{xy,j} = \int_{A_j} y \rho_j(x,y) dA$, $M_{yx,j} = \int_{A_j} x \rho_j(x,y) dA$, $I_{M,j} = \int_{A_j} (x^2 + y^2)\, \rho_j(x,y) dA$, $K_{xx,j} = \sum_{i=1}^{N} x_i^2 k_{x,ij}$, $K_{yy,j} = \sum_{i=1}^{N} y_i^2 k_{y,ij}$, $I_{K,j} = \sum_{i=1}^{N} (x_i^2 k_{x,ij} + y_i^2 k_{y,ij})$, $K_{xy,j} = \sum_{i=1}^{N} x_i y_i k_{x,ij}$, $K_{yx,ji} = \sum_{i=1}^{N} y_i x_i k_{y,ij}$.
If L is the number of storey, the equilibrium equations in terms of the displacement vector are:

$$M \ddot{v} + K v = 0 \tag{14}$$

$$v = \begin{bmatrix} v_1 \\ \vdots \\ v_L \end{bmatrix}^{\mathrm{T}} \quad M = \begin{bmatrix} M_1 & 0 & \dots & 0 \\ 0 & M_2 & \dots & 0 \\ \vdots & \vdots & \ddots & \vdots \\ 0 & 0 & \dots & M_L \end{bmatrix} \quad K = \begin{bmatrix} K_1 & -K_2 & \dots & 0 \\ -K_2 & K_1 + K_2 & \ddots & \vdots \\ \vdots & \ddots & \ddots & -K_{L-1} \\ 0 & \dots & -K_{L-1} & K_L \end{bmatrix} \tag{15}$$

The modal parameters of this model are obtained from the eigenstructure of Eq.(14).

4.2. Model updating

To measure the distance between the estimated modal parameters and the numerical ones, the following objective function is used [30]:

$$C = \sum_{i=1}^{M} \gamma_i \left(\frac{\omega_i^m - \omega_i^c}{\omega_i^m} \right)^2 + \beta \sum_{i=1}^{M} (1 - diag(MAC(\Phi_i^m, \Phi_i^c))) \tag{16}$$

where the apex $(*)^m$ indicates a measured variable, the apex $(*)^c$ a calculated variable, Φ_i is the mode shape vector, M is the number of modes, MAC is the modal assurance criterion [31], while γ_i and β are weighting factors. The weighting factors are set equal to one. Since the storeys are almost identical among each other, except for the roof, the mass of a generic storey M_{storey}, and that of the roof M_{roof} are set as estimand parameters in the optimization. The main reasons for this choice are:

- The mass is known with greater uncertainty than the geometry and stiffness of the CLT walls, whose properties are known from the producer. Except for the self-weight of the CLT floors, the variable load (people, furniture, e.g.) is almost unknown and non-stationary;
- The optimization of both stiffness and mass, based on the natural frequencies and un-scaled mode shapes, may stand as an undetermined problem: the eigenfrequencies depend on the ratio between rigidity and weight; Theoretically, infinite couples of rigidity and weight values could be possible candidates for the optimization.

The computation of the equivalent rigidity of the CLT walls [32–34] is based on the longitudinal and shear elastic moduli declared by the producer. The bending stiffness is calculated considering only the vertical layers and an equivalent shear modulus takes into account the torsional deformation of the lamellae. Specifically, both the shear and the bending deformation of the walls are taken into account in the following:

$$k_{CLT} = \left(\frac{h^3}{12\,EI} + \frac{1.2h}{GA} \right)^{-1} \tag{17}$$

where h is the inter-storey height, E the Elastic modulus, G the shear modulus and A the cross sectional area of the wall.
To reduce the number of modelling simplifications, the entire mass of the storeys is assumed unknown (M_{storey} e M_{roof}). The authors estimated the minimum of the objective function by evaluating the objective function in a discretized domain with a 0.1 KN step. The contour plot of the objective function is shown in Fig.7, the "X" indicates the minimum of the function. The optimized parameters are itemized in Tab.4.

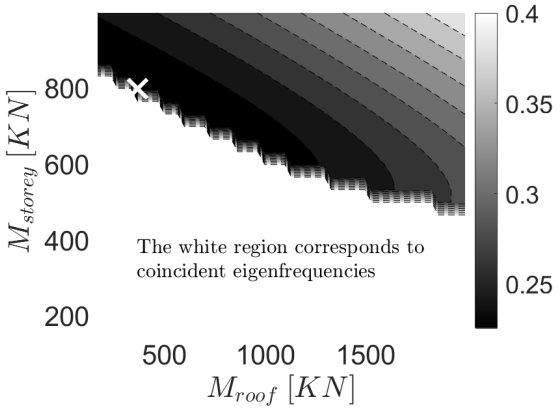

Figure 7: Contour plot of the objective function.

Table 2: Weight values estimated from updating.
Mass

Description	KN	KN/m^2
Roof	365.6	1.042
j-th storey	797.7	2.275
Self Weight of the j-th storey	350.7	1.000
Variable and permanent of the roof	14.9	0.042
Variable and permanent load of the j-th floor	447.0	1.275

Table 3: Comparison between the expected and estimated Self-Weight of the roof

Description	Estimated value	Expected value
Self Weight of the j-th storey [KN/m^2]	1.000	1.100

To evaluate the portion of the storey mass due to the variable and permanent load, the self-weight of the CLT floors is assumed known and subtracted from the M_{storey} and M_{roof} values, Tab.4.
Tab.3 reports the estimated and expected values of the self-weight of the generic floor: the two values are almost coincident. The self-weight of j-th generic floor is

Table 4: Comparison between the experimental and numerical modal parameters.

	Experimental		Numerical	
Mode shapes	**f[Hz]**	ξ **[%]**	**f[Hz]**	**MAC**
1st translational mode	1.913	1.216	1.867	0.99
2nd translational mode	2.414	1.916	2.543	0.98
1st torsional mode	2.693	1.921	2.712	0.92

close to the estimated mass of the roof. This is true, since the sole extra load on the roof was due to the thermal insulation coating and the ventilation system.

5. Discussion

Direct methods or indirect methods can drive the assessment of the role of the connections. The direct method directly estimate the stiffness of the connections by updating all modelling parameters. The indirect method, followed in this paper, derives from proving hypothesis through tests. Let assume a continuum-like behaviour of the building (hypothesis): the connections are neglected in the model updating process (test). If the updated masses match with the expected ones, the hypothesis is proven (proof). In the following part, the authors discuss the causes of the obtained results. Most of the scholars pursue a direct and more conventional approach: a Finite Element Model of the building would have driven the optimization of both the storey masses and the stiffness of the connections. The obtained parameters would have then provided a direct assessment of the role of the connections.

5.1. The role of connections

Comparing the measured natural frequencies with those calculated from the numerical model, it appears that the connections do not significantly contribute to the low-amplitude dynamics. The modal parameters of the numerical model with infinitely rigid connections, in fact, are in great accordance with the experimental ones.

Theoretically, the possible nonlinear response of the building could be evidenced at a very low-level response, when the uplift of the CLT walls arises. Recurring to the experiments by Gavric et al. [9, 35], the ratio between the uplift stiffness at a very first stage, estimated by the tangent to zero of the backbone curve in Fig.8, and the elastic rigidity estimated from Eq.(17) is approximately:

$$r = \frac{k_{uplift}}{k_{elastic}} \approx \frac{11606\,\mathrm{KN/m}}{39387\,\mathrm{KN/m}} = 0.29\% \tag{18}$$

It follows that the CLT building may exhibit important frequency shifts even at the low-level dynamics. This phenomenon (uplift, rocking [36, 37] e.g.) could be easily

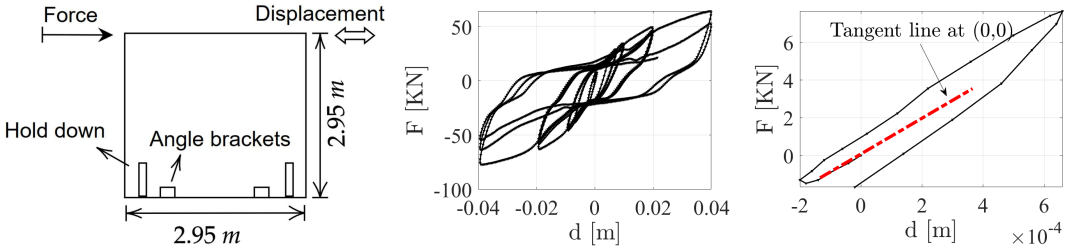

(a) (b) (c)

Figure 8: (a) Layout of the CLT panels tested by Gavric et al. [9]; (b) Hysteresis loops of the tested panel; (c) Representation of the first steps of the cyclic tests shown in (b): the dotted line is the tangent to zero.

estimated from continuous monitoring under different operational conditions (e.g. wind speed). Besides, given the difference between the elastic and the uplift rigidity Fig.9, the model updating with a $\approx 0.3\%$ of the elastic stiffness would lead to an non-realistic increment of the storey masses. Fig.9 is an oversimplification, analytical

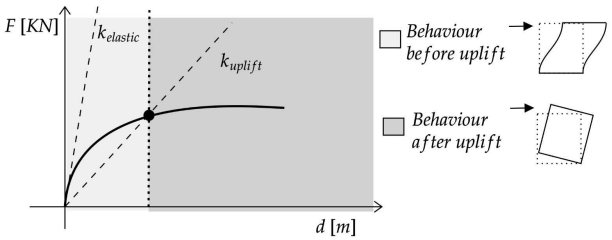

Figure 9: Schematic representation of the CLT wall panel behaviour.

prediction models were discussed by [9, 38]. According to Gavric et al. [9] the lateral displacement on top of a CLT wall can be divided into several contributions: (i) rocking deformation, (ii) sliding deformation, (iii) bending deformation, (iv) shear deformation. However, the incremental deformation due to vertical elongation of the wall anchorage, which is further considered by the Canadian Standard Association [39], is likely to be negligible in operational conditions.

5.2. Correlations to the building height

As evidenced in the previous section, several factors, peculiar of the considered CLT building, may determine the eigenfrequencies in Tab.4:

- Negligible influence of the connections in the very low intensity dynamics;
- High stiffness to weight ratio of CLT panels;

- Redundancy of structural components [13].

The straightforward estimation of the first natural frequency may be important for practitioners: to perform static seismic analyses, in fact, national codes provide a simplified equation for estimating the main frequency of a structure.
The formulations proposed by ASCE 07-16 (2017) [40] and the former Italian Seismic Code [41] are similar (Eq.(19)), while that of the Spanish Code [42] is more complete Eq.(20):

$$f_1(H) = \frac{1}{C_1 H^{3/4}} \tag{19}$$

$$f_1(H) = \frac{\sqrt{H}}{C_2 H \sqrt{\frac{H}{(2L+H)}}} \tag{20}$$

where C_1 and C_2 are constants, H is the building height in metres, L the plan dimension along the direction of oscillation in metres. The current Italian Seismic Code [43] proposes a different formulation:

$$f_1(d) = \frac{1}{2\sqrt{d}} \tag{21}$$

where d is the lateral elastic displacement of the highest point of the structure under the seismic action. The constants C_1, computed by setting f_1 equal to the first experimental eigenfrequency, and C_2, estimated from an Ordinary Least Squares Operator are reported in Tab.5. C_1 is very close to the proposed value for masonry

Table 5: Estimated constants of Eq.(19)-(20) based on the results in Tab.4.

C_1	0.0443
C_2	0.1100

$C_1 = 0.0488$. This might be due to the sharing of a wall-based structure in both typologies, CLT and masonry. It must be remarked that the use of the first eigenfrequency based on simplified formulations is mainly devoted to static linear analysis; Static linear analysis are highly conventional approaches, given the uncertainties on the seismic action estimation and the linear approximations of the structural behaviour.

5.3. Damping estimation

The damping factors estimated by Reynolds at al. [5], which span in the range 4.7-7%, are sensibly higher than those in Tab.4. In particular, the damping factors of the building under test are very close to the damping of timber itself, which is about 2%. However, the building tested by [5] has a RC core, while the current

building has a CLT one. Hence, the RC core might sensibly increase the damping factor, from that of CLT to that of concrete.

6. Conclusions

The results of the dynamic identification in operational conditions of an eight-storey CLT building are interpreted in the light of an elementary analytical model. Three stable modes are detected, two translational and one torsional: the diaphragm-like behaviour of the CLT floors is clearly evidenced by the mode shapes. The analytical model is calibrated on the experimental eigenstructure using a proper objective function, whose estimand parameters were the masses of the storeys. Given the accordance with the analytical model, the building is likely to behave linearly at a very low vibration level, when the contribution of the connections is not activated. However, the contribution of the connections to the global dynamics may possibly be observed by continuous dynamic monitoring under different vibration-induced levels. The first eigenfrequency matches well with that estimated from empirical relations tuned to masonry structures: this may be due to the wall-based construction typology, recurring in both masonry and CLT structures. The damping factors, which span in the range 1.2-1.9%, are very close to those of timber.
The authors will attempt to further investigate the behaviour of tall CLT buildings from Continuous Dynamic Monitoring of this structure.

7. Acknowledgements

The authors thank Andreas S. Fløe, SiÅs and Thomas K. Thiis for their kind support.

References

[1] A. Aloisio, M. Fragiacomo, and G. D'Alò, "The 18th-century baraccato of l'aquila," *International Journal of Architectural Heritage*, pp. 1–15, 2019.

[2] A. Aloisio, M. Fragiacomo, and G. D'Alò, "Traditional tf masonries in the city centre of l'aquila–the baraccato aquilano," *International Journal of Architectural Heritage*, pp. 1–18, 2019.

[3] R. Brandner, G. Flatscher, A. Ringhofer, G. Schickhofer, and A. Thiel, "Cross laminated timber (clt): overview and development," *European Journal of Wood and Wood Products*, vol. 74, no. 3, pp. 331–351, 2016.

[4] M. Izzi, D. Casagrande, S. Bezzi, D. Pasca, M. Follesa, and R. Tomasi, "Seismic behaviour of cross-laminated timber structures: A state-of-the-art review," *Engineering Structures*, vol. 170, pp. 42–52, 2018.

[5] T. Reynolds, D. Casagrande, and R. Tomasi, "Comparison of multi-storey cross-laminated timber and timber frame buildings by in situ modal analysis," *Construction and Building Materials*, vol. 102, pp. 1009–1017, 2016.

[6] T. Reynolds, R. Harris, W.-S. Chang, J. Bregulla, and J. Bawcombe, "Ambient vibration tests of a cross-laminated timber building," *Proceedings of the Institution of Civil Engineers-Construction Materials*, vol. 168, no. 3, pp. 121–131, 2015.

[7] T. Reynolds, R. Harris, and W. Chan, "Dynamic response of tall timber buildings to wind load," in *35th Annual Symposium of IABSE/52nd Annual Symposium of IASS/6th International Conference on Space Structures, London*, 2011.

[8] I. Mugabo, A. R. Barbosa, and M. Riggio, "Dynamic characterization and vibration analysis of a four-story mass timber building," *Frontiers in Built Environment*, vol. 5, p. 86, 2019.

[9] I. Gavric, M. Fragiacomo, and A. Ceccotti, "Cyclic behavior of clt wall systems: Experimental tests and analytical prediction models," *Journal of Structural Engineering*, vol. 141, no. 11, p. 04015034, 2015.

[10] A. Ceccotti, C. Sandhaas, M. Okabe, M. Yasumura, C. Minowa, and N. Kawai, "Sofie project–3d shaking table test on a seven-storey full-scale cross-laminated timber building," *Earthquake Engineering & Structural Dynamics*, vol. 42, no. 13, pp. 2003–2021, 2013.

[11] G. Rinaldin and M. Fragiacomo, "Non-linear simulation of shaking-table tests on 3-and 7-storey x-lam timber buildings," *Engineering Structures*, vol. 113, pp. 133–148, 2016.

[12] M. Follesa, I. Christovasilis, D. Vassallo, M. Fragiacomo, and A. Ceccotti, "Seismic design of multi-storey clt buildings according to eurocode 8. ingegneria sismica," *International Journal of Earthquake Engineering, Special Issue on Timber Structures*, vol. 30, 2013.

[13] I. Lukacs, A. Björnfot, T. Tsalkatidis, and R. Tomasi, "Structural redundancy in cross-laminated timber buildings," *Proceedings of the World Conference on Timber Engineering WCTE2016*.

[14] A. Aloisio, R. Alaggio, and M. Fragiacomo, "Dynamic identification of a masonry façade from seismic response data based on an elementary ordinary least squares approach," *Engineering Structures*, vol. 197, p. 109415, 2019.

[15] A. Aloisio, L. Di Battista, R. Alaggio, and M. Fragiacomo, "Analysis of the forced dynamics of a masonry facade by means of input-output techniques and a linear regression model," in *COMPDYN, 2019, 7th International Conference on Computational Methods in Structural Dynamics and Earthquake Engineering*, 2019.

[16] R. Alaggio, D. Galeota, E. Antonacci, and A. Aloisio, "The s. maria di collemaggio basilica: from the vulnerability assessment tothe first results of shm.," *Atti del XVIII Convegno ANIDIS L'ingegneria Sismica in Italia*, pp. 75–85, 2019.

[17] M. Aoki, *State space modeling of time series*. Springer Science & Business Media, 2013.

[18] K. Arun and S. Kung, "Balanced approximation of stochastic systems," *SIAM journal on matrix analysis and applications*, vol. 11, no. 1, pp. 42–68, 1990.

[19] B. Peeters and G. De Roeck, "Reference-based stochastic subspace identification for output-only modal analysis," *Mechanical systems and signal processing*, vol. 13, no. 6, pp. 855–878, 1999.

[20] A. Aloisio, L. Di Battista, R. Alaggio, and M. Fragiacomo, "Sensitivity analysis of subspace-based damage indicators under changes in ambient excitation covariance, severity and location of damage," *Engineering Structures*, vol. 208, p. 110235, 2020.

[21] A. Aloisio, L. Di Battista, R. Alaggio, E. Antonacci, and M. Fragiacomo, "Assessment of

structural interventions using bayesian updating and subspace-based fault detection methods: the case study of s. maria di collemaggio basilica, l'aquila, italy," *Journal Structure and Infrastructure Engineering*, 2020.

[22] A. A. Antonacci, E., D. Galeota, and R. Alaggio, "The s. maria di collemaggio basilica: from vulnerability assessment to first results of shm," *Journal of Archiectural Engineering*, vol. Forthcoming, p. in press, 2020.

[23] M. Döhler and L. Mevel, "Subspace-based fault detection robust to changes in the noise covariances," *Automatica*, vol. 49, no. 9, pp. 2734–2743, 2013.

[24] M. Döhler, P. Andersen, and L. Mevel, "Data merging for multi-setup operational modal analysis with data-driven ssi," in *Structural Dynamics, Volume 3*, pp. 443–452, Springer, 2011.

[25] E. Reynders, R. Pintelon, and G. De Roeck, "Uncertainty bounds on modal parameters obtained from stochastic subspace identification," *Mechanical systems and signal processing*, vol. 22, no. 4, pp. 948–969, 2008.

[26] B. EN, "1-1: 2004 eurocode 5: Design of timber structures—general—common rules and rules for buildings," 1995.

[27] A. K. Chopra, *Dynamics of structures theory and*. 1995.

[28] G. Tamagnone, G. Rinaldin, and M. Fragiacomo, "Influence of the floor diaphragm on the rocking behavior of clt walls," *Journal of Structural Engineering*, vol. 146, no. 3, p. 04020010, 2020.

[29] G. Tamagnone, G. Rinaldin, and M. Fragiacomo, "A novel method for non-linear design of clt wall systems," *Engineering Structures*, vol. 167, pp. 760–771, 2018.

[30] M. Friswell and J. E. Mottershead, *Finite element model updating in structural dynamics*, vol. 38. Springer Science & Business Media, 2013.

[31] R. J. Allemang and D. L. Brown, "A correlation coefficient for modal vector analysis," in *Proceedings of the 1st international modal analysis conference*, vol. 1, pp. 110–116, SEM Orlando, 1982.

[32] H. J. Blass and P. Fellmoser, "Design of solid wood panels with cross layers," in *8th world conference on timber engineering*, vol. 14, p. 2004, 2004.

[33] F. Boggian, M. Andreolli, and R. Tomasi, "Cross laminated timber (clt) beams loaded in plane: testing stiffness and shear strength," *Frontiers in Built Environment*, vol. 5, p. 58, 2019.

[34] I. Lukacs, A. Björnfot, and R. Tomasi, "Strength and stiffness of cross-laminated timber (clt) shear walls: State-of-the-art of analytical approaches," *Engineering Structures*, vol. 178, pp. 136–147, 2019.

[35] A. Aloisio, R. Alaggio, K. Jochen, and M. Fragiacomo, "Extension of the generalized bouc-wen hysteresis modelling of wood joints and structural systems," *Journal of engineering mechanics*, vol. 146, no. 3, 2020.

[36] A. Di Egidio, R. Alaggio, A. Aloisio, A. M. de Leo, A. Contento, and M. Tursini, "Analytical and experimental investigation into the effectiveness of a pendulum dynamic absorber to protect rigid blocks from overturning," *International Journal of Non-Linear Mechanics*, vol. 115, pp. 1–10, 2019.

[37] P. Stefano, A. Angelo, D. E. Angelo, and A. Rocco, "Investigation into benefits of coupling a frame structure with a rocking rigid block," in *XXIV Congresso AIMETA 2019, Associazione Italiana di Meccanica Teorica e Applicata*, 2019.

[38] D. Casagrande, S. Rossi, T. Sartori, and R. Tomasi, "Proposal of an analytical procedure and a simplified numerical model for elastic response of single-storey timber shear-walls," *Construction and Building Materials*, vol. 102, pp. 1101–1112, 2016.

[39] T. Tannert and P. Eng, "Design provisions for cross-laminated timber structures," in *Structures Congress 2019: Buildings and Natural Disasters*, pp. 171–178, American Society of Civil Engineers Reston, VA, 2019.

[40] A. S. of Civil Engineers, "Minimum design loads and associated criteria for buildings and other structures," American society of civil engineers, 2017.

[41] M. d. I. e dei Trasporti, "Ntc2008–norme tecniche per le costruzioni," tech. rep., DM 14/01/2008 [In Italian], 2008.

[42] D. C. S. NORMA, "Parte general y edificación (ncse-02)," *BOE*, vol. 244, no. 11.10, p. 02, 2002.

[43] N. T. per le Costruzione, "Aggiornamento delle norme tecniche per le costruzioni," tech. rep., decreto 17-1-2018, Gazzetta Ufficiale 42, 20-02-2018, Ordinary Suppl, 2018.

List of Figures

1 (a) North view of the building; (b) Prospects and plan (c)-(d) of the building. 4

2 (a) Signal conditioner and DAQ system of the 10 IEPE piezoelectric accelerometers; (b) View of a couple of accelerometers measuring in two orthogonal directions; (c) Schematic view of the experimental setup of the rooftop. 6

3 (a) Acceleration time-history of a reference accelerometer placed on the rooftop; (b)-(c) FFT of the signals in two orthogonal directions; (d) Stabilization diagram of the merged signals. The stabilization criteria are: $\delta f_i \leq 1\%$, $\delta \xi_i \leq 1\%$, MAC$<$1% [25]. 7

4 Natural frequencies, damping factors and mode shapes of the three stable modes in the frequency range $0 - 10\,Hz$ corresponding to the roof setup. 8

5 Natural frequencies, damping factors and mode shapes of the three stable modes in the frequency range $0{-}10Hz$ corresponding to merged data sets. 8

6 Plan view of a general configuration of the bearing walls of the j-th storey. 9

7 Contour plot of the objective function. 12

8 (a) Layout of the CLT panels tested by Gavric et al. [9]; (b) Hysteresis loops of the tested panel; (c) Representation of the first steps of the cyclic tests shown in (b): the dotted line is the tangent to zero. . . . 14

9 Schematic representation of the CLT wall panel behaviour. 14

Paper IV

IV D. Pasca, A. Aloisio, M. Fragiacomo, R. Tomasi (2020) Dynamic characterization of timber floors sub-assemblies: sensitivity analysis and modelling issues.

Dynamic characterization of timber floors sub-assemblies: sensitivity analysis and modelling issues

Dag Pasquale Pasca[1], Angelo Aloisio[2], Massimo Fragiacomo[3], and Roberto Tomasi[4]

[1]Faculty of Science and Technology, Norwegian University of Life Sciences, Drøbakveien 31, 1433 Ås, Norway. Email: dag.pasquale.pasca@nmbu.no
[2]Department of Civil, Construction-Architectural and Environmental Engineering, Università degli Studi dell'Aquila, Via G. Gronchi 18, 67100 L'Aquila, Italy. Email: angelo.aloisio1@graduate.univaq.it
[3]Department of Civil, Construction-Architectural and Environmental Engineering, Università degli Studi dell'Aquila, Via G. Gronchi 18, 67100 L'Aquila, Italy. Email: massimo.fragiacomo@univaq.it
[4]Faculty of Science and Technology, Norwegian University of Life Sciences, Drøbakveien 31, 1433 Ås, Norway. Email: roberto.tomasi@nmbu.no

ABSTRACT

Timber floors are prone to exhibit vibration levels which can cause discomfort to the occupants. In the last twenty years, ambient vibration tests have become very popular due to the many advantages they have over traditional forced vibration tests, when dealing with civil engineering structures. Furthermore, sensitivity analyses and "black box" optimization algorithms can support the development of refined finite element models that accurately predict the structures' responses based on the experimental modal parameters. Though, applications of these methods and techniques to timber structures are scarce compared to traditional materials. This paper presents and discusses the findings of an experimental testing campaign on a lightweight timber floor. At first, each component of the assembly was tested separately under different boundary conditions. Then the authors evaluated the behaviour of the whole floor assembly. In a second step, the authors carried out a covariance-based sensitivity analysis of FE models representative of the tested structures by varying the different members' mechanical properties. The results of the sensitivity analysis highlighted the most influential parameters and supported the comparison between diverse FE models. As expected, the longitudinal modulus of elasticity is the most critical parameter, although the results are very dependent on the boundary conditions. Then automatic modal updating algorithms tuned the numerical model to test results. As a concluding remark, the experimental and numerical results were compared to the outcomes of a simplified analytical approach for the floor's first natural frequency estimate based on Eurocode 5.

INTRODUCTION

Modal testing represents a standard practice in structural engineering. Traditional modal testing is based on estimating frequency response functions, which basically are the ratio of the output response to the input excitation. This approach is also known as Experimental Modal Analysis (EMA). Other ways to obtain modal properties through testing are the so-called Operational Modal

Analysis (OMA) methods. These approaches are very advantageous in civil engineering, where the tested object is usually massive.

OMA encouraged copious research activities, which spanned from theoretical investigations (Aloisio et al. 2020e; Reynders et al. 2012; Reynders et al. 2016) to practical applications (Bedon and Morassi 2014; Rainieri et al. 2019; Aloisio et al. 2020a; Aloisio et al. 2020c). The scientific literature documents a considerable amount of applications to civil engineering structures: wind turbines (Tcherniak et al. 2011; Devriendt et al. 2014), stadiums (Peeters et al. 2007; Magalhães et al. 2008), dams (Sevim et al. 2011; Pereira et al. 2018), architectural heritages (Kita et al. 2019; Gentile et al. 2019; Antonacci et al. 2020; Aloisio et al. 2020d). The modal features, obtained from OMA, bestow a direct insight into the actual structural behaviour and can guide a heedful assessment about the modelling of the tested structures. A high-quality experimental campaign can yield a reliable estimation of many modal parameters, valuable in understanding the limits and advantages of the possible modelling approaches. The matching between the experimental modal parameters and those obtained from the numerical model endorses the modelling choices. The search for an optimum matching leads to an optimum model, obtained by optimizing the modelling variables via the so-called model updating methods (Friswell and Mottershead 2013). Model updating defines the process of refreshing the modelling variables at each step to minimize a proper objective function, which magnifies the difference between experimental and numerical features. In the digital era, model updating is gaining popularity due to automated optimization algorithms. These algorithms lead to an optimum structural model, which best mirrors the experimental response. The increasing popularity of model updating methods has alimented considerable research. Today, a researcher can use numerous optimization algorithms, which are equally feasible in terms of reliability and computational efforts.

Timber is an excellent construction material with good stiffness-to-mass ratios and carbon-storing properties. These characteristics made timber very popular in the last years. The interest in timber structures has risen, especially in the last two decades, due to the advent of new engineering wood products, like the Cross-Laminated Timber (Ceccotti et al. 2013; Brandner et al. 2016; Izzi et al. 2018; Aloisio et al. 2020b). The low weight of timber, however, is a double-edged sword to the dynamic performance. The use of timber elements is beneficial in reducing dead loads (and inertial forces) on the structure. On the other hand, its low mass makes it prone to reach a higher amplitude of vibrations. The assessment of timber buildings' vibration performances has two primary branches: one focused on evaluating the lateral response(Reynolds et al. 2016; Mugabo et al. 2019; Aloisio et al. 2020f; Aloisio et al. 2021), the other on assessing walk-induced vibrations and the comfort requirements for the users (Smith et al. 2007). While the first field is relatively new, researchers have investigated the second aspect for many years (Ohlsson 1982; Smith and Chui 1988; Hu et al. 2001; Hamm et al. 2010). The serviceability limit state is related to the perception of annoying oscillations caused by walking-induced vibrations. The "live" feel of timber floors is familiar to many, especially in single-family housing with a timber framework. However, this problem is not limited to timber-framed residential buildings. Timber joists can support the flooring system even in masonry buildings (Hu et al. 2001). The trend of seeking large, open-spaced architectural layout and adopting new construction practices certainly affects timber floors' serviceability significantly. The ability to predict timber flooring systems' behaviour remains a difficult task and a topical subject.

There are some applications of ambient vibration tests on timber floors in the scientific liter-

ature (Weckendorf and Smith 2012; Weckendorf et al. 2014; Weckendorf et al. 2016). However, force vibration tests, and EMA methods remain the most known and used procedures to estimate traditional floors' modal properties or more innovative solutions (e.g. CLT and Timber concrete composites) (Casagrande et al. 2018; Xie et al. 2020; Huang et al. 2020). Applications of OMA methods and automated modal updating procedures to timber structures are still not copious. This paper presents and discusses ambient vibration test results of a timber floor and the modelling strategies and techniques adopted to simulate the floor's dynamic response numerically. Specifically, the research studies the response of two glulam beams with plywood decking, which are part of a simply-supported timber floor. At first, each assembly component was tested separately under different boundary conditions; then, the authors evaluated the whole floor assembly's behaviour. In a second step, the authors carried out a covariance-based sensitivity analysis on the FE models representing the tested structures by varying the Moduli of Elasticity of the different members. The sensitivity analysis outcomes evidence the significant structural parameter and drive a definitive comparison between diverse FE modelling methods. The authors used two automated updating algorithms to refine the numerical model's parameters better and match the testing results. The adoption of closed-form analytical solutions is diffuse in engineering practice. Therefore, the authors compared the well-known Euler-Bernoulli model for the simply-supported beam tests with the FE numerical predictions.

MATERIALS AND METHODS

The authors tested a timber floor sub-assembly made by two beams and decking above. The two GL30C beams are 5m long with a 115mm x 315mm cross-section. The nominal average Modulus of Elasticity (MoE) is $13GPa$, while the mean weight is $430kg/m^3$, according to EN 14080 (EN14080 2013). Both beams presented some defect at delivery, see Fig1. "Beam 1" on one end had two cracks (approximately 15cm and 20cm wide), on both faces; while "Beam 2" had a hole on one face that was filled with silicone.

The decking consists of 21 mm thick Plywood 1,5 x 1,5 m sheets made from Birch veneers. According to the producer declaration of performance (DoP) the self-weight is $650kg/m^3$, while the mean values of the MoE span between $6GPa$ and $8GPa$, depending on loading direction, perpendicular or parallel to the external layer fibre orientation, respectively.

In modal testing practice, mechanical parts, machinery and other structural components are tested freely-suspended due to the difficulties in modelling the boundary conditions. Due to the laboratory conditions, it was not possible to suspend the beams. The authors adopted a compromise solution, based on the use of a layer of Rockwool insulation placed under the beams, which successfully simulated the free-free boundary conditions. A single rectangular piece of Rockwool (300mm x 300mm, 100mm thick) located under the mid-span of the beams, or by the centre of the plywood boards yielded the best results, in terms of repeatability, consistency and clearness of both the spectral densities and the stabilisation diagrams. The presence of the Rockwool layer may affect the results in terms of damping. However, reliable damping estimates are always challenging to achieve and are not the primary scope of this investigation.

Pinned-pinned boundary conditions characterized the floor assembly in Fig2. Two metal cylinders, spaced 4.8m, supported each beam, with a 600mm centre-to-centre distance. The decking was made of three square boards with 1.5m long sides. The beams, being 5m long, were not covered by the boards for the last 25cm on each side, see Fig2a. Furthermore, no nailed or screwed connector secured the boards over the beams. Dynamic analyses are susceptible to the

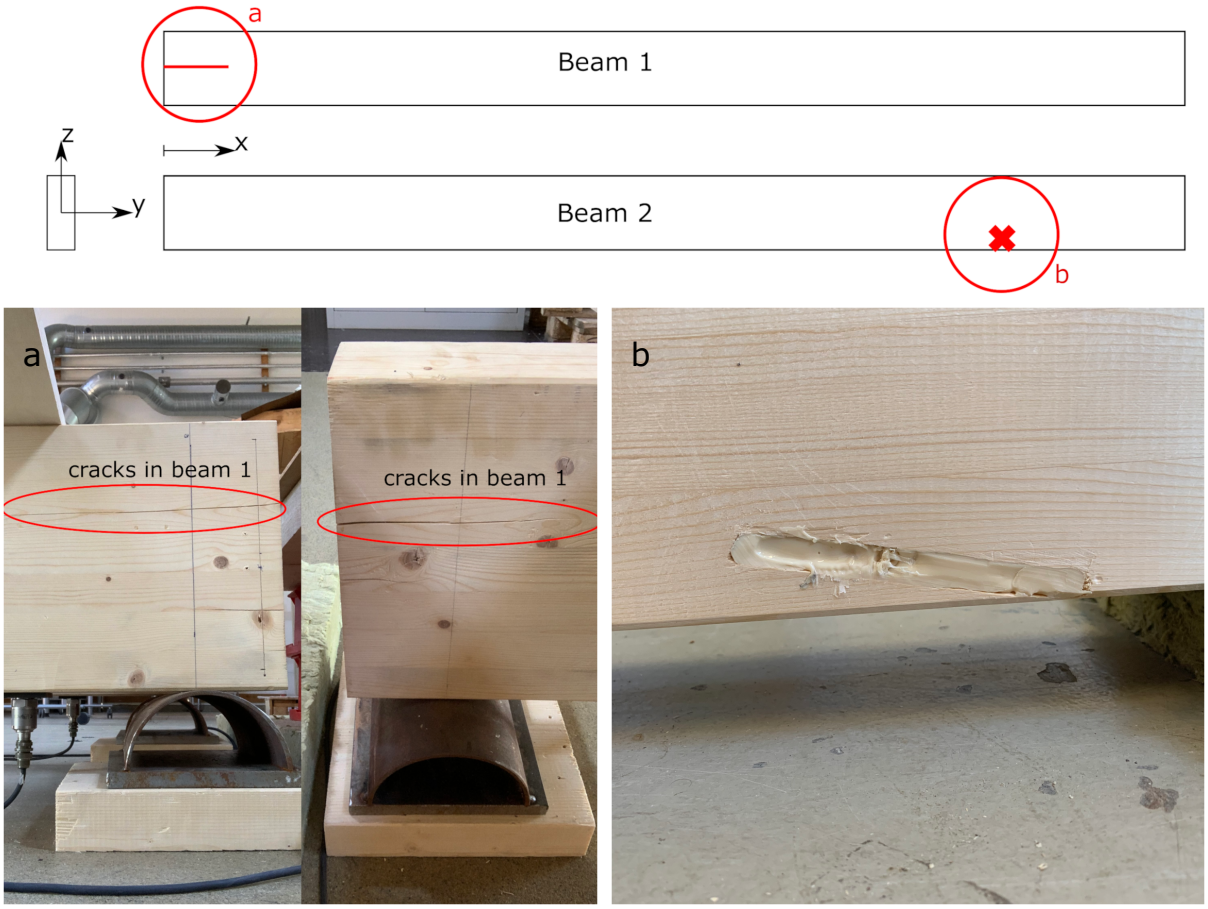

Fig. 1. Location of the defects on "Beam 1" and "Beam 2".

occurrence of little damage or minimal structural modification. The insertion of the connectors would have altered/damaged each component, thus vanishing the efforts to identify the dynamics of each of them accurately. Therefore, the authors devised an alternative solution to study the entire structural arrangement without the need for connectors. They placed a reusable putty-like pressure-sensitive adhesive, which guarantees the joint response of the beams and the decking in the vertical direction. Even if in a real building the decking would be fixed to the beams, thus enhancing the composite interaction and the overall stiffness, the floor would also be much thicker and heavier, due to the finishing. The structural assembly is not intended to be representative of realistic situations, it is a structural archetype useful for the accurate calibration of numerical models able to predict its vibration performance.

A slight and random brushing of the structures using a wooden stick represented the excitation source. This method aims to improve the signal-to-noise ratio of the measurements (Brincker and Ventura 2015). The Enhanced Frequency Domain Decomposition method (EFDD, (Brincker et al. 2001)) and the Stochastic Subspace Identification method (SSI-cov (Peeters and De Roeck 1999), SSI-dat (Van Overschee and De Moor 2012)), implemented by the authors in Python programming language, yielded the modal parameters from the acquired data. The EFDD method, which is a so-called non-parametric, frequency domain procedure, and SSI, which is a parametric, time-domain

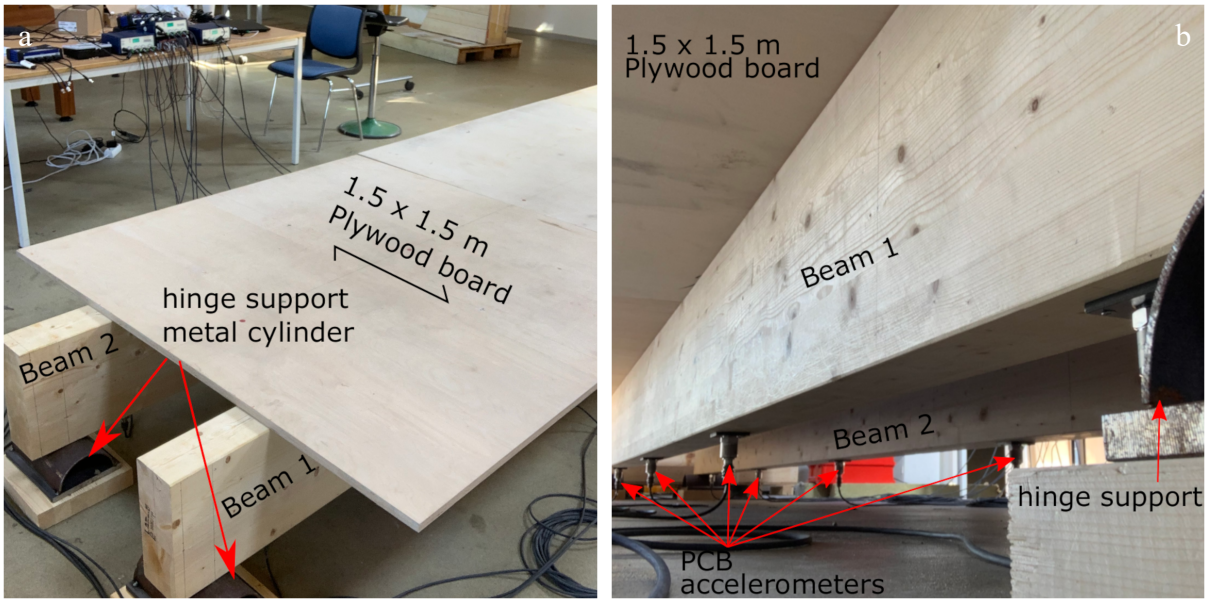

Fig. 2. Floor assembly: left view from above, right view from below.

procedure, are probably among the two most used techniques for OMA.

The numerical characterisation of the dynamic response originated from Finite Element Modelling using the software SAP2000 (SAP2000 1975). The authors developed a set of models for each sub-assembly (i.e. beams and board) before the testing using standardised values for the material properties (i.e. from material standard and DoP). These models provided an expected response, which was useful to derive a proper setup and instrumentation plan. Two models reproduced the dynamics of the beams. The former derived from the one-dimensional "Frame elements" based on the Timoshenko beam theory, the latter originated from the use of "Solid elements", which are eight-node elements for modelling three-dimensional structures. The material property was defined as orthotropic to model the glulam. Thin "Shell elements" modelled the decking, with the plywood of the boards idealised as an orthotropic material. Unfortunately, SAP2000 does not perform a modal analysis of unrestrained objects. Therefore, a "Linear-link" element connected the modelled structures' end corners to the ground. An infinitesimal stiffness was assigned to the link elements to simulate the unrestrained boundary conditions.

The global model of the floor emerged from the sensitivity analysis and model updating of the structural sub-assemblies, see Fig3. "Linear-link" elements connect the beam's nodes to the nodes of the plywood boards. Each element is assumed to be composed of six separate "springs", each associated with a deformational degree of freedom (DoF). Given the type and source of loading, the authors assigned an infinite stiffness to the first local axis of the spring, representing the contact between components (see Fig3).Conversely, the other DoF were kept unrestrained since the boards were not fixed to the beams. The mesh size of the frame elements (50 mm), the solid elements (55x25x30 mm) and the shell elements (50x50 mm) derived from a simple convergence test on the firsts natural frequencies, and represent a possibly satisfactory compromise between accuracy and computational time.

The SAP2000 Open Application Programming Interface (OAPI) was used in combination with

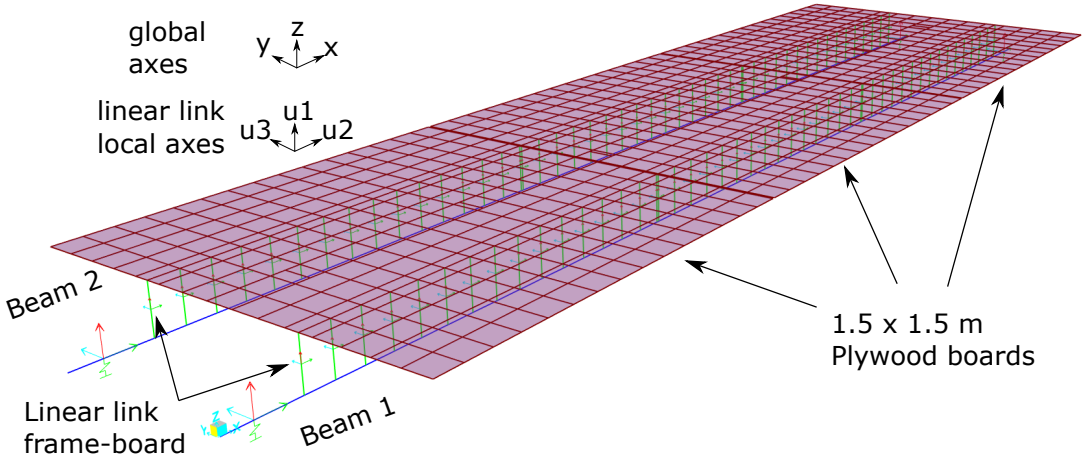

Fig. 3. Sap2000 FE model of the floor.

the open-source programming language Python to develop the routines for the sensitivity analysis and model updating. The OAPI allows third-party products, like Python, to interact with SAP2000, allowing the users to create custom applications.

A Sobol sensitivity analysis (Sobol 1993) evidenced the role of each term of the flexibility matrix of an orthotropic finite element. Namely, the analysis returned the sensitivity indices of the three MoE, E_X E_Y E_Z, the three Shear Moduli, G_{XY} G_{XZ} G_{YZ}, and three Poisson's ratios, ν_{YX} ν_{ZX} ν_{ZY} on the output (modal properties).

Finally, the FE models were tuned to reflect the measured data better using two global optimization algorithms for "black box" functions, the Differential Evolution (DE) (Storn and Price 1997) and the Particle Swarm Optimization (PSO)(Kennedy and Eberhart 1995). The script for the model updating process was written in Python using SAP2000 OAPI along with the Python module PySwarms (Miranda 2018) (to run PSO), and the popular Python toolkit SciPy (Virtanen et al. 2020)(to run DE). The idea behind PSO is to emulate the social behaviour of birds and fishes by initializing a set of candidate solutions to search for an optimum. A set of candidate solutions (called particles) are moved around in the search-space. The movements of the particles are guided by their own best-known position in the search-space as well as the entire swarm's best-known position. Differential evolution is a stochastic population-based method that, at each step, mutates each candidate solution (called agents) by mixing with other candidate solutions to create a trial candidate. If the new position is an improvement, then it is accepted and forms part of the population. Otherwise, the new position is simply discarded.

The following objective function measures the distance between the estimated modal parameters and the numerical ones:

$$C = \sum_{i=1}^{M} \gamma_i \left(\frac{f_i^m - f_i^c}{f_i^m} \right)^2 + \sum_{i=1}^{M} \beta_i \left(1 - MAC(\{\phi^m\}_i, \{\phi^c\}_i)\right) \tag{1}$$

where the apex $(*)^m$ indicates a measured variable, the apex $(*)^c$ a calculated variable, f_i is the i^{th} natural frequency, ϕ_i is the mode shape vector, M is the number of modes, MAC is the Modal Assurance Criterion, while γ_i and β_i are weighting factors.

Practitioner usually rely on simplified equation provided by building codes and standards to design structural elements, rather than rely on cumbersome and time-consuming FE analysis, especially at early design stages. To reflect this aspect the authors drew some comparisons to well-known engineering procedures. The bending vibrations of a beam can be described by the well-known Euler-Bernoulli beam equation:

$$EI\frac{\partial^4 z}{\partial x^4} + \rho A\frac{\partial^2 z}{\partial t^2} = 0 \quad with \quad 0 < x < L \tag{2}$$

where the E is the MoE, I is the second moment of inertia of the cross-section, ρ is the mass density (mass per unith length), A is the cross-section area, z is the vertical displacement, L is the length of the beam and t is time. The solution for Eq.(2) can be found for example by decomposing the displacement into a sum of harmonic vibrations $z(x,t) = Re[\hat{z}(x)e^{-i\omega t}]$. Eq.(2) can then be rewritten as an ordinary differential equation $EI\partial^4\hat{z}/\partial x^4 - \rho\omega^2\hat{z} = 0$, which have a general solution of the form:

$$\hat{z}_n = C_1 cosh(k_n x) + C_2 sinh(k_n x) + C_3 cos(k_n x) + C_4 sin(k_n x) \quad with \quad k_n = \left(\frac{\rho\omega_n^2}{EI}\right)^{1/4} \tag{3}$$

where $C_1 - C_4$ are constants that depends on the boundary conditions, k_n is the wave number and ω_n is the n^{th} natural frequency. Eurocode 5 (EN1995 2004) provides a formula to estimate the first natural frequency of rectangular floor with span L, width B, simply supported along the four edges, which derives from the temporal component of the solution of Eq.(3):

$$f_1 = \frac{\pi}{2L^2}\sqrt{\frac{(EI)_L}{m}} \tag{4}$$

where $(EI)_L$ is the equivalent bending stiffness along the span direction and m is the mass per unit floor area.

DYNAMIC IDENTIFICATION

Experimental setup

The measurement chain was composed by ten seismic ceramic shear piezoelectric accelerometers, an HBM QuantumX data acquisition unit (24-bit analogue-to-digital converter) and a laptop pc. Shielded polyurethane coaxial cables made the connection between the sensors and the acquisition unit. The accelerometers (PCB, model 393B12) have an approximate 10000 mV/g sensitivity, a frequency range from 0.15 Hz to 1000 Hz and a measurement range up to $\approx \pm 5\ m/s^2$.

The accelerometers measured the beam responses parallel to the principal axes of inertia (strong and weak) in the free-free condition, according to the setups shown in Fig4a. Mounting studs and small metal plates screwed to the beams extrados (i.e. top surface) secured the accelerometers to the elements. The second setup for the weak axis allowed the extraction of the torsional modes of the beams, see Fig4c. In this case, three different measurements were processed and then merged to get the mode shapes. The sensors were attached to the beams through adhesive rubber to fasten up the testing operations. Furthermore, the beams were also tested on two metal supports to simulate the simply-supported condition; this time, the measurement axes were parallel to the strong axis of inertia. Fig4b shows the test setup of the decking. The authors tested a single panel out of the

three plywood sheets. The testing of the structural sub-assembly had the sensors placed by the intrados of the beams. This choice allowed to leave the space on top of the floor free, see Fig2b. The accelerometers were evenly distributed along both beams. The distance between the edge accelerometers was lesser than the beam length due to the presence of the supports.

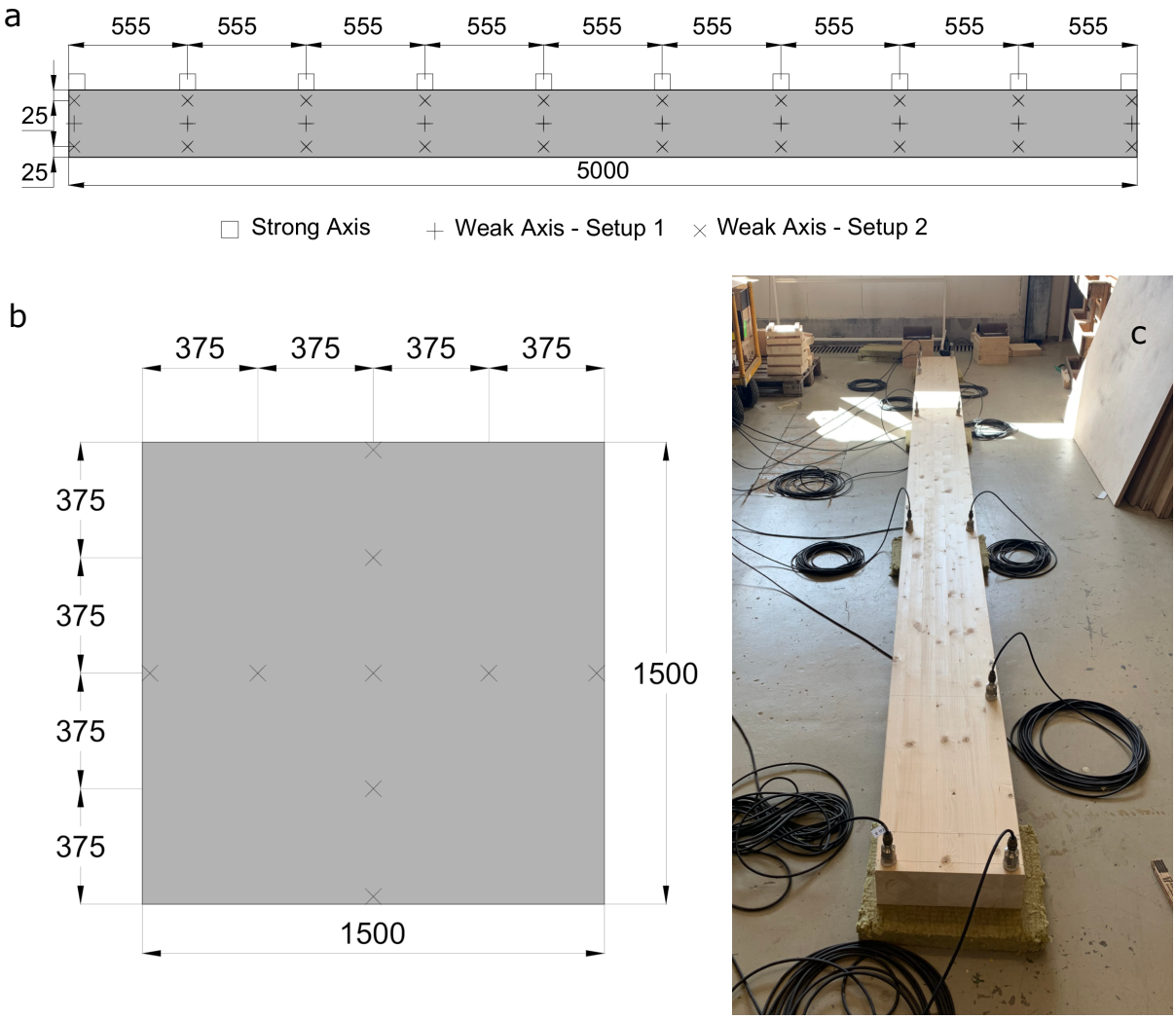

Fig. 4. a)Test setup glulam beams, b)Test setup plywood boards, c)Test setup for torsional modes glulam beams. (all the dimensions are in mm)

The sampling frequency was set to 1200 Hz (the aliasing filter is automatically set by the software embedded in the logger), and the duration was 5 minutes for every test. The data were first detrended to remove the DC offset with the application of a digital high-pass filter, then decimated. Different decimation factors, depending on the frequency bandwidth of interest, were used.

With regards to the EFDD method, the Power Spectral Densities (PSD) were estimated according to the Welch's method, dividing the data so to get a frequency resolution of 0.1 Hz and using a Hanning window with 50% overlap. The MAC rejection level to estimate the singe-DoF PSD "bell"

function was set to 0.95. Twenty consecutive peaks were used to estimate the damped frequency and the damping ratio from the autocorrelation function, ignoring the first 3. For the SSI-cov method, the number of block rows was set to 15, and the maximum model order to 80. As suggested in (Rainieri and Fabbrocino 2014), the stability requirements were set to:

$$\left(\frac{|f(n) - f(n+1)|}{f(n)}\right) < 0,01 \tag{5}$$

$$\left(\frac{|\xi(n) - \xi(n+1)|}{\xi(n)}\right) < 0,05 \tag{6}$$

$$[1 - MAC(\{\phi(n)\}, \{\phi(n+1)\})] < 0,02 \tag{7}$$

where (n) and $(n+1)$ are the n^{th} and $n^{th}+1$ model order, f is the natural frequency, ξ is the damping, and ϕ is the mode shape vector.

Results and discussion

Processing the data yielded nine of the first ten modes of the freely suspended beams in the bandwidth between 0 Hz and 300 Hz, the only exclusion being the first flexural mode along the weak axis. Tab1 shows the results estimated from the EFDD method and SSI-cov, with the results of the preliminary numerical model. As can be seen from the table, the estimated frequencies are very close to each other. The mode shape estimates are very consistent, with CrossMAC values higher than 0.99. Furthermore, the experimental results do not differ too much from the numerical ones. The only exception being the swapping of position between the 1^{st} flexural mode along the strong axis and the 2^{nd} flexural mode along the weak axis in the measured modes, compared to the numerical ones. Fig5 shows the experimental modes: the MAC matrix in Fig6 remarks on the excellent correspondence between experimental and numerical modes. The fact that some off-diagonal terms have very high values could seem odd at first glance, but with a more careful look, one can notice how these are the modes that have similar shape along the two orthogonal axes.

TABLE 1. Results dynamic identification freely suspended beams

	SAP2000	Beam 1 SSIcov		Beam 1 EFDD		Beam 2 SSIcov		Beam 2 EFDD	
Mode	f_n[Hz]	f_n[Hz]	ξ[%]	f_n[Hz]	ξ[%]	f_n[Hz]	ξ[%]	f_n[Hz]	ξ[%]
1-Flex-WA	25.81	-	-	-	-	-	-	-	-
2-Flex-WA	69.96	62.98	0.72%	63.06	0.59%	65.66	0.61%	65.83	0.60%
1-Flex-SA	67.57	65.50	1.03%	65.98	1.00%	67.77	0.89%	67.54	1.13%
1-Tors	72.78	70.32	1.05%	70.52	1.07%	71.94	1.28%	71.51	0.85%
3-Flex-WA	133.75	124.09	0.99%	124.87	1.01%	129.50	0.89%	129.42	0.92%
2-Tors	146.86	149.15	2.12%	148.99	1.61%	154.37	2.24%	153.44	1.96%
2-Flex-SA	166.79	154.07	0.59%	155.97	0.54%	157.90	0.70%	157.91	0.66%
4-Flex-WA	214.06	194.83	0.59%	195.13	0.53%	202.75	0.65%	202.03	0.65%
3-Tors	223.42	220.05	2.53%	219.88	1.60%	227.53	3.55%	222.68	1.49%
3-Flex-SA	286.77	273.90	0.80%	273.68	0.73%	279.31	0.83%	278.40	0.73%

Flex = Flexural mode; Tors = Torsional mode; WA = Weak Axis; SA = Strong Axis
Numerical and analytical model's parameters:
$E_x = 13000\ [MPa]$, $G_{xz} = G_{xy} = 650\ [MPa]$; $\rho = 430\ [kg/m^3]$

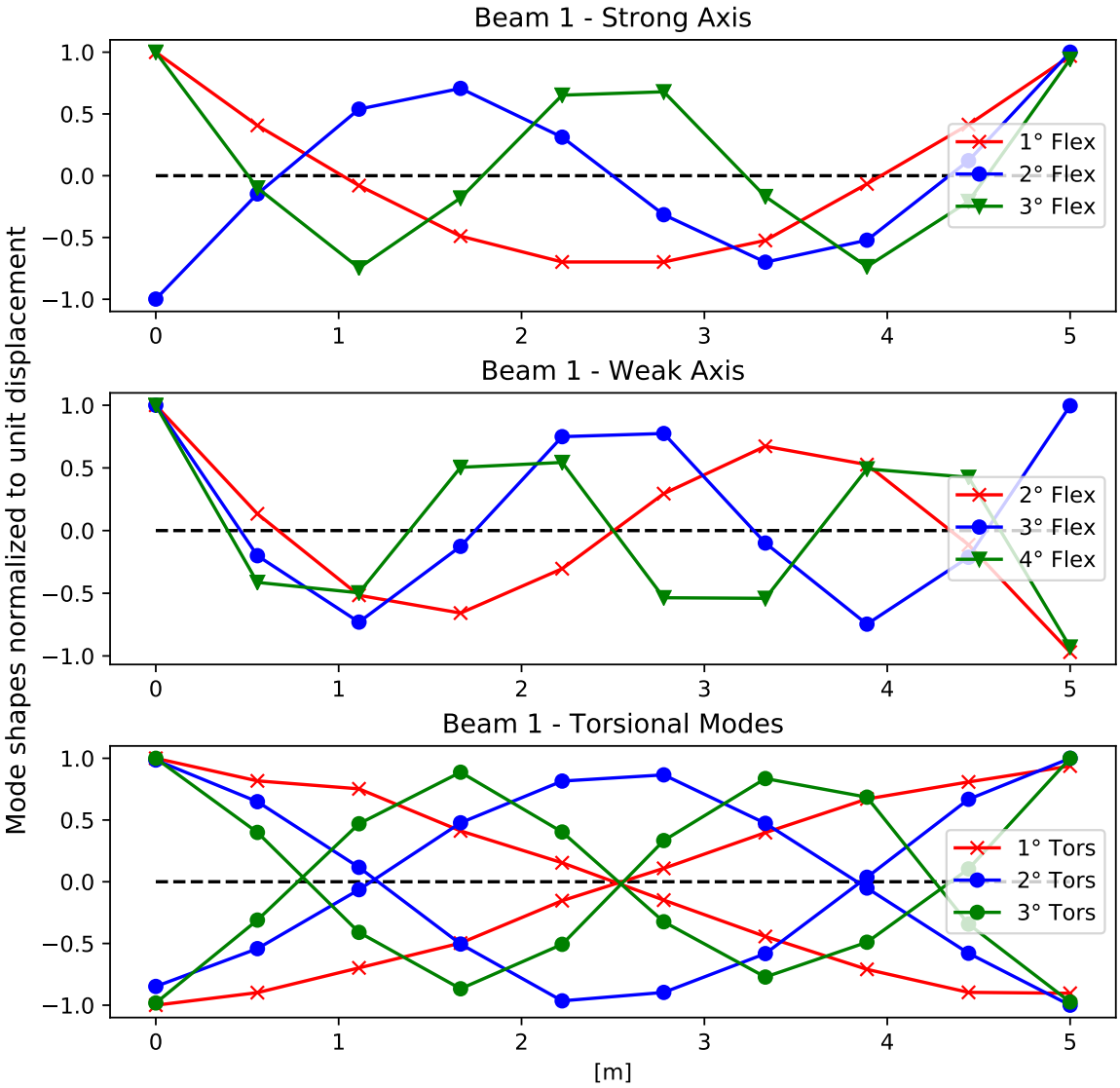

Fig. 5. Experimental modal shapes freely suspended beam.

Three modes were identified in the bandwidth between 0 Hz and 300 Hz when the two beams were simply-supported. Tab2 presents the results of dynamic identification compared to the results of the numerical model and the first three frequency calculated according to Eq.(3). The excellent crossMACs between analytical and numerical mode shapes confirm that the beam's meshing size for the numerical model was appropriately chosen.The experimental mode shapes are depicted in Fig7. A more significant difference between measured and numerical/analytical results is appreciable for the II and the III mode, both in terms of natural frequencies and mode shapes. The differences are probably due to the stiffness of the metal supports, which are not able to restrain the uplift movement.

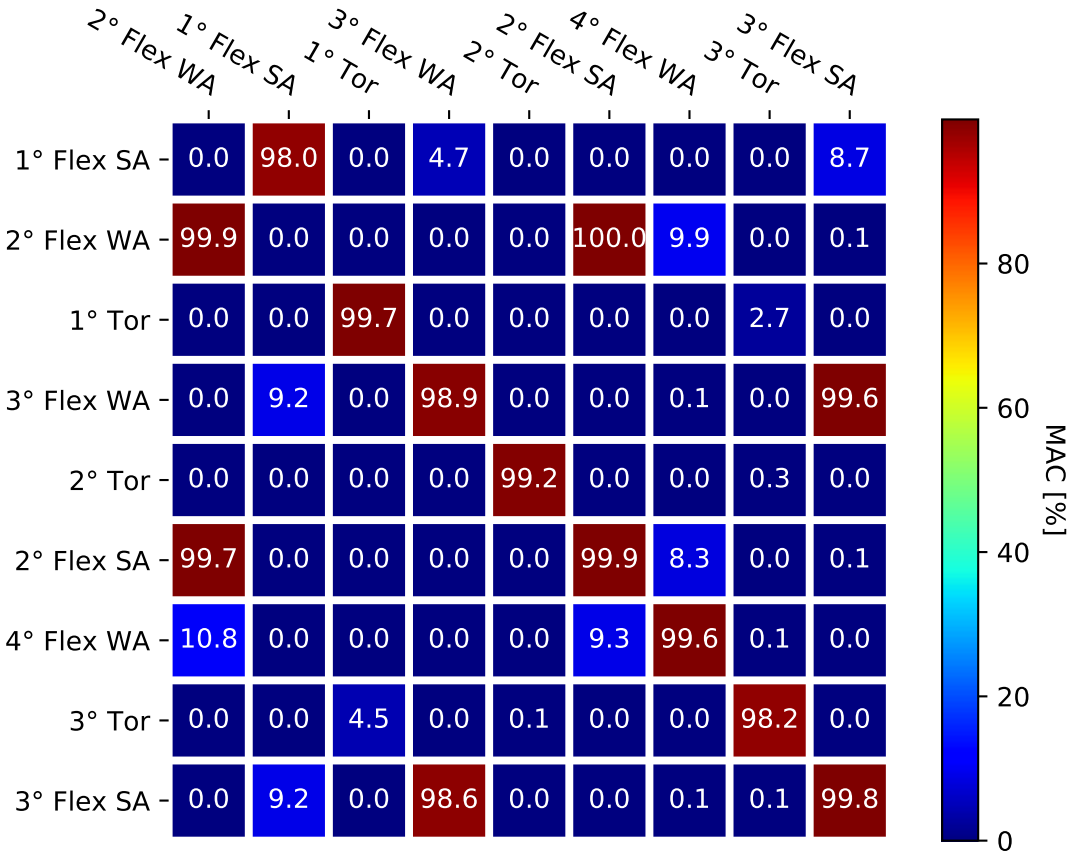

Fig. 6. MAC matrix: measured mode shapes vs numerical.

TABLE 2. Results dynamic identification simply supported beams

Mode	SAP2000	Analytical	Beam 1 - SSIcov		Beam2 - SSIcov	
	f_n[Hz]	f_n[Hz]	f_n[Hz]	ξ[%]	f_n[Hz]	ξ[%]
I	32.72	31.42	28.90	0.70%	29.93	0.75%
II	117.77	125.66	90.22	1.76%	92.53	2.04%
III	230.84	282.74	149.50	1.75%	153.73	1.80%
Numerical and analytical model's parameters: $E_x = 13000\ [MPa]$; $G_{xz} = G_{xy} = 650\ [MPa]$; $\rho = 430\ [kg/m^3]$; $K_{support} = \infty$						

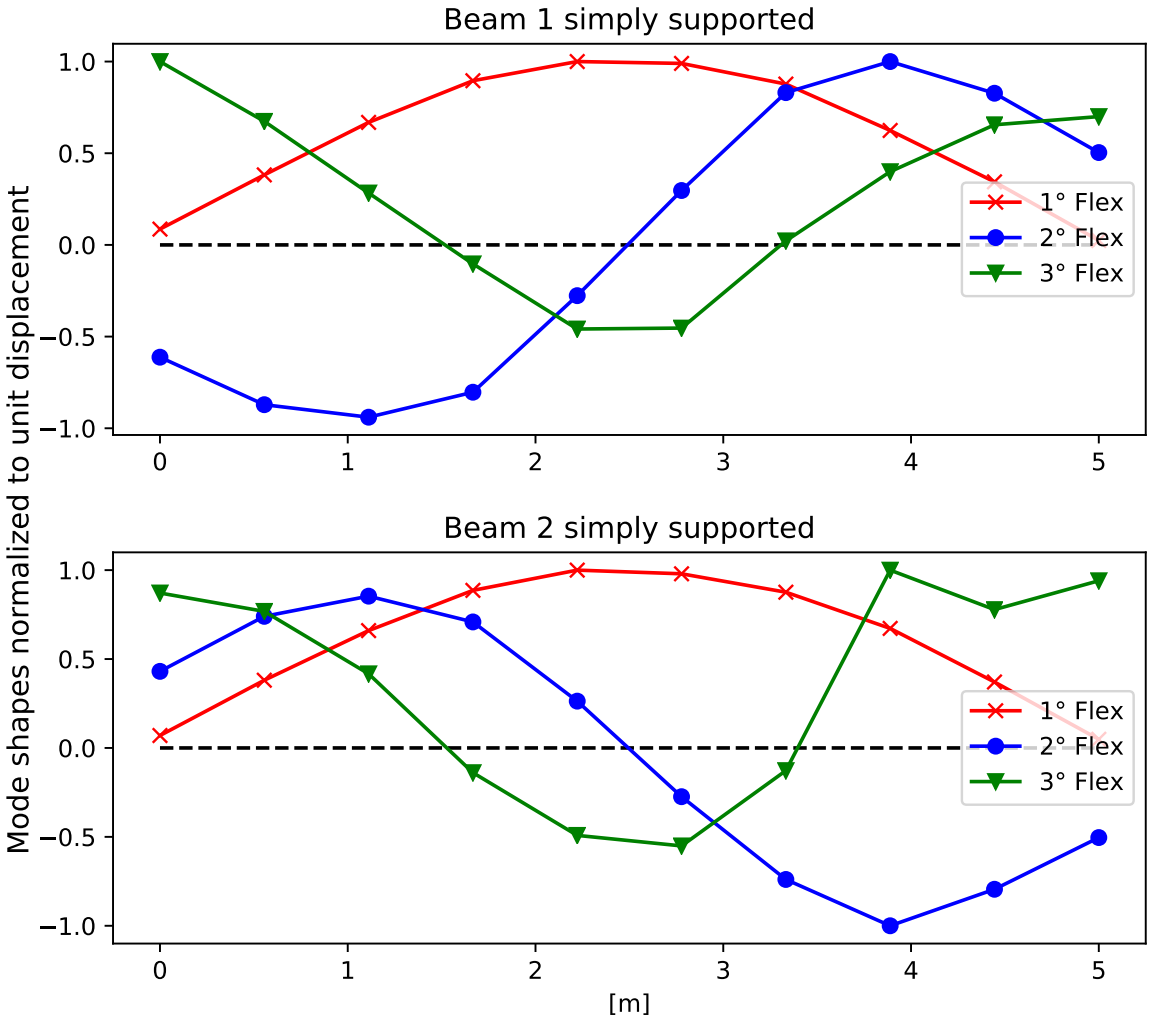

Fig. 7. Experimental modal shapes simply supported beam.

Interestingly, the measured mode shapes, depicted in Fig7, reveal the presence of defects on both beams, which were not detectable when the beam was tested as freely suspended. The visible variations recorded by the accelerometers nearby the location of the damages, especially in the III mode, suggest that higher modes can be used as indicators to localise the presence of damages on structural elements, as already suggested by other authors (Ciambella et al. 2019; Aloisio et al. 2020e).

The identification of the plywood boards in Tab3 returned seven stable modes in the bandwidth $0 - 100\ Hz$. The numerical model evidenced the presence of some modes, not reported here, that could not be identified from the chosen setup. These are those modes where all the positions of the accelerometers correspond to the nodes of the mode shapes (i.e. a point of dynamic equilibrium), and therefore could not be detected. Out of the seven modes, three show a notable agreement with the numerical model, namely: mode I, mode VI and mode VII (see Fig8). The others seem to be more affected by the presence of the Rockwool pad. Looking more carefully at the mode shapes in

Fig8 one can notice how in mode I, VI and VII, the central point is a node of the modal shape and accordingly less affected by the presence of the Rockwool. Whereas modes IV and V, where the centre is an anti-node, are more affected by the insulation piece.Nevertheless, the addition of a small set of springs at the centre of the numerical model, so to simulate the presence of the Rockwool, determine mode IV and mode V to exhibit a satisfactory agreement with the experimental data, as remarked in the following paragraphs.

TABLE 3. Results dynamic identification plywood boards

	SAP2000	Plate - SSIcov			Plate - EFDD		
Mode	f_n [Hz]	f_n [Hz]	ξ [%]	MAC	f_n [Hz]	ξ [%]	MAC
I	28.04	30.42	0.88%	95.8%	30.50	0.88%	96.0%
II	35.48	37.45	1.39%	51.2%	37.32	1.46%	51.6%
III	39.20	39.96	1.62%	47.8%	40.09	1.21%	48.8%
IV	35.36	46.90	2.80%	30.3%	47.05	1.63%	30.1%
V	61.90	74.29	5.86%	92.9%	74.45	5.24%	91.4%
VI	81.16	88.83	1.40%	98.6%	89.03	0.76%	98.9%
VII	93.56	91.24	1.58%	98.6%	91.08	0.74%	98.8%
Numerical model's parameters:							
$E_x = 6000\ [MPa]$, $E_y = 8000\ [MPa]$; $\rho = 650\ [kg/m^3]$							

The dynamic identification of the simply-supported floor assembly returned two stable modes in the bandwidth $0 - 40\ Hz$, that is the suggested bandwidth of interest for timber floors (EN1995 2004). Mode I is a torsional mode were the two beams move out of phase with each other, while mode II is the first bending mode, namely the two beams are in phase. Tab4 reports the estimated frequencies and damping ratios with the results of the numerical model. The particular configuration of the floor, with the board not rigidly fixed to the beams, prompted the numerical model to exhibit several local modes of the boards that had almost none effect on the beams. The mode shapes from the numerical model were extracted from the modal displacement of nodes belonging to the frame elements, so to be faithful to the test setup. The results of the two methods are in excellent agreement, with CrossMAC values higher than 0.99. In a single instance, the damping ratio of the II mode from SSIcov was noticeably higher than that estimated from the EFDD. The adoption of standardized material properties in the numerical model causes a significant error in terms of frequency, although the mode shapes show a satisfactory correspondence with the experimental. Moreover, in Tab4 the first bending frequency (mode II) can also be compared to the first bending frequency calculated according to the analytical Euler-Bernoulli model. The two frequency values reported correspond to the situation when a complete composite action between the beams and the decking and only the beams are respectively considered for the calculation of $(EI)_L$, in Eq.(4).

It is worthwhile to point out that exciting the tested structure did undoubtedly help to increase the signal to noise ratio, but it also partially masked the presence of spurious harmonics. Structures under test may show dominant frequency components which do not represent natural frequencies but derive from deterministic signals superimposed to the stochastic response (e.g., rotating equipment). One of the criteria to identify the presence of such spurious harmonics is by looking at the plot of the singular values of the PSD matrix. The PSD matrix presents a high rank in similar instances, and the spurious frequency is recognizable in the plot of the singular values, which have a sharp-

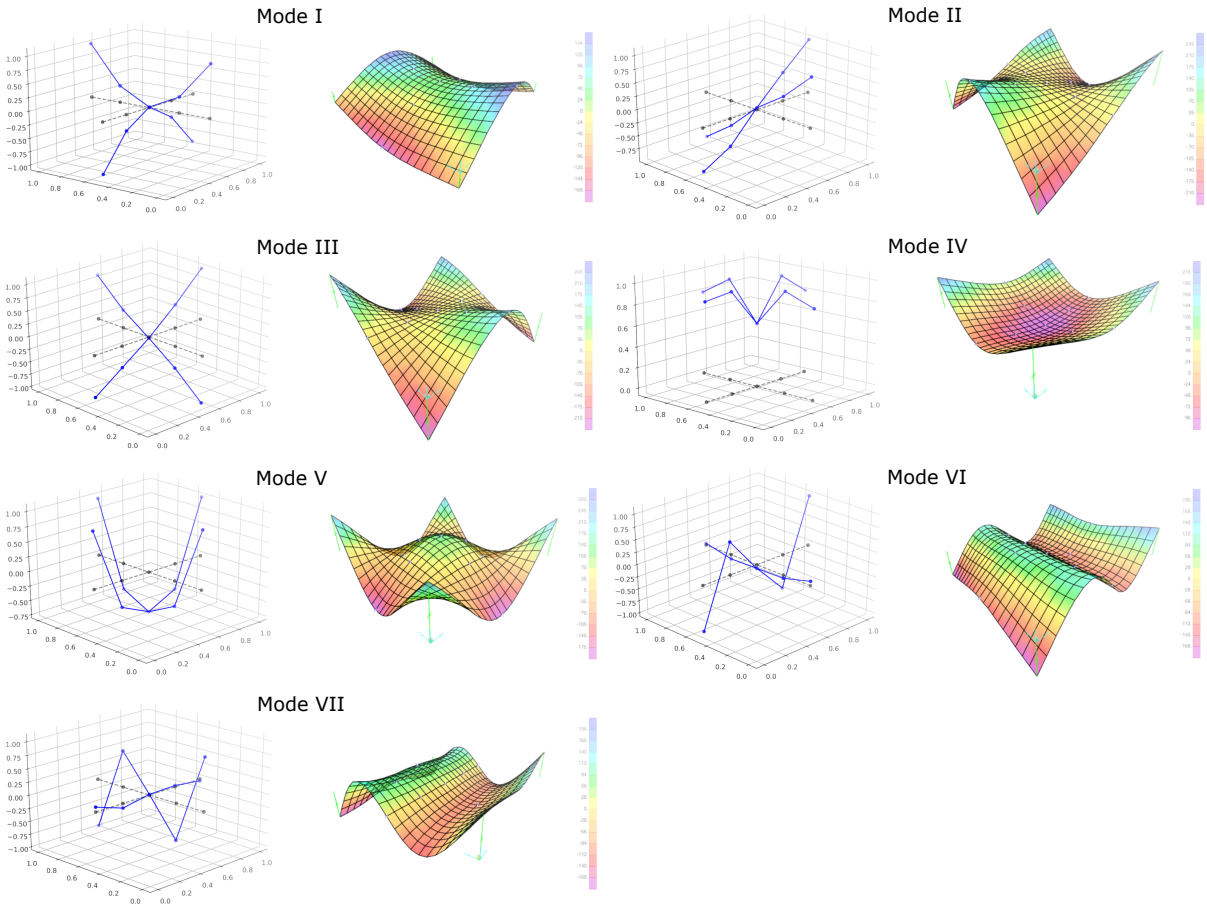

Fig. 8. Experimental and numerical mode shapes of the plywood board.

TABLE 4. Results dynamic identification floor

	SAP2000	Analytical	Floor - SSIcov			Floor - EFDD		
Mode	f_n [Hz]	f_n [Hz]	f_n [Hz]	ξ [%]	MAC	f_n [Hz]	ξ [%]	MAC
I	20.09	-	16.76	3.26%	90.9%	16.81	3.28%	92.2%
II	23.44	26.37 / 23.41	20.28	3.96%	91.5%	20.31	2.40%	93.5%
Numerical model's parameters:								
Glulam: $E_x = 13000\ [MPa]$, $G_{xz} = 650\ [MPa]$; $\rho = 430\ [kg/m^3]$								
Plywood: $E_x = 6000\ [MPa]$, $E_y = 8000\ [MPa]$; $\rho = 650\ [kg/m^3]$								
Supports: $K_{support} = \infty$								

pointed resonance peak. During the excitation, the peaks in the plot of the singular values could be misunderstood for natural frequencies. In the current case, a few tests carried out without the manual excitation revealed the occurrence of the spurious harmonics. Fig9 demonstrates this aspect by comparing the plots of the singular values of the floor assembly.

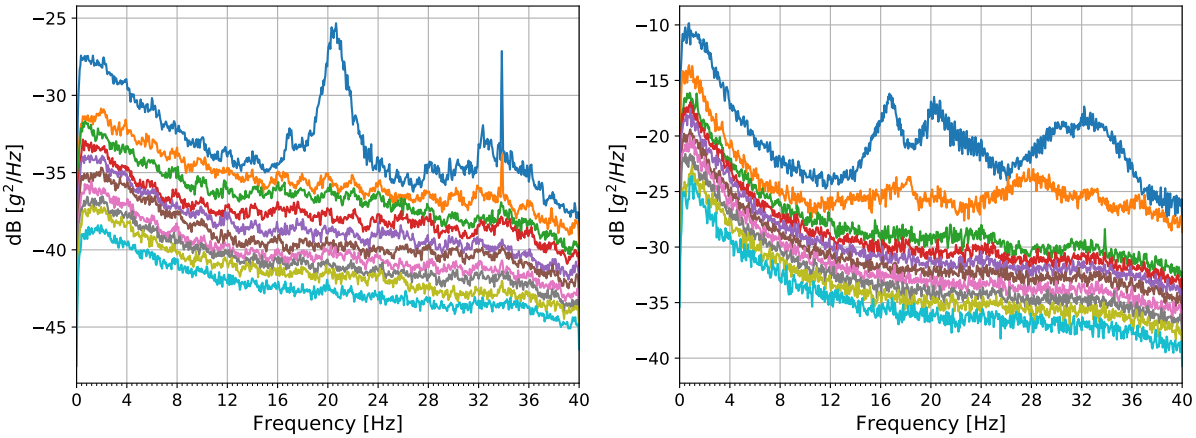

Fig. 9. Singular values plot: left unexcited floor, right excited floor.

SENSITIVITY ANALYSIS AND MODEL UPDATING

Sensitivity analysis

The solid element models of the beams were the base of a variance-based sensitivity analysis. The analysis allowed decomposing the variance of the output (objective function, and natural frequencies) of the model into fractions which can be attributed to the inputs (mechanical properties). The first step was setting the inputs sampling range (mean value ±30%) and generate the model inputs according to the Saltelli's sampling scheme (Saisana et al. 2005) ($N * (2D + 2)$ model inputs were generated, where $N = 100$ is the number of samples, and $D = 9$ is the number of input parameters). After running all the model inputs the first-order (S1) and total-order (ST) sensitivity indices were calculated. S1 and ST measure respectively, the effect of varying a single parameter alone and the contribution to the output variance of the selected parameter including all variance caused by its interactions with the other parameters. Since the results were similar for both beams, Tab5 details those of a single beam. The first two columns express the impact of the mechanical parameters on the total response. The following columns show the impact of the parameters on each mode (SA=Strong axis, WA=Weak axis, Tors=Torsional mode).

From Tab5 it is evident that the dynamic behaviour is mainly influenced by E_X and G_{XZ}, while G_{XY} shows a moderate contribution. The other parameters do not affect the results at all. For the objective function the differences in the first and total order indexes show some degree of interaction between E_X and G_{XZ}. Furthermore, between all the flexural modes, E_X is the most critical parameter. However, in the dynamic parallel to the strong axis, the shear modulus G_{XZ} gain importance in higher modes (see SAIII in Tab5). The fact that G_{XY} show very little influence for the modes along the weak axis agrees with the fact that the cross-section is much higher than wider (115 x 315 mm). This aspect is also evident in the torsional modes, where G_{XZ} is the most crucial

TABLE 5. First-order (S1) and total-order (ST) sensitivity indices for beam 1

	Obj. Fun.		SA I		SA II		SA III		WA II	
	S1	ST	S1	ST	S1	ST	S1	ST	S1	ST
E_X	60%	80%	97%	97%	85%	86%	62%	64%	97%	97%
E_Y	0%	0%	0%	0%	0%	0%	0%	0%	0%	0%
E_Z	0%	0%	0%	0%	0%	0%	0%	0%	0%	0%
ν_{YX}	0%	0%	0%	0%	0%	0%	0%	0%	0%	0%
ν_{ZX}	0%	0%	0%	0%	0%	0%	0%	0%	0%	0%
ν_{YZ}	0%	0%	0%	0%	0%	0%	0%	0%	0%	0%
G_{XY}	0%	5%	0%	0%	0%	0%	0%	0%	0%	0%
G_{XZ}	32%	56%	1%	1%	10%	11%	32%	35%	0%	0%
G_{YZ}	0%	0%	0%	0%	0%	0%	0%	0%	0%	0%

	WA III		WA IV		Tor I		Tor II		Tor III	
	S1	ST	S1	ST	S1	ST	S1	ST	S1	ST
E_X	96%	96%	94%	94%	0%	0%	0%	0%	0%	1%
E_Y	0%	0%	0%	0%	0%	0%	0%	0%	0%	0%
E_Z	0%	0%	0%	0%	0%	0%	0%	0%	0%	0%
ν_{YX}	0%	0%	0%	0%	0%	0%	0%	0%	0%	0%
ν_{ZX}	0%	0%	0%	0%	0%	0%	0%	0%	0%	0%
ν_{YZ}	0%	0%	0%	0%	0%	0%	0%	0%	0%	0%
G_{XY}	1%	1%	3%	3%	3%	3%	4%	4%	5%	5%
G_{XZ}	0%	0%	0%	0%	101%	101%	100%	100%	98%	98%
G_{YZ}	0%	0%	0%	0%	0%	0%	0%	0%	0%	0%

parameter. These observations are in line with what one could expect from the slender nature of the element, which should indeed follow the assumptions of the beam theory.

The fact that some first-order indices add up to values slightly higher than one may derive from the reduced number of samples ($N = 100$). Still, this not affect the substantial interpretation of the results. A 2^{nd} order polynomial was fitted to the values of the objective function to provide a graphical description of the results in the E_X and G_{XZ} domain, see Fig10.

Model Updating

Finite element model updating methods aim at tuning a numerical model to the measured response(Marwala 2010). It is assumed that the measurements are correct, and the model under consideration will need to be updated to reflect the measured data better.

As already mentioned, two global optimization algorithms headed the model updating process: particle swarm optimization (PSO) and differential evolution (DE). Eq.(1) was used in both to minimize the distance between measurements and numerical simulations. The results of the sensitivity analysis supported the adoption of β equal to 0.1. The choice counterbalanced the significant contribution of the second part of the objective function (due to the MAC). The swapping of position between the 1^{st} flexural mode along the strong axis and the 2^{nd} flexural mode along the weak axis resulted, in fact, in very high values of the objective function, see Fig10.

The natural frequencies depend on the ratio between the stiffness and the mass of the system. The direct weighting of the beams and the panel allowed a straightforward calibration of the FE model inertia (Beam 1 = $455kg/m^3$, Beam 2 = $470kg/m^3$, panel = $680kg/m^3$). Tab6 and Tab7 report the frequencies of the initial FE models (with the measured mass), with errors to test results,

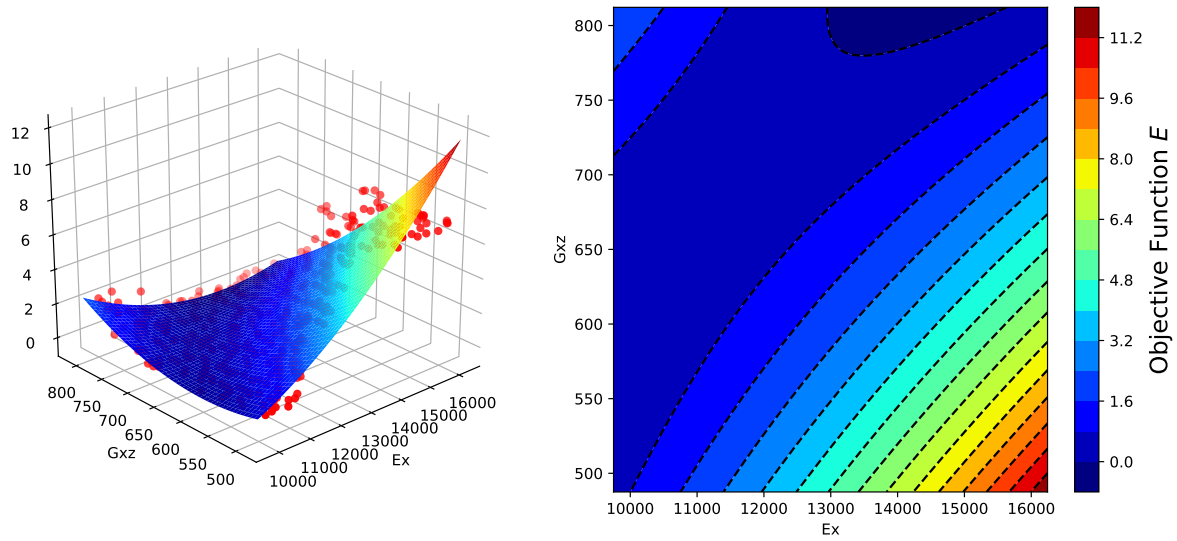

Fig. 10. 2^{nd} order polynomial fit: left 3D view with data points, right contour plot.

referred to the frame and solid element models, respectively. The first update regarded the frame element. Isotropic material properties are used for these elements by SAP2000 even if the material is defined as orthotropic. However, the definition of the material as orthotropic allows to separately define the elastic modulus E_X (axial stiffness and bending stiffness) and the shear modulus G_{XZ} (transverse shear stiffness), which were the selected parameters to be updated in this model. The last columns of Tab6 list the frequencies of the updated FE model, compared to test results. The averages of the optimal solutions of the two algorithms, used to calculate the modes of the updated model, are presented in the lower part of Tab6. The tables reveal that the updating process did improve the agreement between the physical and numerical model. However, the model did not resolve the already mentioned inconsistency due to the swapping of position between modes. Furthermore, the updating of Beam 1 showed that there is a reduction of the elastic modulus E_X compared to the mean value of the standards, while that of Beam 2 E_X increases slightly. Likely, the reduction of the elastic modulus E_X in Beam 1 derives from the wide crack present by the end of the beam. The shear modulus G_{XZ} is higher than expected in both beams, more evident in Beam 2 than Beam 1.

In the second step, the updating regarded the solid beam models. Following the results of the sensitivity analysis, only E_X, G_{XZ} and G_{XY} were updated among the nine mechanical properties. The updating process involved G_{XY}, although the sensitivity analysis showed that this parameter has minimal effect on the dynamic behaviour in the selected frequency range. Similarly to the frame element model, Tab7 reports the results of the solid beam models. The last columns show the frequencies and the error of the updated model, while the lower part of the table reports the averages of the optimal solutions found by the two algorithms. This model yielded a significant improvement in the results. Still, as occurred in the frame-like models, the updating did not resolve the inconsistency due to the swapping of position between modes. There is a similar reduction of the elastic modulus E_X in Beam 1, probably caused by the cracks. Similar observations about the frame element model are valid about the shear modulus G_{XZ} of both beams. The shear modulus

TABLE 6. Result of the model updating on the "Frame elements" beam model

Beam 1					
	Experimental	FE Initial model		Optimised model	
Mode	f_n[Hz]	f_n[Hz]	Error	f_n[Hz]	Error
1-Flex-SA	65.50	66.14	-0.97%	62.94	3.92%
2-Flex-WA	62.98	68.08	-8.09%	64.61	-2.59%
3-Flex-WA	124.09	129.17	-4.09%	123.76	0.26%
2-Flex-SA	154.07	163.31	-5.99%	157.12	-1.98%
4-Flex-WA	194.83	207.78	-6.65%	198.49	-1.88%
3-Flex-SA	273.90	280.09	-2.26%	272.34	0.57%
Optimal parameters: E_x = 11800 $[MPa]$; G_{xz} = 670 $[MPa]$; ρ = 455 $[kg/m^3]$					

Beam 2					
	Experimental	FE Initial model		Optimised model	
Mode	f_n[Hz]	f_n[Hz]	Error	f_n[Hz]	Error
1-Flex-SA	67.77	65.21	3.77%	65.01	4.07%
2-Flex-WA	66.24	67.12	-1.33%	66.74	-0.76%
3-Flex-WA	129.86	128.19	1.28%	127.83	1.56%
2-Flex-SA	157.90	161.02	-1.98%	162.40	-2.85%
4-Flex-WA	202.75	204.87	-1.05%	205.07	-1.15%
3-Flex-SA	279.31	276.16	1.13%	281.68	-0.85%
Optimal parameters: E_x = 13100 $[MPa]$; G_{xz} = 700 $[MPa]$; ρ = 467 $[kg/m^3]$					

G_{XY} exhibits an increment to values suggested by the standards in the Beam 2. In contrast, there is a decrease in the shear modulus G_{XY} in Beam 1. The results in terms of MAC are very high (≈ 0.99), except for the inconsistency between the first modes.

The sensitivity analysis and the model updating process confirm that the "solid elements" model does not determine a significant enhancement of the results to the "frame elements" model. For these reasons, the use of "solid elements" for the FE model of the floor assembly is worthless, given the enormous computational costs related to the use of the "solid elements" model.

The use of low-stiffness linear links (100 N/mm) placed by the middle of the plate, in correspondence of the Rockwool pad, enhance the quality of the results referred to mode IV and V. The first column of Tab3 and the second column of Tab8 prove this aspect. Conversely, the low-stiffness linear links did not affect the results of mode I, VI and VII: the centre is a node in these modes. Accordingly, the authors used only mode I, VI and VII to update the FE model with the optimization algorithms as carried out in the beam models. The last columns of Tab8 summarize the results, while the lower part of the table reports the optimal solutions (rounded).

The numerical model of the floor assembly descended from the updating of the single structural components. As already mentioned, frame elements were used to model the beams and shell elements the plywood boards. The boards were "lifted" to the centre of mass of the beams. Link elements, with infinite stiffness in the axial direction and zero stiffness to all the others, model the connection between the elements. The updated parameters of the single sub-assemblies yield already a good match with the measurements (compare the first columns of Tab9). However, it was decided to enhance it further, by changing the supports' stiffness from infinite into a finite value.

TABLE 7. Results of the updating on the "Solid elements" beam model

Beam 1					
	Experimental	FE Initial model		Optimised model	
Mode	f_n[Hz]	f_n[Hz]	Error	f_n[Hz]	Error
1-Flex-SA	65.50	65.76	-0.39%	62.54	4.52%
2-Flex-WA	62.50	68.08	-8.94%	64.35	-2.97%
1-Tors	70.32	70.83	-0.73%	72.15	-2.60%
3-Flex-WA	124.17	130.17	-4.83%	123.12	0.85%
2-Tors	149.15	142.92	4.17%	145.20	2.65%
2-Flex-SA	154.07	162.32	-5.35%	156.52	-1.59%
4-Flex-WA	193.55	208.32	-7.63%	197.20	-1.89%
3-Tors	220.05	217.43	1.19%	219.99	0.03%
3-Flex-SA	273.90	279.08	-1.89%	272.75	0.42%
Optimal parameters: E_x = 11600 $[MPa]$; G_{xz} = 690 $[MPa]$; G_{xy} = 620 $[MPa]$; ρ = 455 $[kg/m^3]$					

Beam 2					
	Experimental	FE Initial model		Optimised model	
Mode	f_n[Hz]	f_n[Hz]	Error	f_n[Hz]	Error
1-Flex-SA	67.77	64.84	4.32%	64.71	4.50%
2-Flex-WA	65.66	67.13	-2.24%	66.74	-1.65%
1-Tors	71.94	69.84	2.92%	74.15	-3.07%
3-Flex-WA	129.50	128.35	0.89%	127.86	1.26%
2-Tors	154.37	140.92	8.71%	149.27	3.30%
2-Flex-SA	157.90	160.05	-1.36%	161.62	-2.36%
4-Flex-WA	201.36	205.40	-2.01%	205.14	-1.87%
3-Tors	227.53	214.38	5.78%	226.28	0.55%
3-Flex-SA	279.31	275.17	1.48%	281.06	-0.63%
Optimal parameters: E_x = 12800 $[MPa]$; G_{xz} = 740 $[MPa]$; G_{xy} = 700 $[MPa]$; ρ = 467 $[kg/m^3]$					

TABLE 8. Results of the updating of the Plywood board

	Experimental	FE Initial model		Optimised model		
Mode	f_n[Hz]	f_n[Hz]	Error	f_n[Hz]	Error	MAC
I	30.42	28.31	6.9%	29.51	3.0%	99.8%
II	37.45	35.57	5.0%	37.60	-0.4%	47.8%
III	39.96	39.27	1.7%	38.87	2.7%	51.5%
IV	46.90	44.07	6.0%	44.66	4.8%	95.9%
V	74.29	71.02	4.4%	71.58	3.7%	98.9%
VI	88.83	81.39	8.4%	89.23	-0.5%	98.2%
VII	91.24	93.75	-2.8%	92.10	-0.9%	98.3%
Optimal parameters: E_X = 6500 $[MPa]$; E_Y = 7500 $[MPa]$; ρ = 680 $[kg/m^3]$						

The simplicity of the problem encouraged a manual update based on trial and error. Tab9lists the results of the updated FE model with the optimal solution. As further validation, the estimated stiffness value of the supports was applied to the simply-supported beam models. The adoption of a finite value of stiffness of the supports determine a further enhancement of the results, see Tab10. It was observed that a higher stiffness for the supports was needed to reduce the frequency discrepancy further.

The findings of the investigation confirm that the dynamic response of a timber floor is highly sensitive to every parameters that describe its components and its boundary conditions. Unfortunately predicting accurately the dynamical behaviour of a timber floor with simplified analytical approach is rarely possible. Even if well-known and understood analytical models are certainly useful at preliminary design stages, more detailed numerical models are needed if high level of performance of the floor are desired. It is possible to obtain numerical models very faithful to reality, however updating every element that compose the system is not feasible in practical applications. To assess the behaviour of an existing floor in a building, a researcher would need update all the parameter "at once" with an inevitable loss of detail. A careful examination of the drawings corroborated by on-site inspections is therefore of paramount importance in order to build a detailed and representative numerical model. Furthermore the level of detail of the experimental campaign will set the basis for the success of the updating process.

TABLE 9. Results of the updating of the floor

	Experimental	FE Initial model		Optimised model		
Mode	f_n [Hz]	f_n [Hz]	Error	f_n [Hz]	Error	MAC
I	16.76	18.62	-11.11%	17.15	-2.32%	94.0%
II	20.30	21.77	-7.22%	20.30	0.00%	93.5%
Optimal parameters:						
Glulam: see Tab6						
Plywood: see Tab8						
Supports: $K_{support}$ = 6000 $[N/mm]$						

TABLE 10. Simply supported beam with updated parameters

	Experimental		FE Updated		FE Updated	
Mode	Beam 1	Beam 2	Beam 1	MAC	Beam 2	MAC
I	28.90	29.93	28.77	99.9%	29.74	100.0%
II	90.22	92.53	90.49	99.8%	92.17	99.5%
III	149.50	153.73	150.48	96.0%	151.67	92.5%
Optimal parameters:						
Glulam: see Tab6						
Supports: $K_{support}$ = 9000 $[N/mm]$						

CONCLUSIONS

This paper investigates the dynamic behaviour of a simply-supported timber floor assembly and its composing elements. A sensitivity analysis revealed the influence of mechanical parameters on the dynamic response. As the last step, the numerical models were updated to reflect the findings of the measurements better. The main findings are:

- OMA techniques can be used, instead of EMA techniques, to test not only massive civil engineering structures, but also smaller structural elements, such as floors, beams etc., and their results can be used to calibrate the parameters of numerical models.
- It is helpful to continuously and randomly excite the tested components, for example, by rubbing something onto it, to increase the signal-to-noise ratio. Significant attention must, however, be paid not to mistake spurious harmonics for natural frequencies.
- Small pieces/layers of insulation material, can be used to recreate free-free boundary conditions if the suspension of the element is not possible.
- Higher modes were found more susceptible to damages and defect when the beams were tested as simply-supported. They could therefore be used as damage indicators to assess the state of health and/or to localise defects in it. When the beams were tested as freely suspended, however, the damages seemed not to affect the modal shapes.
- The results of the identification, for any component, are very susceptible to the nature of the boundary conditions and even small variations in them significantly affect the results.
- The results confirm that the use of the well-known beam model is more than capable of correctly predicting the behaviour of slender components. The significant computational time needed for a solid element model is not worth the gain in terms of precision.

This research was preliminary to more-in-depth investigations about the walked-induced vibration response of timber floors. The authors aim at using the assembled floor system and the updated numerical model to study different walking models further and compare numerical simulations with walking tests. This investigation will allow studying the various metrics used by building codes and relevant standards to evaluate and assess building floor vibrations.

DATA AVAILABILITY STATEMENT

Some or all data, models, or code that support the findings of this study are available from the corresponding author upon reasonable request.

ACKNOWLEDGEMENTS

The authors acknowledge the significant role of Prof. Rocco Alaggio, who shared with the authors his thirty years experience in dynamic identification.

REFERENCES

Aloisio, A., Alaggio, R., and Fragiacomo, M. (2020a). "Dynamic identification and model updating of full-scale concrete box girders based on the experimental torsional response." *Construction and Building Materials*.

Aloisio, A., Alaggio, R., and Fragiacomo, M. (2020b). "Fragility functions and behavior factors estimation of multi-story cross-laminated timber structures characterized by an energy-dependent hysteretic model." *Earthquake Spectra*, 8755293020936696.

Aloisio, A., Alaggio, R., and Fragiacomo, M. (2020c). "Time-domain identification of elastic modulus of simply supported box girders under moving loads: method and full-scale validation." *Engineering Structures*.

Aloisio, A., Alaggio, R., and Fragiacomo, M. (2021). "Equivalent viscous damping of cross-laminated timber structural archetypes." *Journal of Structural Engineering*, 147(4), 04021012.

Aloisio, A., Battista, L. D., Alaggio, R., Antonacci, E., and Fragiacomo, M. (2020d). "Assessment of structural interventions using bayesian updating and subspace-based fault detection methods: the case study of s. maria di collemaggio basilica, l'aquila, italy." *Structure and Infrastructure Engineering*, 1–15.

Aloisio, A., Di Battista, L., Alaggio, R., and Fragiacomo, M. (2020e). "Sensitivity analysis of subspace-based damage indicators under changes in ambient excitation covariance, severity and location of damage." *Engineering Structures*, 208, 110235.

Aloisio, A., Pasca, D., Tomasi, R., and Fragiacomo, M. (2020f). "Dynamic identification and model updating of an eight-storey clt building." *Engineering Structures*, 213, 110593.

Antonacci, E., Aloisio, A., Galeota, D., and Alaggio, R. (2020). "The s. maria di collemaggio basilica: From vulnerability assessment to first results of shm." *Journal of Architectural Engineering*, 26(3), 05020007.

Bedon, C. and Morassi, A. (2014). "Dynamic testing and parameter identification of a base-isolated bridge." *Engineering Structures*, 60, 85–99.

Brandner, R., Flatscher, G., Ringhofer, A., Schickhofer, G., and Thiel, A. (2016). "Cross laminated timber (clt): overview and development." *European Journal of Wood and Wood Products*, 74(3), 331–351.

Brincker, R. and Ventura, C. (2015). *Introduction to operational modal analysis*. John Wiley & Sons.

Brincker, R., Zhang, L., and Andersen, P. (2001). "Modal identification of output-only systems using frequency domain decomposition." *Smart materials and structures*, 10(3), 441.

Casagrande, D., Giongo, I., Pederzolli, F., Franciosi, A., and Piazza, M. (2018). "Analytical, numerical and experimental assessment of vibration performance in timber floors." *Engineering Structures*, 168, 748–758.

Ceccotti, A., Sandhaas, C., Okabe, M., Yasumura, M., Minowa, C., and Kawai, N. (2013). "Sofie project–3d shaking table test on a seven-storey full-scale cross-laminated timber building." *Earthquake Engineering & Structural Dynamics*, 42(13), 2003–2021.

Ciambella, J., Pau, A., and Vestroni, F. (2019). "Modal curvature-based damage localization in weakly damaged continuous beams." *Mechanical Systems and Signal Processing*, 121, 171–182.

Devriendt, C., Magalhães, F., Weijtjens, W., De Sitter, G., Cunha, Á., and Guillaume, P. (2014). "Structural health monitoring of offshore wind turbines using automated operational modal analysis." *Structural Health Monitoring*, 13(6), 644–659.

EN14080 - Timber structures. Glued laminated timber and glued solid timber. Requirements (2013). European Committee for Standardisation.

EN 1995-1-1: 2004—Eurocode 5: Design of timber structures—Part 1-1: General—Common rules and rules for buildings (2004). European Committee for Standardisation.

Friswell, M. and Mottershead, J. E. (2013). *Finite element model updating in structural dynamics*, Vol. 38. Springer Science & Business Media.

Gentile, C., Ruccolo, A., and Canali, F. (2019). "Long-term monitoring for the condition-based structural maintenance of the milan cathedral." *Construction and Building Materials*, 228, 117101.

Hamm, P., Richter, A., and Winter, S. (2010). "Floor vibrations–new results." *Proceedings of 11th World Conference on Timber Engineerig (WCTE2010), Riva del Garda*.

Hu, L. J., Chui, Y. H., and Onysko, D. M. (2001). "Vibration serviceability of timber floors in residential construction." *Progress in Structural Engineering and Materials*, 3(3), 228–237.

Huang, H., Gao, Y., and Chang, W.-S. (2020). "Human-induced vibration of cross-laminated timber (clt) floor under different boundary conditions." *Engineering Structures*, 204, 110016.

Izzi, M., Casagrande, D., Bezzi, S., Pasca, D., Follesa, M., and Tomasi, R. (2018). "Seismic behaviour of cross-laminated timber structures: A state-of-the-art review." *Engineering Structures*, 170, 42–52.

Kennedy, J. and Eberhart, R. (1995). "Particle swarm optimization." *Proceedings of ICNN'95-International Conference on Neural Networks*, Vol. 4, IEEE, 1942–1948.

Kita, A., Cavalagli, N., and Ubertini, F. (2019). "Temperature effects on static and dynamic behavior of consoli palace in gubbio, italy." *Mechanical Systems and Signal Processing*, 120, 180–202.

Magalhães, F., Caetano, E., and Cunha, Á. (2008). "Operational modal analysis and finite element model correlation of the braga stadium suspended roof." *Engineering Structures*, 30(6), 1688–1698.

Marwala, T. (2010). *Finite element model updating using computational intelligence techniques: applications to structural dynamics*. Springer Science & Business Media.

Miranda, L. J. V. (2018). "PySwarms, a research-toolkit for Particle Swarm Optimization in Python." *Journal of Open Source Software*, 3.

Mugabo, I., Barbosa, A. R., Riggio, M., and Batti, J. (2019). "Ambient vibration measurement data of a four-story mass timber building." *Frontiers in Built Environment*, 5, 67.

Ohlsson, S. V. (1982). *Floor vibrations and human discomfort*. Chalmers University of Technology, Division of Steel and Timber Structures.

Peeters, B. and De Roeck, G. (1999). "Reference-based stochastic subspace identification for output-only modal analysis." *Mechanical systems and signal processing*, 13(6), 855–878.

Peeters, B., Van der Auweraer, H., Vanhollebeke, F., and Guillaume, P. (2007). "Operational modal analysis for estimating the dynamic properties of a stadium structure during a football game." *Shock and Vibration*, 14(4), 283–303.

Pereira, S., Magalhaes, F., Gomes, J. P., Cunha, A., and Lemos, J. V. (2018). "Dynamic monitoring of a concrete arch dam during the first filling of the reservoir." *Engineering Structures*, 174, 548–560.

Rainieri, C. and Fabbrocino, G. (2014). "Operational modal analysis of civil engineering structures." *Springer, New York*, 142, 143.

Rainieri, C., Magalhaes, F., Gargaro, D., Fabbrocino, G., and Cunha, A. (2019). "Predicting the variability of natural frequencies and its causes by second-order blind identification." *Structural Health Monitoring*, 18(2), 486–507.

Reynders, E., Houbrechts, J., and De Roeck, G. (2012). "Fully automated (operational) modal analysis." *Mechanical Systems and Signal Processing*, 29, 228–250.

Reynders, E., Maes, K., Lombaert, G., and De Roeck, G. (2016). "Uncertainty quantification in operational modal analysis with stochastic subspace identification: validation and applications." *Mechanical Systems and Signal Processing*, 66, 13–30.

Reynolds, T., Casagrande, D., and Tomasi, R. (2016). "Comparison of multi-storey cross-laminated timber and timber frame buildings by in situ modal analysis." *Construction and Building Materials*, 102, 1009–1017.

Saisana, M., Saltelli, A., and Tarantola, S. (2005). "Uncertainty and sensitivity analysis techniques as tools for the quality assessment of composite indicators." *Journal of the Royal Statistical Society: Series A (Statistics in Society)*, 168(2), 307–323.

SAP2000 (1975). "Integrated software for structural analysis & design." *Computer and Structures,*

Inc., Berkeley, CA, USA.

Sevim, B., Bayraktar, A., and Altunişik, A. C. (2011). "Finite element model calibration of berke arch dam using operational modal testing." *Journal of vibration and control*, 17(7), 1065–1079.

Smith, A. L., Hicks, S. J., and Devine, P. J. (2007). *Design of floors for vibration: A new approach*. Steel Construction Institute Ascot, Berkshire, UK.

Smith, I. and Chui, Y. H. (1988). "Design of lightweight wooden floors to avoid human discomfort." *Canadian Journal of Civil Engineering*, 15(2), 254–262.

Sobol, I. M. (1993). "Sensitivity estimates for nonlinear mathematical models." *Mathematical modelling and computational experiments*, 1(4), 407–414.

Storn, R. and Price, K. (1997). "Differential evolution–a simple and efficient heuristic for global optimization over continuous spaces." *Journal of global optimization*, 11(4), 341–359.

Tcherniak, D., Chauhan, S., and Hansen, M. H. (2011). "Applicability limits of operational modal analysis to operational wind turbines." *Structural Dynamics and Renewable Energy, Volume 1*, Springer, 317–327.

Van Overschee, P. and De Moor, B. (2012). *Subspace identification for linear systems: Theory—Implementation—Applications*. Springer Science & Business Media.

Virtanen, P., Gommers, R., Oliphant, T. E., Haberland, M., Reddy, T., Cournapeau, D., Burovski, E., Peterson, P., Weckesser, W., Bright, J., van der Walt, S. J., Brett, M., Wilson, J., Jarrod Millman, K., Mayorov, N., Nelson, A. R. J., Jones, E., Kern, R., Larson, E., Carey, C., Polat, İ., Feng, Y., Moore, E. W., Vand erPlas, J., Laxalde, D., Perktold, J., Cimrman, R., Henriksen, I., Quintero, E. A., Harris, C. R., Archibald, A. M., Ribeiro, A. H., Pedregosa, F., van Mulbregt, P., and Contributors, S. . . (2020). "SciPy 1.0: Fundamental Algorithms for Scientific Computing in Python." *Nature Methods*, 17, 261–272.

Weckendorf, J., Hafeez, G., Doudak, G., and Smith, I. (2014). "Floor vibration serviceability problems in wood light-frame buildings." *Journal of Performance of Constructed Facilities*, 28(6), A4014003.

Weckendorf, J. and Smith, I. (2012). "Dynamic characteristics of shallow floors with cross-laminated-timber spines." *World*, 15, 19.

Weckendorf, J., Ussher, E., and Smith, I. (2016). "Dynamic response of clt plate systems in the context of timber and hybrid construction." *Composite Structures*, 157, 412–423.

Xie, Z., Hu, X., Du, H., and Zhang, X. (2020). "Vibration behavior of timber-concrete composite floor under human-induced excitation." *Journal of Building Engineering*, 101744.